Full-Duplex Millimeter-Wave-Band Radio Over Fiber Transmission System

Gang Zhou

A Thesis

In

The Department

Of

Electrical and Computer Engineering

Presented in Partial Fulfillment of the Requirements
for the Degree of Master of Applied Science at
Concordia University
Montreal, Quebec, Canada

December 2004

Your file Votre référence
ISBN: 0-494-04410-1
Our file Notre référence
ISBN: 0-494-04410-1

Abstract

Full-Duplex Millimeter-Wave-Band Radio Over Fiber Transmission System

Gang Zhou

A broadband 30-GHz-band radio over fiber (RoF) transmission system has been investigated by using a combination of novel techniques in this thesis. Our efforts focus on star-tree architecture as well as bus architecture connecting remote antenna base stations (BSs) to a central control office (CO) by incorporating OTSSB, SCM, DWDM and frequency-downshifting schemes. These schemes allow the sharing equipment at the CO and therefore enable simple radio distribution architecture to be implemented.

In this thesis, we have shown that chromatic dispersion can be almost overcome by implementing a simple method using the dual electrode MZM modulation. An important issue related to maximizing spectral utilization in millimeter-waved-band RoF system has been solved by using wavelength-interleaving DWDM technique incorporating OTSSB modulation. Novel WI-Mux, WI-DeMux and WI-OADM, which are the critical components in wavelength-interleaved DWDM system, have also been studied. Moreover, we have demonstrated a 30-GHz full-duplex RoF network using only a signal light source from CO. In this configuration, BSs are simplified by removing local light sources. In uplink, in addition, a novel technique, frequency-downshifting technique, is used for channel selection and frequency downconversion without electrical frequency downconverter. The principle underlying this novel technique is explained theoretically.

Our design features three frequency-interleaved DWDM channel signals in both downlink and uplink, and each optical carrier carries two different 155Mb/s DPSK

signals. The use of 155Mb/s allows for a distribution network of ten customers, and each is able to access 15.5Mb/s of broadband data. In our simulation, wavelength-interleaved OTSSB/DWDM/SCM millimeter-wave-band RoF signals after transmitting over a 50-km-long SMF have been successfully demonstrated and desired BER, Q parameter and eye diagram were achieved without any serious fiber dispersion and channel crosstalk.

Acknowledgments

At the outset I would like to express my most sincere appreciation to my thesis supervisor, Dr. John Xiupu Zhang for being a guiding force necessary for this work and creating a friendly environment during the entire course of this thesis. Without his guidance, support and encouragement, this work would not have been accomplished.

The members at the Broadband RoF Project provided a precious collaborative working environment that will be hard to forget. I thank Dr. Raman Kashyap (Ecole Polytechnique), Dr. Ke Wu (Ecole Polytechnique), and Dr. Jianping Yao (University of Ottawa) for their full support and coordination for this project.

I wish to express my gratitude to all professors who ever have taught me at Concordia University. Their enlightening lectures that allowed me to broaden my view and deepen my professional expertise are sincerely acknowledged.

I would like to thank my fellow students who offered me their hand to solve all of kinds of problem I encountered during the progress of my work. I will not forget those friends who were always on my side when I felt down.

My special thanks are also extended to my friends in Canada and China. I believe that their encouragement and trust, which have been accompanying me all these years, are driving me to success.

I am indebted to my parents and all my family for their encouragement and moral support they have provided me throughout my academic career. No words can express my gratitude to them.

Table of Contents

Chapter 4 A Single Light-Source Configuration

Chapter 5 Novel Optical Components in Millimeter-Wave-Band RoF System

Chapter 6 Optical Heterodyne Detection

Chapter 7 Simulation Demonstration and Result Discussion

Chapter 8 Conclusion and Future Work

List of Acronyms and Symbols

Acronym	Definition
ASE	Amplified Spontaneous Emission
AWG	Arrayed-Waveguide Grating
BER	Bit Error Rate
BPF	Band Pass Filter
BS	Base Station
CS	Central Station
CU	Customer Unit
CW	Continue-wave
DSF:	Dispersion Shift fiber
DeMux	Demultiplexer
DPSK	Differential Phase-Shift Keying
Demod.	Demodulator
Mod.	Modulator
DSB	Double Side Band
DWDM	Dense Wavelength Division Multiplexing
EAM	Electroabsorption Modulator
EBPF	Electrical Band Pass Filter
EDFA	Erbium-Doped Fiber Amplifier
EWG	Electrical Sinusoidal Waveform Generator
FBG	Fiber Bragg Grating
FDM	Frequency-Division Multiplexing
FP	Fabry-Perot
IF	Intermediate Frequency

IM/DD	Intensity Modulation with Direct Detection
ITU	International Telecommunications Union
LD	Laser Diode
LSB	Low Sideband
Mux	Multiplexer
MZ	Mach-Zehnder
MZM	$LiNbO_3$ Mach-Zehnder Modulator
OBPF	Optical Band Pass Filter
OC	Optical Circulator
OPPL	Optical Phase Locked Loop
ORC	Optical Carrier Recovery
OSSB	Optical Single Sideband
OTSSB	Optical Tandem Single Sideband
PC	Polarization Controller
PD	Photodetector
PLL	Phase Locked Loop
PRBS	Pseudo Random Bit Sequence
PS	Phase Shifter
RF	Radio Frequency
RN	Remote Node
RoF	Radio over Fiber
SCM	Subcarrier Multiplexing
SMF	Single-Mode Fiber
SNR	Signal Noise Ratio
SSB	Single Sideband

USB Upper Sideband

VOA Variable Optical Attenuator

WI-DeMux Wavelength Interleaved Demultiplexer

WI- Mux Wavelength Interleaved Multiplexer

Chapter 1

Introduction

1.1 Preview

Future wireless communication systems are expected to offer broadband radio access and mobile multimedia services to a large number of subscribers. Consequently, the carrier frequency of such wireless systems will be within the millimeter-wave- band where a sufficient number of channels with wide bandwidth is available. Since the electrical transmission of such millimeter-wave-band signals over long distance is not feasible, radio over fiber system has attracted great interests as it is considered to form the backbone of future broadband millimeter-wave-band wireless communication system. Recently, the millimeter-wave-band frequency is considered between 24-31 GHz to be used in Canada. In a typical architecture of a millimeter-wave-band wireless access system with optical fiber, the radio signals are generated at a central location before distribution via fiber to a number of remote antenna base stations for wireless distribution [1]-[3]. Such architecture moves the radio signal-processing and routing functions to the central office, allowing the remote BSs to share resources, thereby simplifying the network architecture. The requirement for more BSs due to the small coverage of millimeter-wave-band frequency radio signals demands the installation of functionally simple and compact

BSs. This can be achieved by implementing the RoF transport scheme where the radio signal is distributed to and from the BS as a millimeter-wave-band modulated optical signal, which reduces the complexity of the electronics required at BSs, since frequency conversion hardware is not required there [4], [5]. However, the performance of RoF transport scheme may be severely limited by fiber chromatic dispersion, which may degrade the received RF power of the millimeter-wave-band radio signals. This effect can be overcome by using optical single sideband with carrier modulation [6]. DWDM offers a number of advantages in terms of simplified upgrade and management of the radio network. However, implementing DWDM in millimeter-wave-band systems will lead to poor optical spectral efficiency since the typical DWDM channel spacing is in excess of 25 GHz. However, wavelength-interleaving technique can increase the optical spectral efficiency in millimeter-wave-band DWDM RoF system. In this scheme, the spectral efficiency of the optical network is much greater than conventional DWDM systems with standard wavelength channel spacing of 25 or 50 GHz. Moreover, using optical tandem single sideband modulation can double the frequency efficiency than using the conventional single sideband modulation.

In addition, a BS can be further simplified with no local light or RF sources. The optical carrier for the uplink is sent along with the downlink optical signal to a remote BS. It is looped back to the central station after being modulated with uplink RF signals [7].

1.2 The Architecture of Millimeter-Wave-Band RoF Networks

In DWDM, individual optical carrier is modulated by RF signals and multiplexed in the optical domain. The use of DWDM can simplify the network architecture using different wavelengths to feed different antenna BSs, support multiple interactive services on one fiber; and greatly simplify network upgrades by enabling the introduction of new services and the deployment of additional BSs. Figure 1.1 shows a possible architecture of the combination of star-tree and bus connection for a millimeter-wave-band RoF network incorporating DWDM. In the star-tree topology, for the downlink case, the wavelengths are multiplexed together at the CO and demultiplexed at the RN, while in the uplink direction the wavelengths are multiplexed at the RN and demultiplexed at the CO. The uplink signal transmission is achieved by modulating the uplink radio signals onto an optical carrier at the same BS wavelength. In the bus topology, it also allows the allocation of a single wavelength to particular two BSs and the wavelength routing is enabled via optical add-drop multiplexers (OADMs). Note that the same wavelength can be reused in the different fiber transmissions under the same CO.

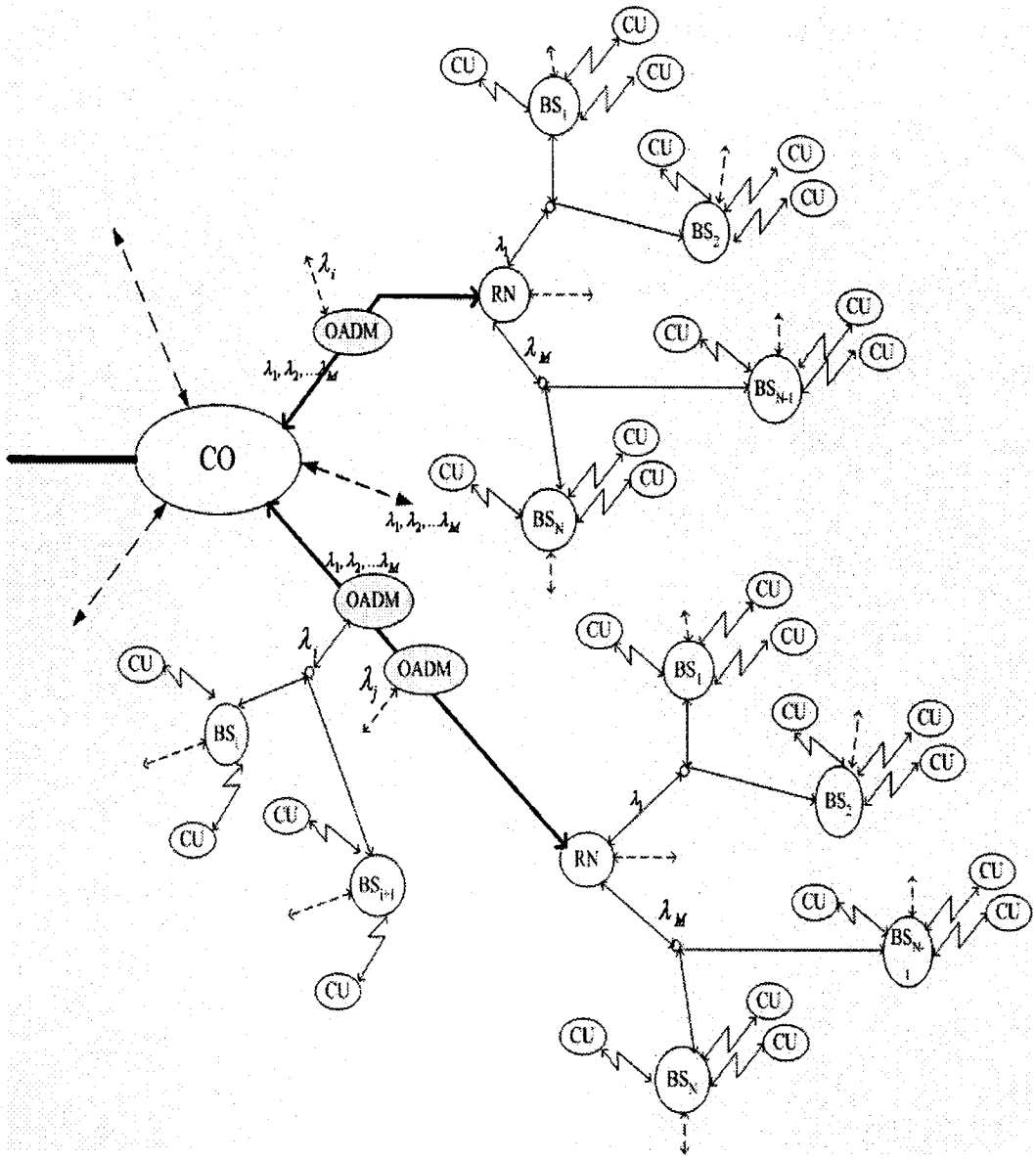

Figure 1.1 The architecture of the combination of star-tree and bus connection in millimeter- wave-band RoF system incorporating DWDM.

1.3 Literature Review

Since the last decade, many millimeter-wave-band ROF systems have been studied. For initial deployment, a simple and low-cost BS design is desirable. This can be realized by putting all the ROF complexities into the CS and by sharing the cost over the

BSs. This concept also enables the ease of maintenance and quick upgradability of entire systems. Moreover, it is concluded that an external modulation technique is one of the best ways to achieve the desired BS design. In addition, a variety of SCM/ DWDM ROF systems have been studied to increase the channel capacity in existing optical fibers.

1.4 Subcarrier Transmission over Fiber

A fiber-optic millimeter-wave-band uplink system can be classified by the following subcarrier frequencies of signals transmitted in an optical fiber link:

1) Baseband (no subcarrier);

2) Microwave IF subcarrier;

3) Millimeter-wave-band RF subcarrier.

In the baseband transmission, influence of the fiber dispersion effect is negligible, but the BS configuration is the most complex. Since, without a subcarrier frequency, it has no choice but to adopt time-division or code-division multiplexing. This requires higher-speed electrical processors. In the IF subcarrier transmission, the fiber dispersion effect does not cause a serious problem. Subcarrier multiplexing can be applied, but downconversion from a millimeter-wave-band to an IF band is required at the BS. However, the IF subcarrier transmission in downlink can work well without using the electrical frequency upconversion, the details will be discussed in Chapter 7. In the RF subcarrier transmission, the BS configuration can be simpli-fied only if a millimeter–wave-band optical external modulator and a high frequency PD are respectively applied to the electric-to-optic (E/O) and the optic-to-electric (O/E) converters. For a simpler BS configuration, the millimeter-wave optical external modulation technique will be one of the best solutions [8].

Chapter 2

Optimal Spectral design in Millimeter-Wave-Band RoF System

One of critical challenges from making millimeter-wave-band practical for commercial deployment is to provide high volume transmission over fiber. Integrating optical wavelength-interleaving, optical tandem SSB modulation, subcarrier and DWDM technologies into a millimeter-wave-band RoF system can achieve a high volume transmission capacity.

2.1 DWDM in Millimeter-Wave-Band RoF Systems

Due to the small coverage of millimeter-wave frequency radio signals, the RoF system demands numerous BSs to be connected with a CO. The capability to deal with large amount of data capacity of the DWDM transmission technology should be applied to the millimeter-wave-band RoF systems. For example, when the L-band (1570 –1610 nm) is allocated as the optical transmission band of the uplink, the maximum number of DWDM channel is estimated to be 160[≈ (C/1570nm-C/1610nm)/channel spacing, where C is the speed of light in fiber, assuming the refractive index is 1.45, then C=2068nm/ps; also assuming the channel spacing is 0.2nm] per optical fiber. If the C–band (1530–1565 nm) is allocated for the downlink,

full-duplex transmission will also be possible [9]. This allows about 160 BSs to be connected to the single CO via an optical fiber. Assuming that one BS covers an area of $10\times10m^2$, the total area of service coverage with 160 BSs estimated will be only $16\ 000\,m^2$. Note that the wavelength band can be exploited by reusing the same band in all the areas under the coverage of a single CS. This architecture of millimeter-wave-band ROF system demonstrates the capability of accommodating a large number of BSs by introducing the DWDM technique. Therefore, we can conclude that DWDM technology will be indispensable in the millimeter-wave-band ROF networks.

2.2 Wavelength-Interleaved DWDM

In this thesis, we assume that the carrier frequency of the millimeter-wave-band signal is at 30-GHz band and the bandwidth of the millimeter-wave-band signal is 310 megahertz. From a view of cost reduction, it is preferable to use the channel allocation in accordance with ITU grid because of the availability of optical components. Therefore, the minimum channel spacing in this case is 100GHz. Thus, the optical spectrum cannot be highly utilized because the bandwidth of the millimeter-wave-band signal is much narrower than the millimeter-wave-band carrier frequency. The problem can become even worse when the architecture of millimeter-wave-band RoF system requires enough capacity to accommodate a large number of BSs. The solution to this demerit is to interleave the optical frequencies along the whole spectrum. Figure 2.1 shows the conventional optical spectrum with DSB modulation format incorporating DWDM for a millimeter-wave-band RoF. Figure 2.2 shows the frequency-interleaved millimeter-wave-band DWDM millimeter-wave-band RoF system [10]. Comparing the two figures, four times of the optical spectral efficiency can be achieved in the case of 25-GHz channel spacing. Note that frequency

interleaving technique can also be well applied to optical SSB modulation format in a millimeter-wave-band RoF system.

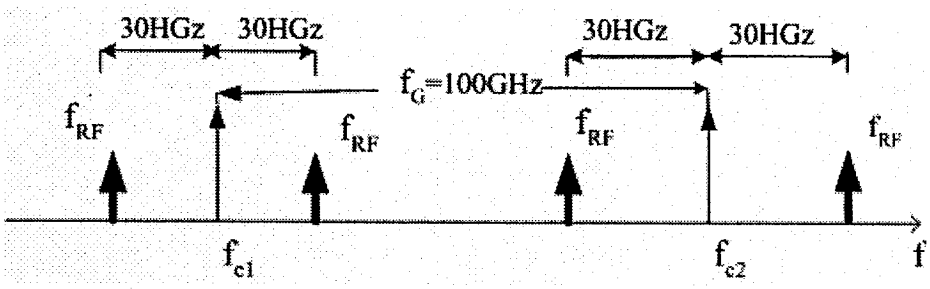

Figure 2.1 The conventional optical spectrum with DSB modulation format incorporating DWDM for a millimeter-wave-band RoF system.

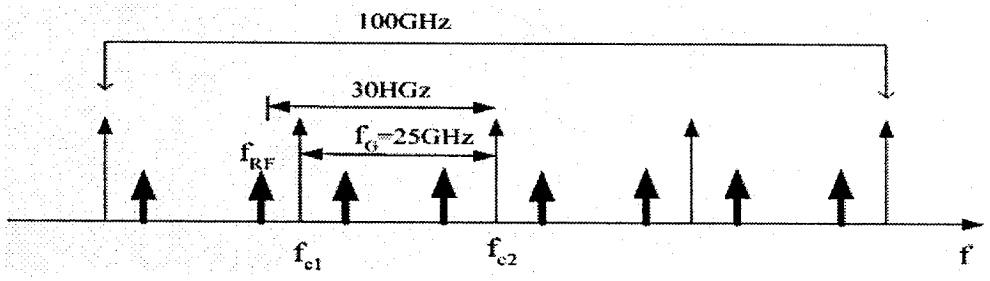

Figure 2.2 The wavelength-interleaved millimeter-wave-band DWDM RoF system.

2.3 Optical Single Sideband Modulation Format and Impact of Chromatic Dispersion

The simple technique for the optical generation and distribution of a RF signal, modulated with data, is a direct-detection scheme via direct or external modulation. In order to avoid the effects of laser frequency chirp as well as decreasing the complexity of the configuration of BS, however, externally modulated optical fiber link is the preferred choice. In traditional intensity modulation, the optical carrier is

modulated to generate a carrier and two sidebands. At the optical receiver side, each sideband beats with the optical carrier to generate two beat signals which constructively interfere to produce a single component at RF. When DSB signals are transmitted via fiber link, fiber chromatic dispersion causes each frequency component to experience different phase shifts depending on the fiber link distance, modulation frequency, and fiber dispersion parameter. If the phase difference is π, destructive mixing will cancel all power at RF frequency [11]-[13].

In a standard single-mode fiber, each optical frequency travels through the fiber at different velocity due to the chromatic dispersion properties of the fiber. It can be shown that phase changes in the optical sidebands alter the resultant phase of the RF beat signals and the RF power of the generated radio frequency will vary approximately as [14]:

$$P_{RF} \propto \cos\left[\frac{\pi L D \lambda_C^{\,2} f_{RF}^{\,2}}{C}\right] \tag{2.1}$$

where P_{RF} is received RF power; D is the fiber dispersion parameter; λ_C is the wavelength of the optical carrier; and f_{RF} is the frequency of RF signal. From Equation 2.1, the received RF power f_{RF} periodically fluctuates with frequency of RF signal f_{RF} change. As f_{RF} increases, the fluctuation period decreases; and thus it can lead to a more serious dispersion. As a result, the fiber link distance becomes severely limited. The argument of the cosine function in Equation 2.1 also indicates that for a fixed radio frequency f_{RF}, the fiber lengths at which power cancellation occurs will be given by

$$L = \frac{NC}{2D\lambda_c^{\,2} f_{RF}^{\,2}}, \quad \text{N=1, 3, 5, } \cdots \tag{2.2}$$

The effect of dispersion on the BL product can be estimated by using the criterion [15]

$$BL|D|\Delta\lambda < 1 \tag{2.3}$$

However, RF signals modulated in OSSB format have essentially solved the fiber dispersion problem. The OSSB of a modulated signal, in which one of the sideband is eliminated, carries full information. OSSB format can also decrease the optical power and bandwidth. An OSSB modulator made of an optical filter to suppress one of the two sidebands has been developed to generate the OSSB. However, the delay-time difference should be compensated by using an electrical delay equalizer in the receiver and phase-synchronization is achieved with a pilot carrier PLL in the transmitter. Thus, this technique could be complex to implement. On the other hand, this technique is also limited by the filter characteristics (for example, this kind of filter is the Mach-Zehnder-type filer) [16]. A preferable technique requiring no optical filtering and only a single dual MZM biased at quadrature to produce OSSB with carrier is clearly a better option, which will be investigated in Chapter 3.

2.4 Optical Tandem Single Sideband Modulation Format

In this thesis, a modification of the OSSB technique, called OTSSB, has been made for our RoF system. Different data streams are placed on each of the two sidebands of the same optical carrier. The two sidebands, each having different data, are then transmitted in tandem, Figure 2.3 (a), (b) show the spectra of OSSB and OTSSB modulation, respectively. In Figure 2.3 (b), the two sidebands contain different information in OTSSB modulation, thus it doubles the information in the two sidebands of the same carrier. However, a photodetector cannot directly detect OTSSB signals because the two sidebands would interfere to produce a single

component at the RF domain. Therefore, two sideband signals should be separately photo-detected by two PDs. In this thesis, a new type of heterodyne detection scheme is proposed to enable the reception of OTSSB signals in the uplink

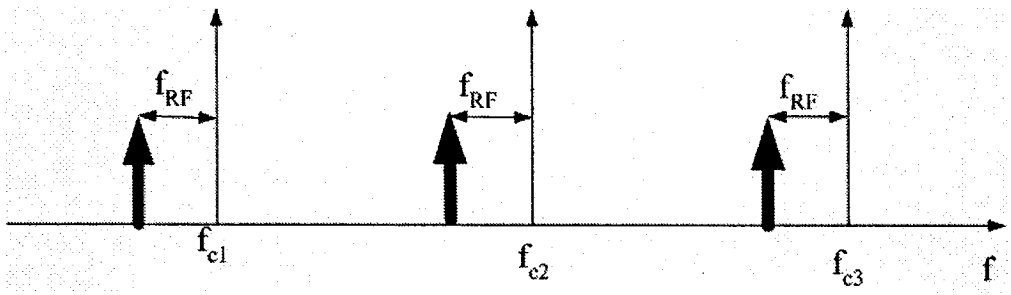

(a)

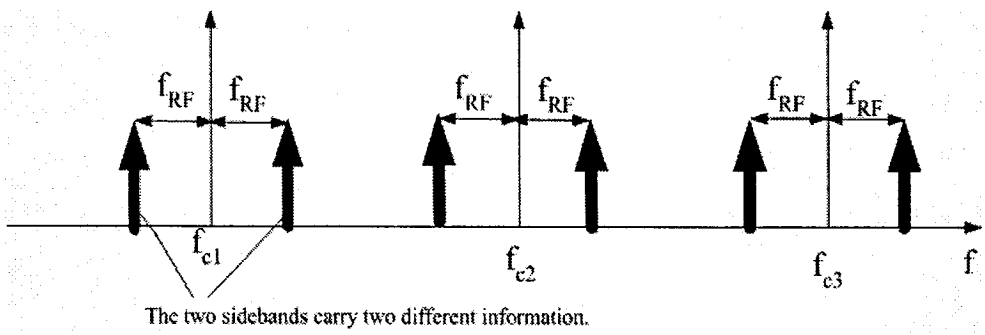

(b)

Figure 2.3 (a) The spectrum of OSSB modulation. (b) The spectrum of OTSSB modulation.

2.5 Subcarrier Multiplexing

To make the optical bandwidth provided by optical fibers more efficiently, SCM is introduced in this thesis. In the electrical domain, the different information channels are multiplexed on RF carriers, and the entire RF signal modulates the power of the lightwave carrier, thus forming a subcarrier-multiplexed signal (SCM) [17], 18]. Note

that, in our RoF system, the bit rate of each channel is relatively low (15.5Mb/s for each of ten users) but the number of channels can become quite large.

Chapter 3

Optimum Modulation in Milli-meter-Wave-Band RoF System

3.1 Introduction

The Mach Zehnder ($LiNbO_3$) optical Modulators (MZM) are indispensable for high-bit-rate millimeter-wave-band RoF system because of their wide wavelength-band operations. Many applications such as optical subcarrier generators, frequency shifters, and SSB modulators can be done based on MZM for the realization of the next-generation optical communication systems. SSB technology brings us special advantages in optical fiber communication systems, such as higher-density wavelength multiplexing and longer-haul fiber transmission due to the reduced optical power and less nonlinear optical effects.

3.2 Mach Zehnder ($LiNbO_3$) Optical Modulator

The Mach Zehnder ($LiNbO_3$) optical Modulator (MZM) is a critical component in millimeter-wave-band RoF system. It is composed of a 3dB **Y** junction optical splitter, and a 3dB **Y** junction combiner, and it incorporates three input port and an output port (see Figure 3.1). A narrow line-width CW polarized optical signal, generated by the laser diode, is applied at the input of MZM. The optical signal is then divided and fed

into two equal paths by 3dB Y junction splitter. If a voltage is applied at the RF input port, an interaction between the optical signal and the RF electrical signal will alter the phase of the optical signal. Through this process, two sets of optical signals are generated: in-phase and out-of-phase. At the Y junction combiner, the in-phase signals are coupled into the optical fiber, while the out-of-phase signals, transformed into a higher order mode, are dissipated into the substrate of the modulator. The transfer function of the modulator is expressed by [19]

$$I(t) = aI(\theta)\cos^2\left(\frac{V_\pi}{2V}\right) \tag{3.1}$$

where $I(t)$ is the intensity of the output modulated signal, a is the insertion loss of the modulator, $I(\theta)$ is the laser diode intensity at the input of the modulator, V is the voltage applied at the Bias Control port, and V_π is the modulator driver voltage required to achieve 180^0 phase shift. A typical MZM transfer curve is illustrated in Figure 3.2 [19].

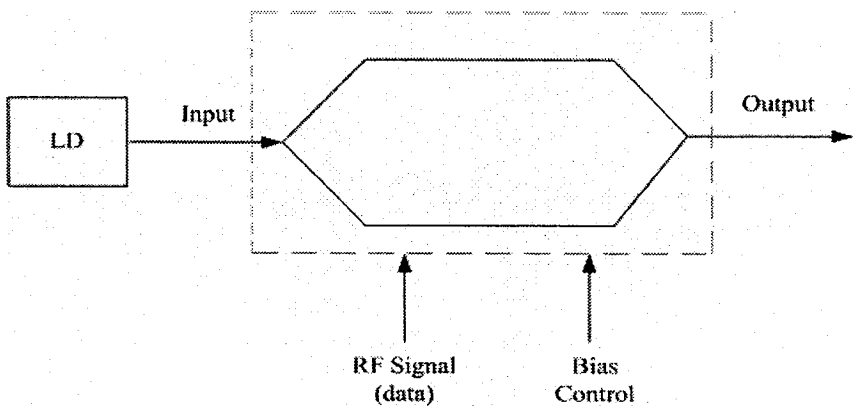

Figure 3.1 The Mach Zehnder ($LiNbO_3$) optical Modulator.

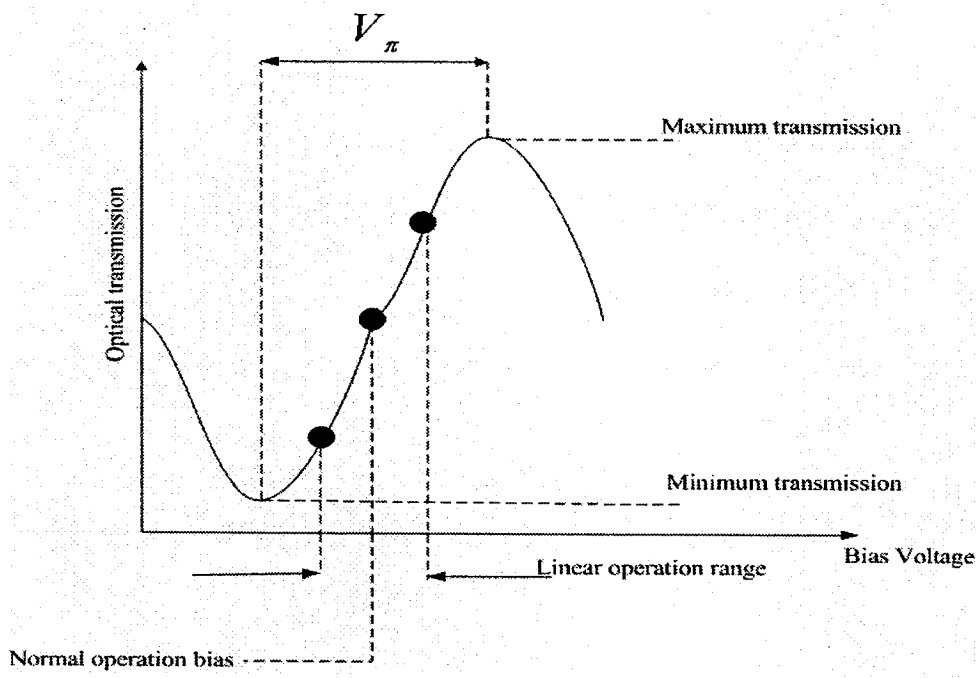

Figure 3.2 The transfer function curve for a Mach Zehnder ($LiNbO_3$) optical modulator.

3.3 Dual Electrode MZM

The dual-electrode MZM can be modeled as two phase modulators in parallel, where the amplitudes of the RF drive signals applied to each electrode are equal. A continuous-wave (CW) light from a laser with amplitude A and frequency f_c is externally modulated by an RF signal with peak-to-peak amplitude $2V_{ac}$ and frequency f_{RF} , which is split and applied to each drive electrode. A phase difference of θ can exist between each drive electrode. If the modulator has a dc-bias voltage of V_{dc} on one electrode while the other dc terminal is grounded, then the output optical field is represented by

$$E(t)=\frac{A}{2}\{\cos(\omega_C t+\gamma\pi+\alpha\pi\cos\omega_{RF}t)$$

$$+\cos(\omega_c t+\alpha\pi\cos[\omega_{RF}t+\theta])\} \tag{3.2}$$

where $\omega_C=2\pi f_c$, $\omega_{RF}=2\pi f_{RF}$, $\gamma=(V_{dc}/V_\pi)$ is the normalized bias voltage, V_π is the switching voltage of the MZM and $\alpha=(V_{ac}/V_\pi)$ is the normalized amplitude of the drive signal. This equation can be expanded in terms of Bessel functions to give

$$E(t)=\frac{A}{2}\{J_0(\alpha\pi)[\cos(\gamma\pi)+1]\cos(\omega_C t)$$

$$-J_0(\alpha\pi)\sin(\gamma\pi)\sin(\omega_C t)$$

$$-J_1(\alpha\pi)\cos(\gamma\pi)[\sin(\omega_c-\omega_{RF})t$$

$$+\sin(\omega_C+\omega_{RF})t]-J_1(\alpha\pi)\sin(\gamma\pi)[\cos(\omega_C-\omega_{RF})t$$

$$+\cos(\omega_C+\omega_{RF})t]-J_1(\alpha\pi)[\sin\{(\omega_C-\omega_{RF})t-\theta\}$$

$$+\sin(\omega_C+\omega_{RF})t+\theta\}]+\cdots\} \tag{3.3}$$

where J_0 and J_1 are the zeroth- and first-order Bessel function, respectively.

When both RF electrode of the MZM are driven with the same signal and a phase difference of $\theta=\pi$ in one arm, and if the applied dc voltage biases the MZM at quadrature ($\gamma=\frac{1}{2}$), then Equation (3.3) simplifies to

$$E(t)=\frac{A}{2}\{J_0(\alpha\pi)\cos(\omega_C t)-J_0(\alpha\pi)\sin(\omega_C t)$$

$$-J_1(\alpha\pi)[\cos(\omega_c-\omega_{RF})t+\cos(\omega_C+\omega_{RF})t]$$

$$+J_1(\alpha\pi)[\sin(\omega_C-\omega_{RF})t+\sin(\omega_C+\omega_{RF})t]$$

$$+\cdots\} \tag{3.4}$$

The Fourier transform of the autocorrelation of E(t) will give the power-spectral density, $S_E(\omega)$:

$$S_E(\omega) = \frac{\pi A^2}{4}[J_0^2(\alpha\pi)\pi\delta\{\omega+\omega_C\}$$

$$+J_1^2(\alpha\pi)\delta\{\omega+(\omega_C-\omega_{RF})\}$$

$$+J_1^2(\alpha\pi)\delta\{\omega+(\omega_C+\omega_{RF})\} \quad (3.5)$$

where $\delta\{\cdot\}$ represents a delta function. This spectrum consists of optical carrier at ω_C, with DSB modulation showing components at $\omega_C-\omega_{RF}$ and $\omega_C+\omega_{RF}$.

The chirp parameter is important in externally modulated systems as it indicates the phase of the output signals from the modulator. Fortunately, MZ interferometer-type intensity modulators can be designed to operate completely chirp-free [20]-[22].

3.4 OSSB Modulation

The preferable technique for generating an optical carrier with SSB modulation to overcome the effect of dispersion in RoF system is to use an external modulator. The technique is simple as no optical filtering is required and it uses only one dual-electrode Mach-Zehnder modulator to produce optical SSB [23]-[25]. The optical SSB generator using the dual-electrode MZM is shown in Figure 3.3(a). When a phase difference of $\theta = \pm\frac{\pi}{2}$ is applied in the two RF electrodes of the dual-electrode MZM, as shown in Figure3.3, Equation 3.3 simplifies to

$$E(t) = \frac{A}{2}[J_0(\alpha\pi)\cos(\omega_C t) - J_0(\alpha\pi)\sin(\omega_C t)$$

$$\pm 2J_1(\alpha\pi)\cos(\omega_C \pm \omega_{RF})t] \quad (3.6)$$

and the power-spectral density, $S_E(\omega)$ is given by

$$S_E(\omega) = \frac{\pi A^2}{4}[J_0^2(\alpha\pi)\pi\delta\{\omega+\omega_C\}$$

$$+\frac{A^2}{2}J_1^2(\alpha\pi)\pi\delta\{\omega+(\omega_C \pm \omega_{RF})\} \qquad (3.7)$$

The first term in (3.7) is the optical carrier at wavelength $\lambda_c = 2\pi c/\omega_c$, while the second term represents either a lower or upper sideband at the optical frequencies $\omega_c - \omega_{RF}$ and $\omega_c + \omega_{RF}$, respectively [see Figure 3.3 (b) and (c)].

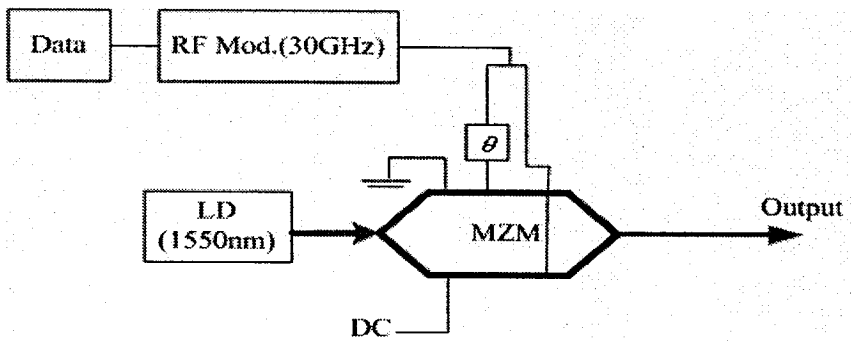

(a)

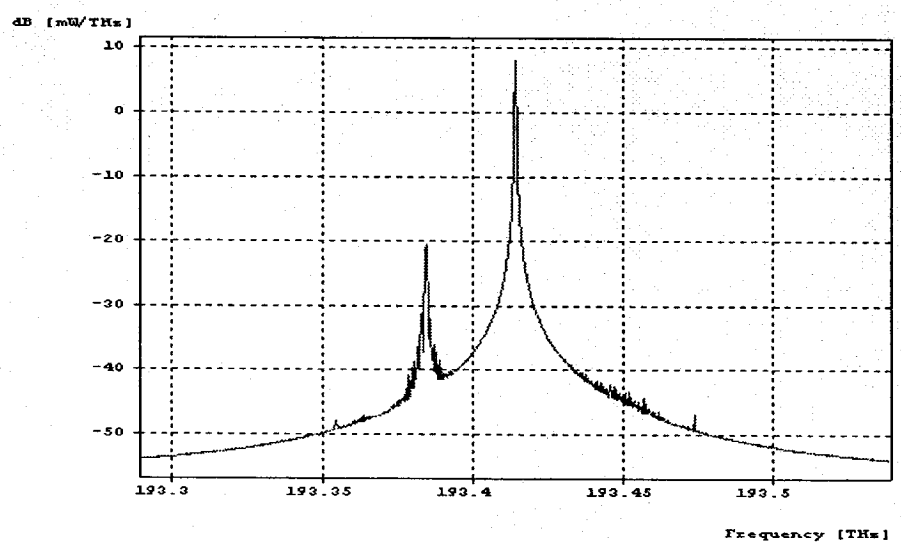

(b)

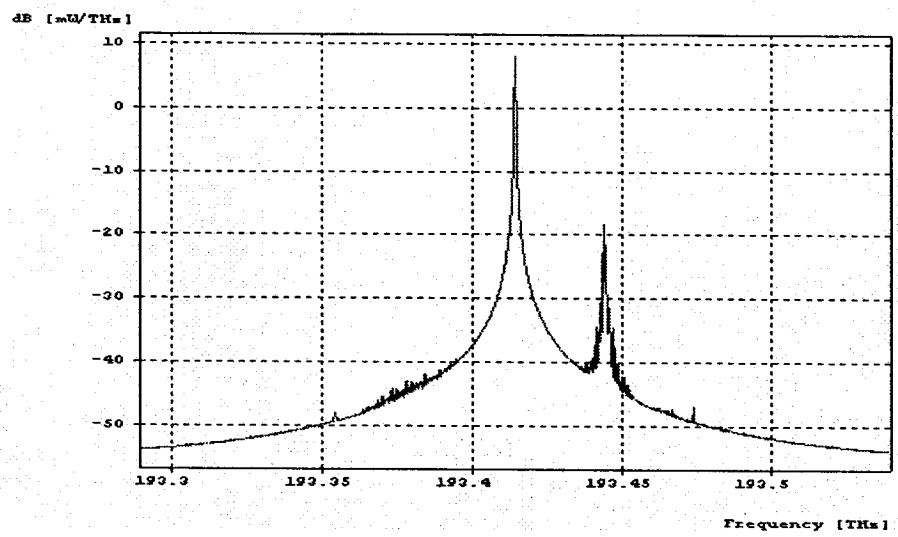

(c)

Figure 3.3 (a) Schematic diagram of OSSB generator. (b) Simulated optical spectrum from the output of MZM with $f_{RF} = 30GHz$ and $\lambda_c = 1550nm$ when $\theta = \pi/2$. (c) Simulated optical spectrum from the output of MZM with $f_{RF} = 30GHz$ and $\lambda_c = 1550nm$ when $\theta = -\pi/2$.

3.5 Optical Tandem SSB Generator

The "tandem" approach modifies the concept by allowing different information to be transmitted in each sideband of the same optical wavelength, thus doubling the information-carrying capacity. A block diagram of the simulation setup for generating TSSB signals is shown in Figure 3.4(a). The light source is a CW laser diode tuned to $f_c = \frac{c}{1550nm}$. The light from the laser is coupled into a dual-electrode Mach–Zehnder modulator through a polarization controller. Two externally triggered pattern generators with $2^{23} - 1$ pseudorandom bit sequences (PRBSs) provide two baseband signals. The data is used to modulate a subcarrier at 30-GHz. The two signals in arms

A and B are then fed to the two inputs of a 90^0 hybrid coupler, the outputs of which are used to drive the MZM at quadrature. The signal that emerges from the MZM is an OTSSB signal consisting of an optical carrier at f_c, a lower sideband at ($f_c - 30$ GHz), and an upper sideband at (f_c+30GHz). The OTSSB spectrum is shown in Figure 3.4(b).

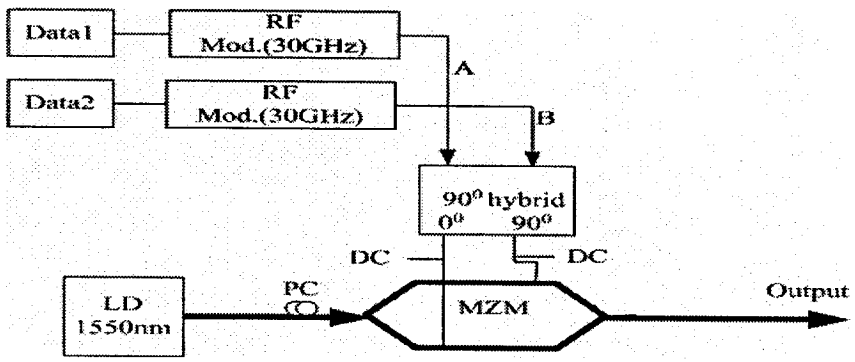

(a)

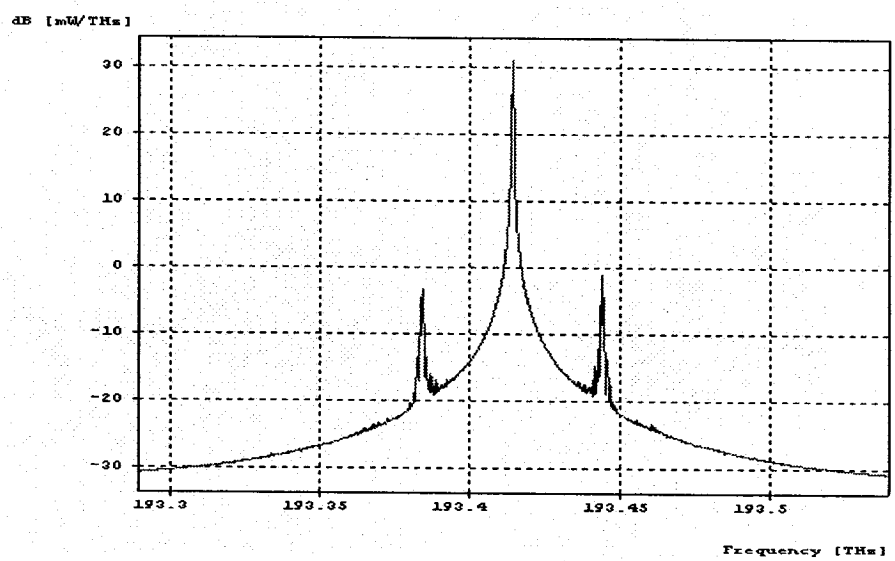

(b)

Figure 3.4 (a) Block diagram of the simulation setup for OTSSB generator.

(b) Simulated OTSSB spectrum at the output of MZM.

Chapter 4

A Single Light-Source Configuration

4.1 Introduction

The key to make millimeter-wave-band RoF systems practical for commercial deployment is to develop a low-cost BS [26], [27]. The external modulation technique is one of the best solutions in order to provide a simple system configuration [28]. In this chapter, a simple full-duplex RoF system using a single light source is described. A BS is simplified by removing local light. The optical carrier for the uplink is sent along with the downlink optical signal to a remote BS. It is looped back to the central station after being modulated with uplink RF signals. The configuration of the proposed system is simpler because one light source is shared by the downlink and uplink. The single light-source configuration is show in Figure 4.1; for simplicity, optical power loss or gain in each optical component is omitted.

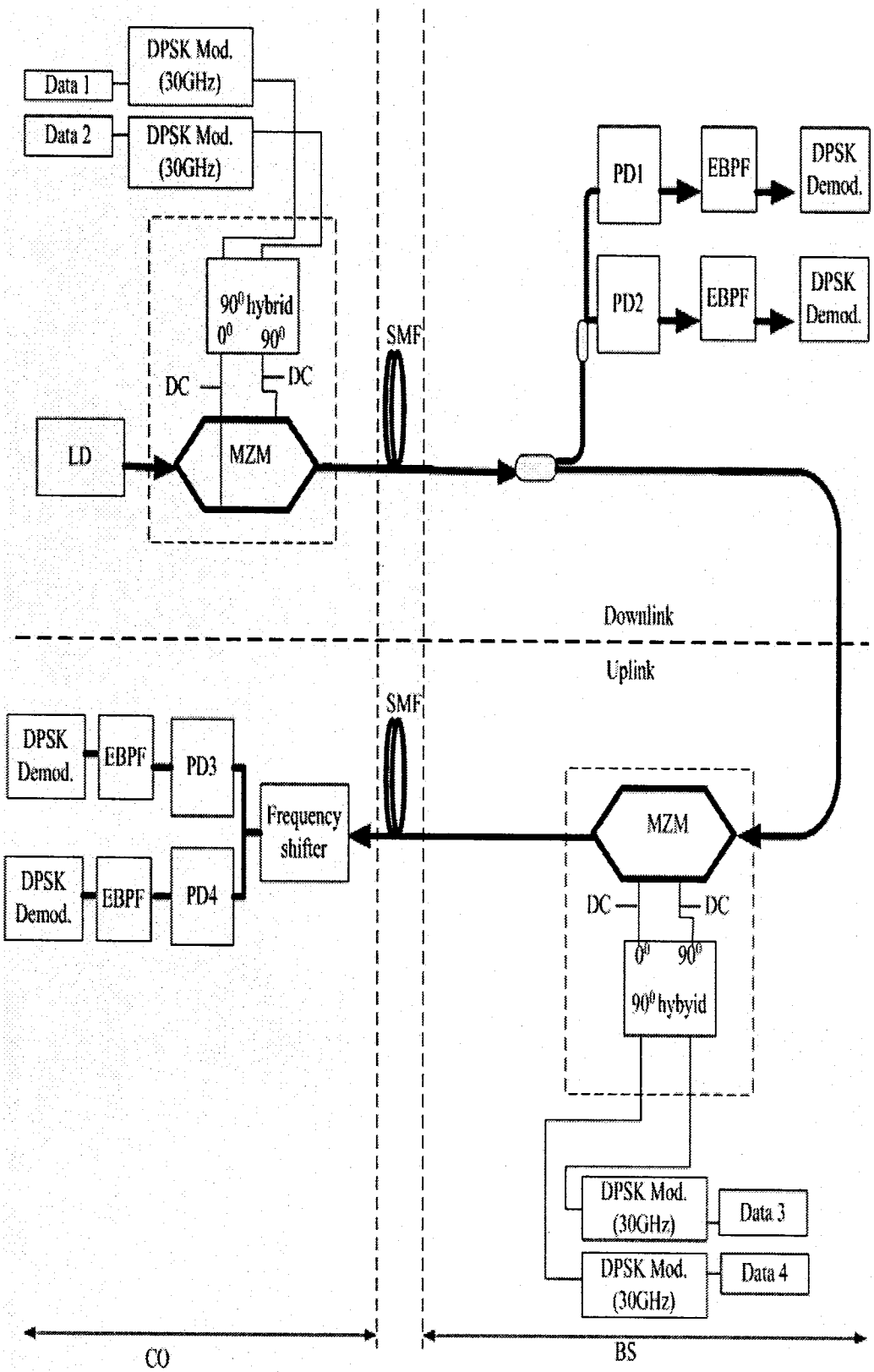

Figure 4.1 Fundamental configuration of a single light source system.

4.2 Techniques for the Single Light-Source Configuration

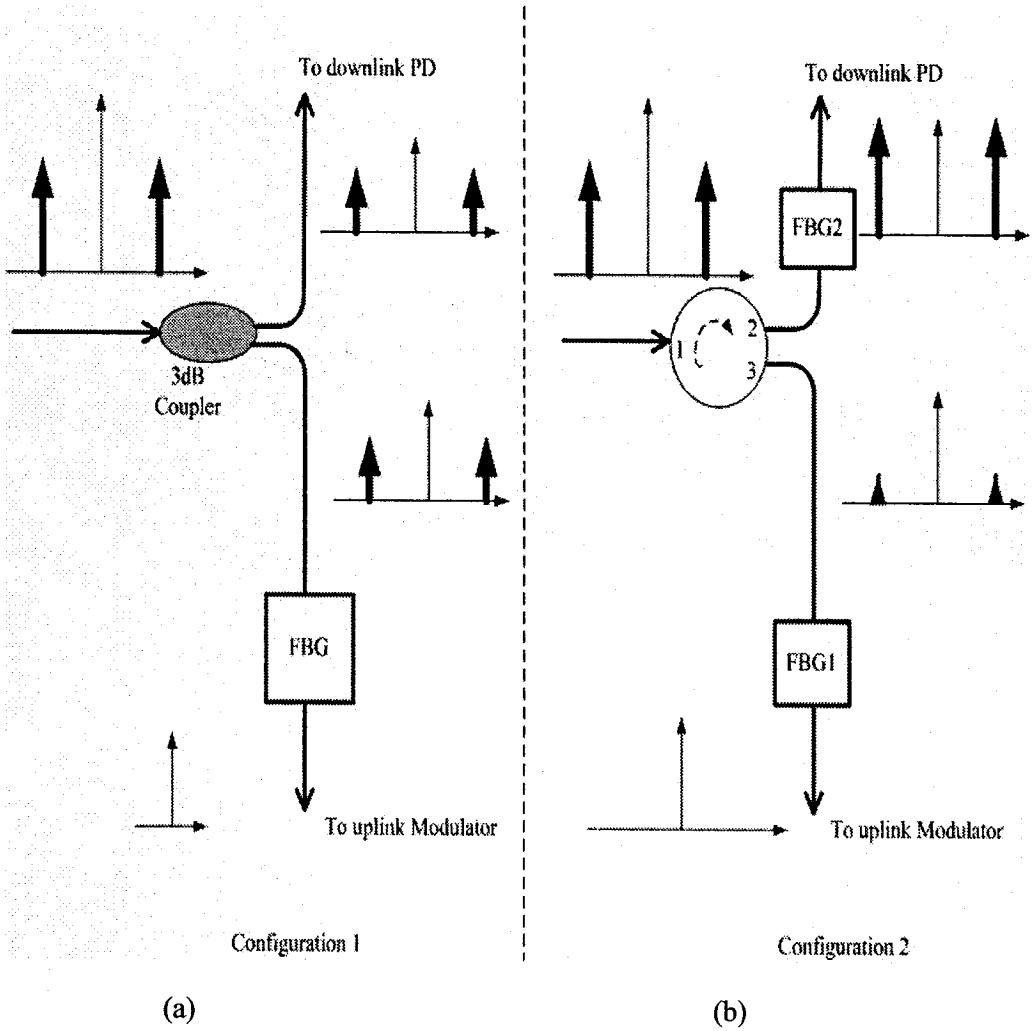

Figure 4.2 (a) The conventional configuration for optical carrier recovery interface.

(b) The improved configuration for optical carrier recovery interface.

The conventional and improved optical interfaces, which eliminate the need for housing an optical source at the BS, are shown in Figure 4.2 (a) and 4.2 (b). In Figure 4.2 (a), the optical signal from the 3dB (50:50) coupler is passed through a customer designed FBG, which filters out the two optical modulation sidebands with downlink

data, thereby extracting the downlink optical carrier signal. FBG has 100% reflectivity at the wavelength corresponding to the modulation sideband of the downlink signal and 0% reflectivity elsewhere. The recovered optical carrier then feeds the uplink optical modulator. However, during this process of optical carrier recovery, useful powers of the two sideband signals are seriously wasted because half of the modulation sidebands are not utilized.

In Figure 4.2 (b), it uses all of the modulation sideband optical powers in the detection of the downlink signal. The downlink signal is launched into an optical circulator and the signal output from port 2 of the circulator is then passed through a custom designed FBG which has 50% reflectivity at the wavelength corresponding to the downlink optical carrier and 0% reflectivity at all other wavelengths. The output of FBG2 which feeds the downlink PD has 3 dB less optical power at the carrier wavelength and nearly the same power in the modulation sideband as compared to the input signal. The reflected carrier (50%) is collected at port 3 of the circulator and passed through another custom designed FBG1 which removes any residual sideband component with downlink data, thereby extracting the downlink optical carrier signal.

The improved interface is also suitable for BSs interconnected to the CO via a wavelength-interleaved DWDM network for both star-tree and bus architectures, in which a wavelength-interleaved DeMux or OADM can be used to filter a channel signal, i.e. a carrier and the two associated sideband signals. The wavelength-interleaved DeMux /OADM will be investigated in Chapter 5.

4.3 Mathematical Description for Millimeter-Wave-Band RoF Signals

Figure 4.1 shows the fundamental configuration of a single light source system. In millimeter-wave-band RoF system, only the optical carrier and two first-order sidebands are of interest.

An optical carrier with the constant power of P_c, carrier frequency of f_c, and phase noise of $\phi_c(t)$ from a single-mode light source is generated from a single-mode light source. The complex electric field of optical carrier $e_c(t)$ is usually expressed by

$$e_c(t) \propto \sqrt{2p_c}\exp\{j\varphi_c(t)\} \tag{4.1}$$

$$\varphi_c(t) = 2\pi f_c t + \phi_c(t) \tag{4.2}$$

An optical modulator (MZM_C) modulates the optical carrier $e_c(t)$ with two RF downlink signal $m_d(t)$ and $m_d'(t)$

$$m_d(t) = V_d.\exp\{j\varphi_d(t)\} \tag{4.3}$$

$$m_d'(t) = V_d'.\exp\{j\varphi_d'(t)\} \tag{4.4}$$

$$\varphi_d(t) = 2\pi f_d t + \theta_d(t) \tag{4.5}$$

$$\varphi_d'(t) = 2\pi f_d' t + \theta_d' \tag{4.6}$$

V_d, f_d and $\theta_d(t)$ are the amplitude, carrier frequency, and pay-load data of the upper-sideband RF downlink signal , respectively. V_d', f_d' and θ_d' are the amplitude, carrier frequency and pay-load data of the low-sideband RF downlink signal, respectively. The complex electric field of the modulated optical signal $e_1(t)$ is, in general, written as

$$e_1(t) = M_c[m_d(t) + m_d'(t)]\cdot e_c(t)$$

$$= \sqrt{2P_c} \sum_{p=-\infty}^{\infty} \sum_{q=-\infty}^{\infty} a_{p.q} \cdot e^{j(\varphi_c(t)+p\varphi_d(t)+q\varphi_d'(t))} \tag{4.7}$$

$M_c[\cdot]$ generally represents the response function of MZM and depends on the modulation scheme. In this case, it is the intensity modulation [29]. $a_{p.q}$ is given as the two-dimensional Fourier coefficient as a function of V_d and V_d'. The complex electric field of OTSSB signal $e_2(t)$ is then expressed as

$$e_2(t) \propto \sqrt{2P_c}[a_{-1,0} \cdot e^{j\{\varphi_c(t)-\varphi_d(t)\}} + a_{0,-1} \cdot e^{j\{\varphi_c(t)-\varphi_d'(t)\}} + a_{0,0} \cdot e^{j\varphi_c(t)}] \tag{4.8}$$

$a_{-1,0}$, $a_{0,-1}$, and $a_{0,0}$ represent the relative amplitudes of upper-sideband, low-sideband of RF signal of downlink, and carrier components, respectively. This is transmitted to a remote BS as an optical downlink signal. After transmitted over a downlink optical fiber with the length of L_d and the propagation constant of $\beta_d(f)$, the optical downlink signal is split by an optical power divider. It is assumed that, for the simplicity, the USB and LSB signals transmit through same distance L_d and have same propagation constant of $\beta_d(f)$ due to that the frequency difference are not too much between them. It is also assumed that the propagation loss of the downlink optical fiber is compensated by optical amplifiers. One part of the optical downlink signal is used to regenerate the RF downlink signal in the BS; the other part is used to transmit RF uplink signals. The complex electric fields of former and later optical signals $e_{2d}(t, L_d)$ and $e_{2u}(t, L_d)$ are then written as

$$\begin{aligned} e_{2d}(t, L_d) &= \sqrt{\alpha_{opd}} \cdot \left(\frac{\pi}{2} - \theta\right) \cdot e_2(t) \cdot \exp\{-j\beta_d(f) \cdot L_d\} \\ &\propto \sqrt{2\alpha_{opd}P_c} \times \left[a_{-1,0} \cdot e^{j\psi_{-1,0}(t,L_d)} + a_{0,-1} \cdot e^{j\psi_{0,-1}(t,L_d)} + a_{0,0} \cdot e^{j\psi_{0,0}(t,L_d)}\right] \end{aligned} \tag{4.9}$$

$$e_{2u}(t, L_d) = \sqrt{(1-\alpha_{opd})} \cdot e_2(t) \cdot \exp\{-j\beta_d(f) \cdot L_d\}$$

$$\propto \sqrt{2(1-\alpha_{opd})P_c} \times \left[a_{-1,0} \cdot e^{j\psi_{-1,0}(t,L_d)} + a_{0,-1} \cdot e^{j\psi_{0,-1}(t,L_d)} + a_{0,0} \cdot e^{j\psi_{0,0}(t,L_d)} \right] \tag{4.10}$$

where $\psi_{p,q}(t,L_d)$ is defined as

$$\psi_{p,q}(t,L_d) \equiv \psi_c(t) + \varphi_c(t) + p\varphi_d(t) + q\varphi_d'(t) - \beta_d(f) \cdot L_d \tag{4.11}$$

Here, α_{opd} is the bifurcation ratio of the optical power divider, the propagation constant $\beta_d(f)$ is approximated as

$$\beta_d(f) \approx \beta_{d0} + \beta_{d1} \cdot 2\pi(f - f_c) + \frac{1}{2}\beta_{d2}\{2\pi(f - f_c)\}^2 \tag{4.12}$$

Here, $\beta_{d1}L_d$ corresponds to the group-delay time, and β_{d2} is related with the dispersion of downlink fiber D_d as

$$\beta_{d2} = -\frac{\lambda^2}{2\pi c} \cdot D_d \tag{4.13}$$

λ and c are the wavelength in the fiber and the velocity in the vacuum, respectively. By using the two photodetectors in the BS, two interest photocurrents are individually generated from the split optical downlink signal $e_{2d}(t,L_d)$

$$i_{c,d}(t,L_d) = \Re_B \alpha_{opd} P_c \cdot a_{0,0} a_{-1,0} \cdot \exp\left\{ j\varphi_{c,d}(t,L_d) \right\} \tag{4.14}$$

$$i'_{c,d}(t,L_d) = \Re_B \alpha_{opd} P_c \cdot a_{0,0} a_{0,-1} \cdot \exp\left\{ j\varphi'_{c,d}(t,L_d) \right\} \tag{4.15}$$

In the above equations, $\Re_B$ is the responsivity of PD in the BS and then $\varphi_{c,d}(t,L_d)$ and $\varphi'_{c,d}(t,L_d)$ are, respectively, given as

$$\begin{aligned} \varphi_{c,d}(t,L_d) &= \psi_{0,0}(t,L_d) - \psi_{-1,0}(t,L_d) \\ &= 2\pi f_d(t - \beta_{d1}L_d) + \theta_d(t - \beta_{d1}L_d) \\ &\quad -\frac{1}{2}\beta_{d2}(2\pi f_d)^2 L_d \end{aligned} \tag{4.16}$$

$$\varphi'_{c,d}(t,L_d) = \psi_{0,0}(t,L_d) - \psi_{0,-1}(t,L_d)$$

$$= 2\pi f_d'(t-\beta_{d1}L_d)+\theta'_d(t-\beta_{d1}L_d)$$

$$-\frac{1}{2}\beta_{d2}(2\pi f_d')^2 L_d \qquad (4.17)$$

We neglect the dispersion effect due to the laser phase noise $\phi_c(t)$, the downlink data $\theta_d(t)$ and θ'_d(t) because they do not seriously influence the system performance in actual fiber-optic access networks with standard SMFs. For example, the linewidth of the laser will be 10 MHz at most, the maximum data rate of the RF signal will be within 300 Mb/s, the total fiber length will be less than 50 of kilometers, and the fiber dispersion will be typically17ps/nm/km. In this case, since the maximum difference of group delay will be 1ps at most, it is trivial when compared with the several hundred megabit-per-second data. Only the desired downlink RF signal $i_{c,d}(t,L_d)$ or/and $i'_{c,d}(t,L_d)$ is then selected by EBPF, and propagated via a millimeter-wave-band antenna to a terminal. Note that in Equations 4.16 and 4.17, the last term is a constant phase, and there is no laser phase noise term. If the payload data of the RF downlink signal $\theta_d(t)$ and θ'_d are differentially encoded and the propagating RF downlink signals $i_{c,d}(t,L_d)$ and $i'_{c,d}(t,L_d)$ are then demodulated by the differential detection, the data for the downlink can be extracted without any serious fiber dispersion effect, as well as no laser phase noise [30], [31].

The other fraction of the optical downlink signal $e_{2u}(t,L_d)$ is used to provide the optical carrier for the uplink as described in Section 4.2, and then the optical carrier is modulated with the RF uplink signals $m_u(t)$ and $m'_u(t)$ by another optical modulator (MZM_B) in the BS. The mathematic descriptions of the uplink signals before the frequency-down-shifter are similar to the ones of the downlink. What we should note is that, after the frequency-down-shifter, downshifted frequency components will be

generated, only several pairs of interested signals are selected to photodetect in order to produce desired IF signals. The frequency-down-shifter is investigated in Chapter 6.

Chapter 5

Novel Optical Components in Millimeter-Wave-Band Radio over Fiber System

5.1 Introduction

Several novel optical components are desired candidates in the implementation of wavelength-interleaved DWDM millimeter-wave-band RoF technology. Among them are wavelength-interleaved multiplexers, wavelength-interleaved demulti-plexers, and wavelength-interleaved add-drop multiplexers. Wavelength-interleaved multiplexers not only simply combine the output of several transmitters, but also interleave the optical carriers and sidebands according to the designed spectrum. Wavelength-interleaved demultiplexers split the received multi-channel signals, i.e. optical carriers and sidebands into individual channel destined to different BSs. Wavelength-interleaved add-drop multiplexers, which can add or drop the desired channel signal at an add or drop port. This chapter focuses on either their scenarios or less-costs in the implementation of our millimeter-wave-band RoF system.

5.1.1 Some Definition

5.1.1.1 Loss

The multiplexer must combine the signals with minimal losses. The losses P_j are expressed in dB at each wavelength λ_j by:

$$P_j = 10 \log\left(\frac{\Phi_j}{\Phi_0}\right) \tag{5.1}$$

where Φ_j is the optical power injected into the transmission line and Φ_0 is the incident power at λ_j.

5.1.1.2 Crosstalk

At the other end of the fiber, the signals at the different wavelengths are separated by a demultiplexer which, like the multiplexer, must have minimal losses. The optical crosstalk D_{ij} of a channel i on a channel j is:

$$D_{ij} = 10 \log\left(\frac{\Phi_{ij}}{\Phi jj}\right) \tag{5.2}$$

where Φ_{ij} is the residual optical power of channel i at wavelength λ_j in channel j and Φjj is the exit optical power in channel j at wavelength λ_j.

The total optical crosstalk in channel j is:

$$D_j = 10 \log\left(\frac{\sum_{i \neq j} \Phi_{ij})}{\Phi jj}\right) \tag{5.3}$$

5.2 Wavelength Interleaved Multiplexer

5.2.1 MZ, Fiber Coupler and FBG Multiplexers

Mach-Zehnder (MZ) devices are based on interference with optical path length difference between both arms. The optical path length difference provides a wavelength-dependent phase shift between the two arms. The path-length difference is chosen such that the total input power from two input ports at different wavelengths appear at only one output port [32]. A Cascaded MZ interferometers is shown in Figure 5.1

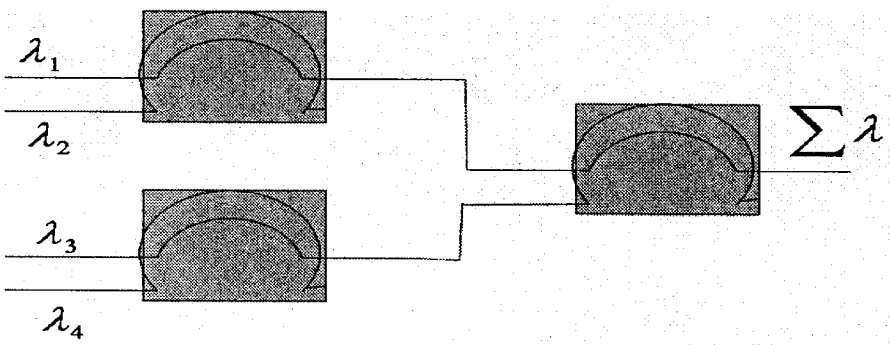

Figure 5.1 Cascaded MZ interferometers.

For simultaneously multiplexing all N channels, the multiplexer would require $(2^N - 1)$ MZ units. Therefore, the device is generally used with few channels only. In millimeter-wave-band RoF system, there is large number of channel signals, so MZ multiplexer is not a suitable candidate to develop towards WI-Mux.

Multiplexer based on the fiber coupler, similar to that shown in Figure 5.1, cannot be used as WI-Mux in millimeter-wave-band RoF system too, since its channel spacing is relatively large ($>10nm$). It is only suitable for coarse WDM applications.

For FBG, most of the power of the light travels in the core with a small part corresponding to the evanescent wave that travels outside the core in the cladding.

This wave is perturbed by the constant index-grating planes perpendicular to the axis. A weak reflection at each grating plane takes place. The contributions of each reflection add constructively in the backward direction for wavelengths defined by the grating period. The principle of FBG is shown in Figure 5.2.

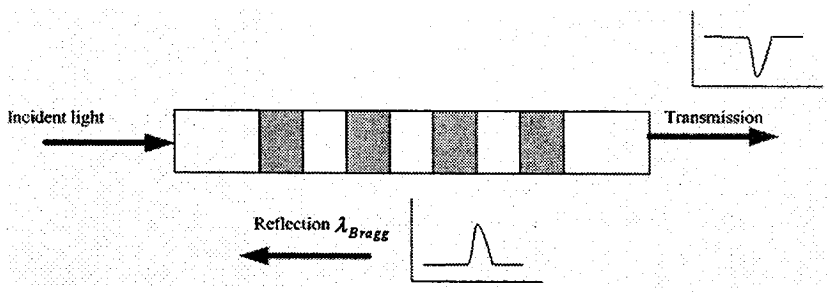

Figure 5.2 Principle of FBG.

The FBG filter cannot be used as a WI-Mux because the number of channels is too high and the wavelengths are too close in our RoF system.

5.2.2 Novel WI-Mux Based on Diffraction Grating

Diffraction grating is preferable to be used in WI-Mux because the main advantage of this grating is the simultaneous diffraction of all wavelengths, so it is possible to construct simple devices with a large number of channels [33], [34]. This grating has the property of diffracting light in a direction related to its wavelength (see Figure 5.3).

A diffraction grating cannot directly work as WI-Mux, since each channel signal consists of an optical carrier and two sidebands in our spectrum design. Therefore,

before the lights enter the diffraction grating, they should be separated by a demultiplexer (see Figure 5.4, as an example, only two channel signals are plotted.)

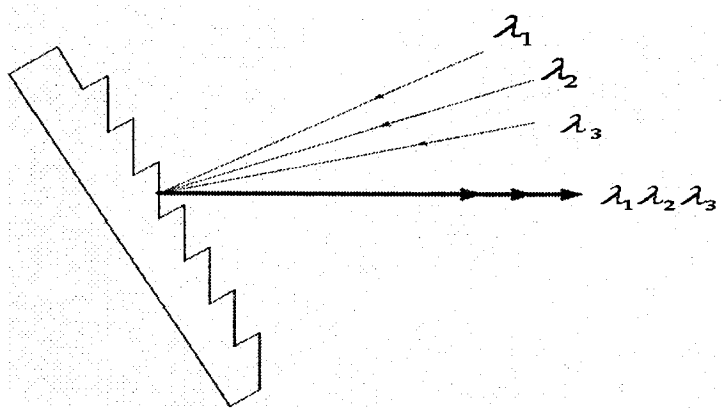

Figure 5.3 Principle of multiplexing by diffraction on an optical grating.

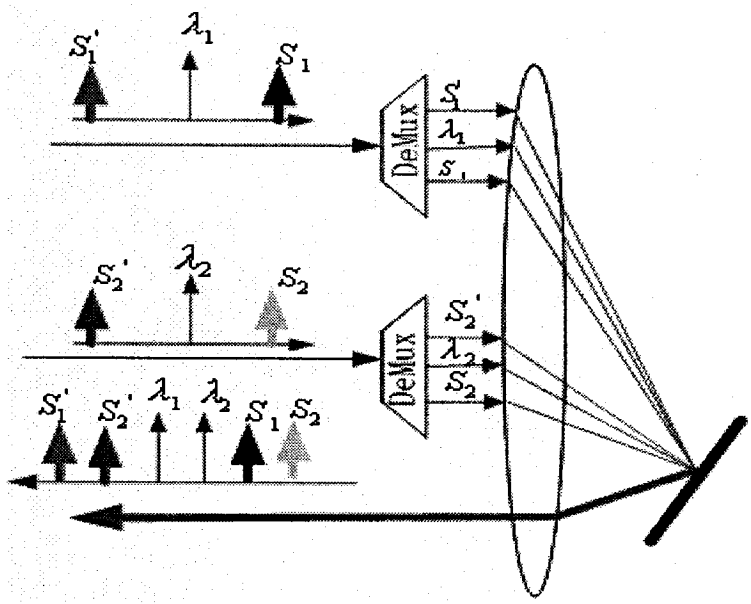

Figure 5.4 Novel WI-Mux based on the diffraction grating.

5.3 Novel Wavelength Interleaved Demultiplexer

5.3.1 WI-DeMux Based on Diffraction Grating

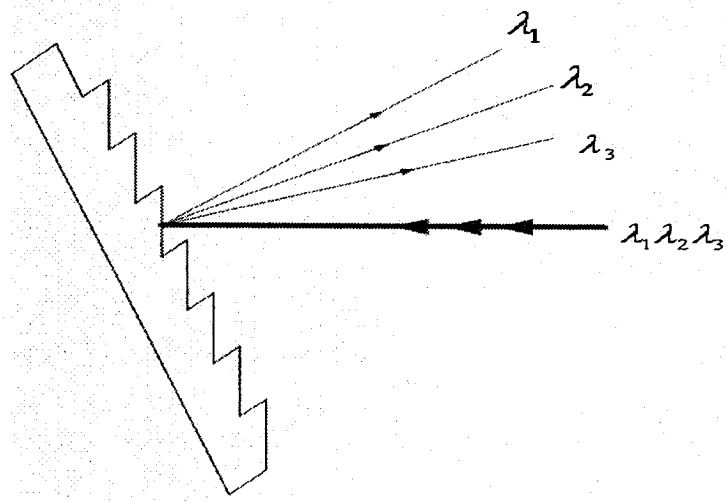

Figure 5.5 Principle of demultiplexing by diffraction on an optical grating.

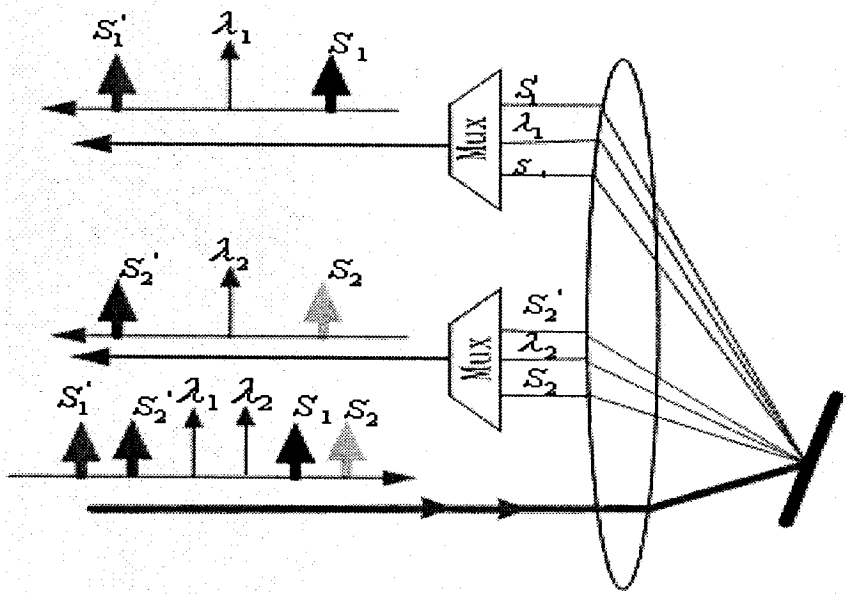

Figure 5.6 Novel WI-DeMux based on the diffraction grating.

For the same reason described in Section 5.2, MZ, fiber coupler and FBG multiplexers are not the suitable candidates for making WI-DeMux in millimeter-wave-band RoF system. For the diffraction grating demultiplexer, an incident beam with several wavelengths is angularly separated in different directions (see Figure 5.5). Using only diffraction grating cannot implement the complete function of WI-DeMux, since individual optical carrier and its associated two modulation sidebands should transmit to the same BS. A conventional multiplexer should work together with the diffraction grating to satisfy the requirement of our spectrum design (see Figure 5.6, as an example, only two channel signals are plotted.)

5.3.2 Possible Configuration of WI-DeMux Based on AWG

The configuration for the WI-DeMux based on AWG is shown in Figure 5.7 (as an example, only two channel signals are plotted; N: total channel number.) [35]. It consists of an OC, a FP etalon and an AWG. The modulated optical signals inputs to OC, all carriers can transmit through FP to input to the AWG while the sideband signals are reflected from FP. The reflected sideband signals from another output port of OC are also input to the AWG. Finally, the AWG combines these two input signals, the output of the AWG consists of individual channel signal, i.e. one carrier and its associated two sidebands. The free spectral range of the FP is adjusted to the channel spacing. The AWG is designed to filter only desired carrier and its associated two sideband signals [35].

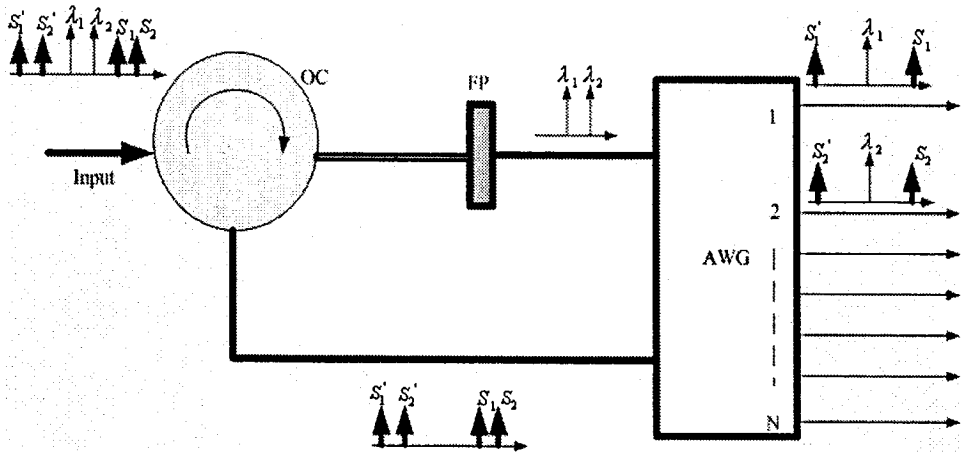

Figure 5.7 Possible configuration of WI-DeMux based on AWG. (After Ref. [35])

5.4 Wavelength Interleaved Add-Drop Multiplexer

Add-drop multiplexers are needed for wide-area and metro-area networks in which one or more channels need to be dropped or added while preserving the integrity of other channel. Such devices avoid the need for demultiplexing all channels. If only a small portion is filtered out, such a device acts as an "optical tap" as it leaves the contents of the DWDM signal intact. The wavelength interleaved add-drop multiplexer in our system employs the use of multiple fiber Bragg gratings (FBGs) in cascades in order to filter out the desired carrier wavelengths and their associated modulation sidebands. Therefore, using this WI-OADM incorporating OTSSB modulation helps to improve the spectral efficiency in addition to having the added advantage of reducing fiber chromatic dispersion effects [36]-[38]. The transmission-amplitude response of the proposed novel WI-OADM is shown in Figure 5.8(b). This WI-OADM reflection profile indicates that it selects a desired channel carrier and its two associated sidebands, for example, λ_1, S_1 and $S_1^{'}$.

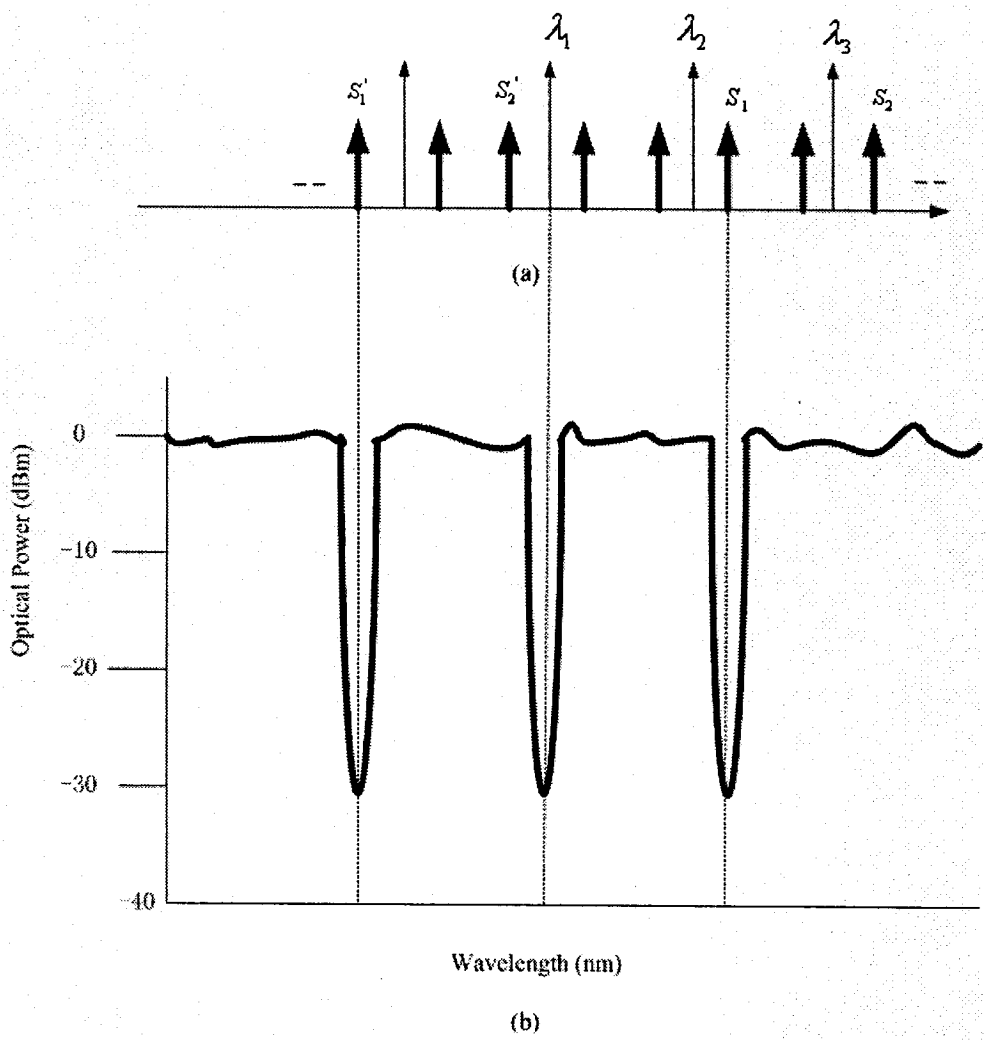

Figure 5.8 (a) The spectrum of WI-interleaved DWDM channel. (b) The transmission response of FBG with three notches corresponding to (λ_1) and its two sideband signals (S_1, S_1').

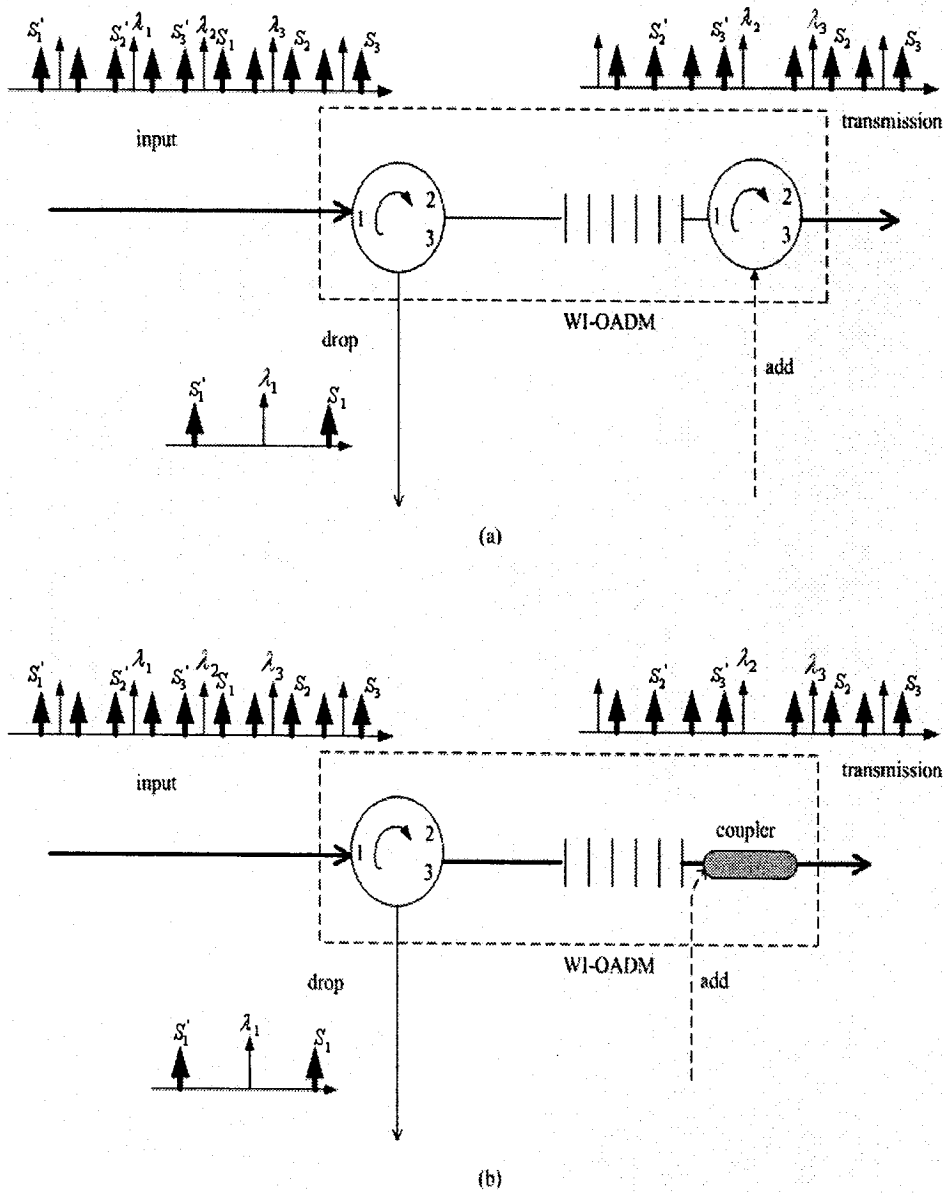

Figure 5.9 (a) The configuration of WI-Add-drop multiplexers using an OC at the add- port. (b) The configuration of WI-Add-drop multiplexers using a optical coupler at the add-port.

A 3-dB bandwidth of < 0.04 nm for each notch was required in order to minimize crosstalk from adjacent channels, as well as high reflectivity to reduce unwanted transmission of the reflected carrier and sideband [39], [40]. The transmission band between the three reflection notches also required a 3-dB bandwidth with a flat top to

avoid unwanted reflections. The transmission profiles are about 30dB lower at wavelength λ_1, S_1 and $S_1^{'}$. The configuration of WI-Add-drop multiplexer is shown in Figure 9(a). Based on Figure 9(a), an improved WI-Add-drop multiplexer is shown in Figure 9(b), in which an optical coupler is used instead of an OC at the add-port for the purpose of low-cost.

Chapter 6

Optical Heterodyne Detection

6.1 Introduction

Coherent detection is composed of homodyne and heterodyne detection techniques. With coherent detection, the receiver sensitivity can be increased up to 20dB compared with that of IM/DD system and it allows a more efficient utilization of the bandwidth provided by the optical fiber. Figure 6.1 illustrates the principle of a coherent detection scheme [41].

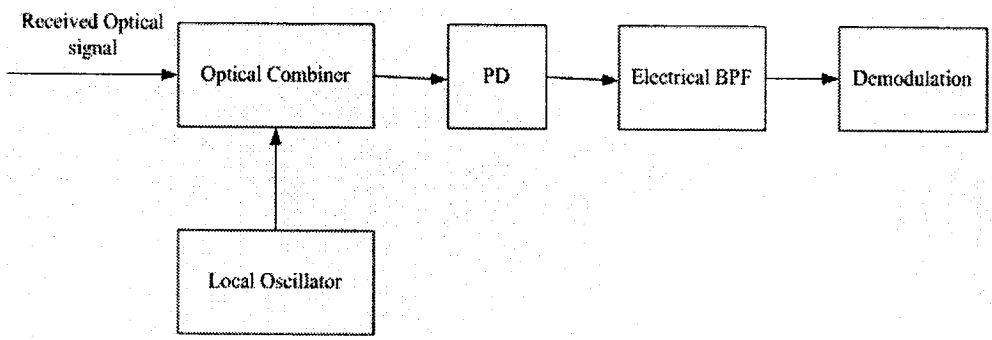

Figure 6.1 The illustration of the principle of a coherent detection scheme.

A received optical signal in Figure 6.1 can be written as [41]

$$E_S = A_S \exp[-i(\omega_0 t) + \phi_s] \qquad (6.1)$$

where ω_0 is the optical carrier frequency, A_S is the amplitude, and ϕ_s is the phase. The local oscillator signal is expressed as

$$E_{LO} = A_{LO} \exp[-i(\omega_{LO}t + \phi_{LO})] \tag{6.2}$$

where A_{LO}, ω_{LO}, and ϕ_{LO} is the amplitude, frequency, phase of the local oscillator, respectively. Assume the polarizations of Es and E_{LO} are matched, then the combined optical power input PD is given

$$P = K\left|E_s + E_{LO}\right|^2 = P_s + P_{LO} + 2\sqrt{P_s P_{LO}}\cos(\omega_{IFT} + \phi_S - \phi_{LO}) \tag{6.3}$$

where K is a constant of proportionality, and

$$P_S = KA_S^2, \quad P_{LO} = KA_{LO}^2, \quad \omega_{IF} = \omega_0 - \omega_{LO} \tag{6.4}$$

if ω_{IF} does not equal zero, it is known as heterodyne detection technique. Consider that $P_{LO} >> P_S$, $I = RP$, and electrical BPF can remove direct-current term, the heterodyne current is now given by the alternating-current (ac) term

$$I_{ac}(t) = 2R\sqrt{P_s P_{LO}}\cos(\omega_{IF}t + \phi_s - \phi_{LO}) \tag{6.5}$$

It can be known from the equation (6.5), the local oscillator amplifies the received signal by a large factor, thereby improving the SNR. Another advantage is that an OPPL is no longer necessary for the frequency stabilization of the local light at receiver [42].

6.2 A Novel Technique in Heterodyne Detection

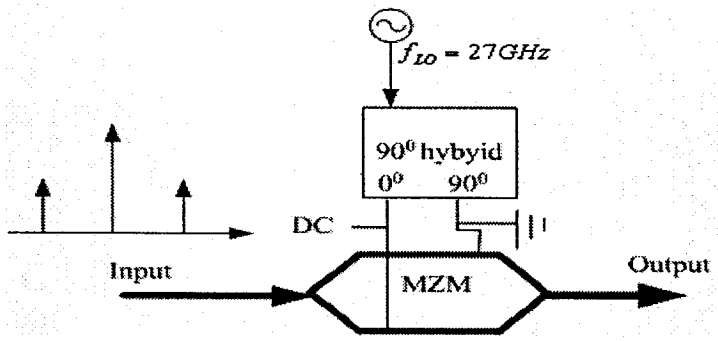

(a)

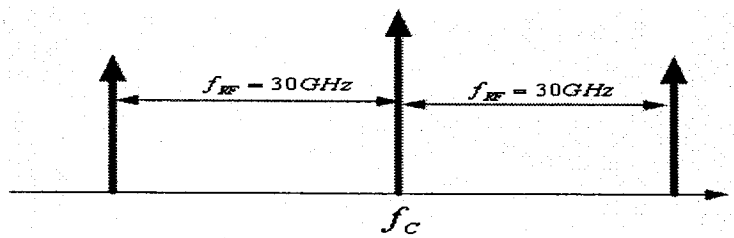

(b)

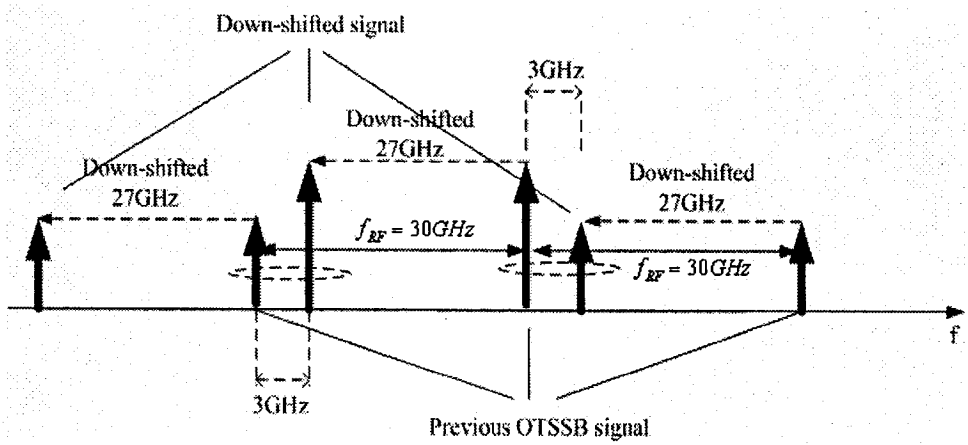

(c)

Figure 6.2 (a) Block diagram of the simulation setup for frequency-down-shifter.

(b) Spectrum at the input of MZM. (c) Spectrum at the output of MZM.

OTSSB signals cannot be directly detected by a photodetector since the two sidebands would interfere in the microwave domain. Using two coarse optical filters to distinguish between the sidebands can be used in the downlink, where the terminal frequency interval is 30GHz and there is enough spacing to accommodate a large guardband between the sidebands and optical carrier [43]. However, it is impossible to achieve an enough guardband in the uplink, since the terminal frequency interval here is 3GHz. In this section, a novel heterodyne detection technique is proposed to enable the reception of OTSSB signals in the uplink.

MZM can also act as a frequency-down-shifter, which is our preferable technique to be used in the uplink of the millimeter-wave-band RoF system [see Figure 6.2 (a)]. At the receiver, the OTSSB signal is coupled to a quadrature biased MZM. Only one input-port of the hybrid is used and the MZM works as a frequency-down-shifter which down-shifts the incoming optical spectrum by f_{LO}, while suppressing the up-shifted version. In this case, the electrical sinusoidal waveform frequency f_{LO} is set to 27GHz.

The optical spectrum at this stage would then consist of the original spectrum centered at f_cGHz, a LSB at ($f_c - 30$ GHz), and an USB) at (f_c+30GHz) and a copy of it centered at ($f_c - 27GHz$) GHz, LSB at $[(f_c - 30) - 27]GHz$, USB at $[(f_c + 30) - 27]GHz$. When these signal are incident on a photodetector, the optical carrier at f_cGHz and the down-shifted version of the optical carrier at ($f_c - 27GHz$), both serve as LOs and beat with the original, as well as with the down-shifted sidebands. Since there are two LOs and four sidebands (two original and two up-shifted), we would expect a total of $2 \times 4 = 8$ major terms from the heterodyning. Table 6.1 shows a list of the eight heterodyne terms expected. In Table 6.1, the term 3 and 5 are desirable for the uplink.

Term	LO frequency	Sideband frequency	LSB/USB	Frequency (after beating)
1	f_c	f_c+30	USB	30
2	f_c	f_c-30	LSB	30
3	f_c	(f_c+30)-27	USB	3
4	f_c	(f_c-30)-27	LSB	57
5	f_c-27	f_c+30	USB	3
6	f_c-27	f_c-30	LSB	57
7	f_c-27	(f_c+30)-27	USB	30
8	f_c-27	(f_c-30)-27	LSB	30

Table 6.1 Heterodyning terms present after PD. (the frequency unit in this figure is GHz).

Note that the input signal is equally power-split into two parts after the frequency-down-shifting, one half for previous version, and another half for frequency-down-shifted version. However, generated power in each of the two parts after the MZM is larger than the half of the original input signal power due to the heterodyning detection.

6.3 Mathematic Description for Frequency-Down-Shifting Technique

Let us assume that the transmitted or received signal has a central frequency of f_c and is modulated by two RF signal (f_{RF}) in tandem format, as shown in Figure 6.2(b). The normalized signal after L-long fiber-optic transmission is

$$e_A(t,L) = ae^{j\varphi_{s,-1}(t,L)} + e^{j\varphi_{s,0}(t,L)} + ae^{j\varphi_{s,1}(t,L)} \tag{6.6}$$

$$\begin{aligned}\varphi_{s,n}(t,L) &= 2\pi(f_c + nf_{RF})(t-\beta_1 L) \\ &+n\theta(t-\beta_1 L - 2\pi\beta_2 nf_{RF}L) \\ &+\phi_C(t-\beta_1 L - 2\pi\beta_2 nf_{RF}L) \\ &-\beta_2(2\pi\beta_2 nf_{RF})^2 L/2 \\ &+(2\pi f_c\beta_1 - \beta_0)L\end{aligned} \tag{6.7}$$

In Equation 6.6, the first, second and the third term individually represents the complex electric field of LSB, carrier, USB. If intensity modulation is performed and the modulation index m is small, $a \approx \sqrt{2}(m/4)/\{1-(m/4)^2\}$ [44]. To carry out frequency-down-shifting, the signal is split into two equal components; the generated frequencies components are previous version and frequency-down-shifted version, as shown in Figure 6.2(c). The result is expressed as

$$e_B(t,L) = \frac{e^{-j2\pi f_{LO}t}+1}{\sqrt{2}} \cdot e_A(t,L) \tag{6.8}$$

Then, only two pairs of components are filtered out for photo-detection. The spectrum after frequency-down-shifting is shown in Figure 6.3 (it is the same one as Figure 6.2 (c) except for some marks).

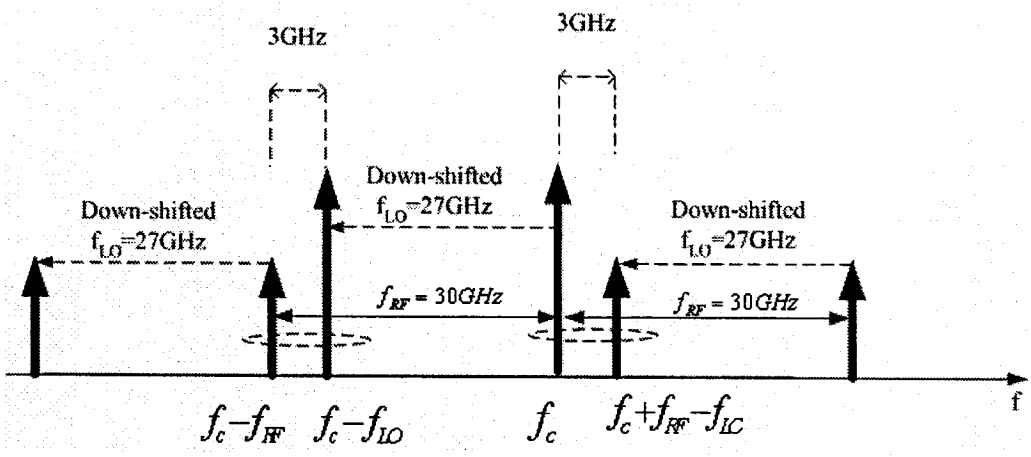

Figure 6.3 The spectrum after frequency-down-shifting.

One pair of interested components is at $f_c - f_{RF}$ and $f_c - f_{LO}$, its frequency difference is 3GHz. This pair can be expressed as

$$e_C(t,L) = a \cdot e^{j\varphi_{s,-1}(t,L)} / \sqrt{2}$$
$$+e^{j\{\varphi_{s,0}(t,L)-2\pi f_{LO}t\}} / \sqrt{2} \qquad (6.9)$$

Another pair of interested components is at f_c and $f_c + f_{RF} - f_{LO}$, the frequency difference is 3GHz too. This pair can be expressed as

$$e_C^{'}(t,L) = e^{j\varphi_{s,0}(t,L)} / \sqrt{2}$$
$$+a \cdot e^{j\{\varphi_{s,1}(t,L)-2\pi f_{LO}t\}} / \sqrt{2} \qquad (6.10)$$

A normalized IF signal generated after the photodetection is expressed as $e^{j\varphi_{IF}(t)}$, where

$$\varphi_{IF}(t) = 2\pi f_{IF}(t-\beta_1 L) + n\theta(t-\beta_1 L - 2\pi\beta_2 n f_{RF} L)$$
$$-2\pi f_{LO}\beta_1 L - \beta_2(2\pi n f_{RF})^2 \cdot L/2 \qquad (6.11)$$

From the above equation, no laser phase noise affects the detected signal. The last two phase components are constant. Because the optical filter extracts only two

optical components for the photodetection, the IF signal is not seriously affected by the fiber-dispersion effect when the data is differentially encoded [45], [46].

6.4 Extracting the IF Signals for WI-DWDM

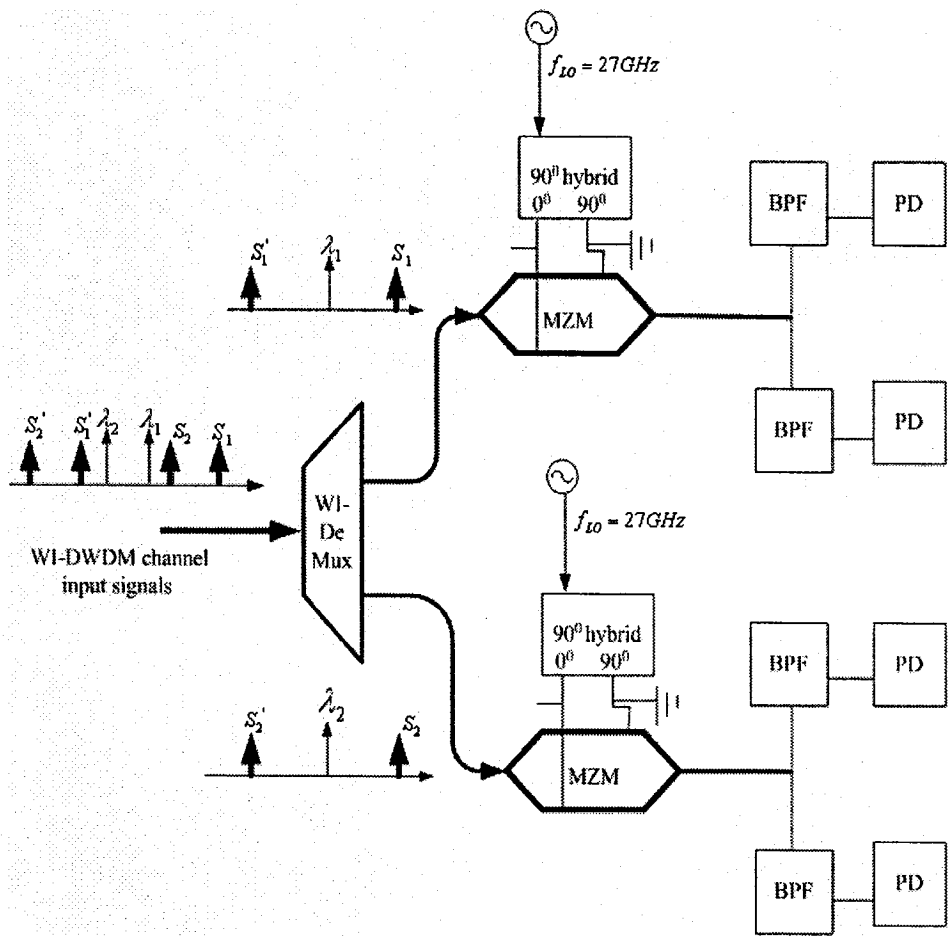

Figure 6.4 Block diagram of the simulation setup for the two-channel wavelength-interleaved OTSSB/SCM/DWDM receiver.

In our RoF system, we should recover each channel signal by WI-DeMux (or WI-OADM) before putting it into the frequency-down-shifter. Figure 6.4 shows the

block diagram of the simulation setup for the two-channel wavelength-interleaved OTSSB/SCM/DWDM receiver. After frequency-down-shifting, only interested signal pair related to generate the desired IF component is filtered out for photodetection. Finally, desired IF signal is generated after photodetection, i.e. S_1, S_1', S_2 and S_2' are individually extracted at 3GHz. If data recovery is required after the photodetection, IF-band demodulator is needed in the receiver.

Chapter 7

Simulation Demonstration and Result Discussion

7.1 Overall Description

To confirm the validity of the principle underlying our design, we performed the simulations with three channel signals transmission over a 50-km-long standard SMF for both downlink and uplink. The three channel signals consisted of three 25GHz spaced DWDM optical carriers; each individually modulated by two 30GHz subcarri - ers with 155Mb/s DPSK data. In addition, we have also successfully simulated IF subcarrier transmission over fiber for downlink and a single frequency-down-shifter serving the all uplink receiver. The distinctive features of our proposed system are as follows:

1) A single light source configuration for full-duplex system: there is no local light or RF sources in BSs;
2) Robustness regarding the chromatic fiber-dispersion effect: Since only two components (a carrier and one of the first-order sideband components) in a certain channel are used for the detection. This refers to the same effect as detecting an optical SSB signal with the carrier, resulting in fiber-dispersion tolerance [47]-[49];
3) No OPLLs: Our technique does not need OPLLs for the purpose of frequency stabilization of the local light because of the OTSSB modulation or/and the heterodyne detection technique;

4) Maximizing spectral utilization: Our design integrate the four spectrum techniques, i.e. optical wavelength-interleaving, OTSSB, SCM and DWDM into one RoF system;

5) No optical narrow BPF: In the uplink, the frequency-downshifting technique mean that an optical BPF with a narrow bandwidth is not needed to select a desired signal;

6) IF-band signal processing: In the uplink, the frequency conversion of heterodyning enables signal processing in an intermediate-frequency band (such as microwave or a lower frequency band) rather than in an RF band (such as millimeter-wave or a higher frequency band).This will help to reduce the need for expensive RF components;

7) High receiver sensitivity: In the uplink, the receiver sensitivity in optical heterodyne detection systems is expected to be higher than that in optical direct detection systems because it is hard in practice to achieve an ideal noise figure of 3 dB in optical amplifiers [50], [51]. The high receiver sensitivity means that optical amplifiers can be eliminated or their number can be reduced. This contributes to the high system performance.

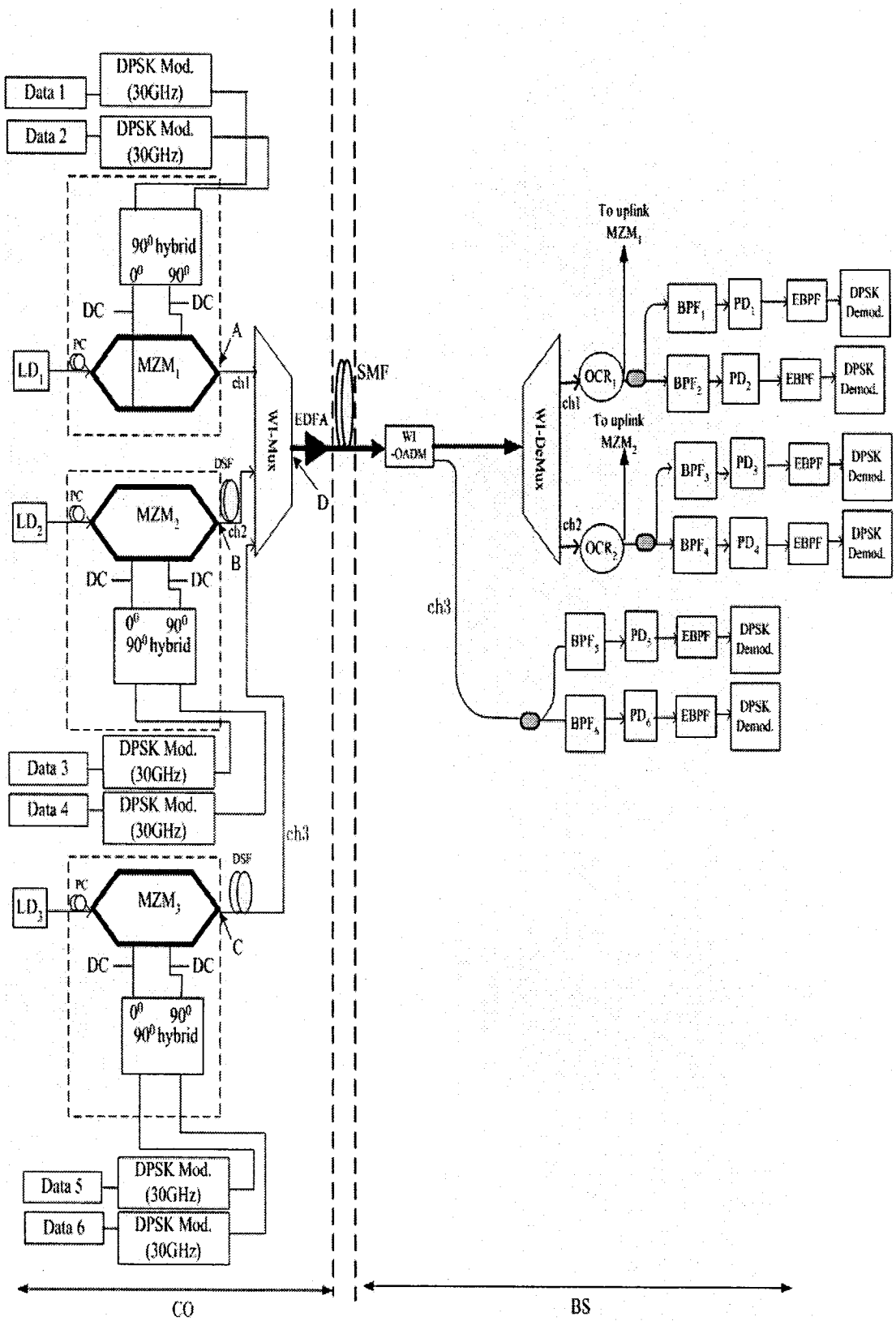

Figure 7.1 Simulation setup of millimeter-wave-band RF over fiber for the downlink.

7.2 RF over Fiber in Downlink

The block diagram of simulation setup for downlink is shown Figure 7.1. Parameters used in the simulation are summarized in Table 7. 1.

Parameter	Frequency or bandwidth
$f_{c1}(\lambda_1)$	193. 4144THz (1550nm)
$f_{c2}(\lambda_2)$	193. 4394THz (1549. 8nm)
$f_{c3}(\lambda_3)$	193. 4644THz (1549. 6nm)
$f_G(\lambda - grid)$	25 GHz
f_{RF} (RF carrier)	30 GHz
R (bit rate)	155Mb/s
B (RF bandwidth)	310MHz
$\Delta\nu$ (line-width)	10MHz

Table 7. 1 Parameters used in the simulation

In this simulation, three 25GHz separated optical carriers and OTSSB signals multiplexed by WI-Mux were used. Six uplink data with a rate of 155Mb/s were generated by six data-source generators with PRBS of $2^{23}-1$, respectively. These downlink data were directly modulated to RF at the frequency of 30GHz via DPSK RF modulators. Three optical carriers from independent signal mode CW light sources with center emission frequencies of $f_{c1}(=\frac{c}{\lambda_{c1}}, \lambda_{c1}=1550nm)$, $f_{c2}(=\frac{c}{\lambda_{c2}},$

$\lambda_{c2} = 1549.8nm$) and $f_{c3}(=\frac{c}{\lambda_{c3}}, \lambda_{c3} = 1549.6nm)$ were individually intensity modulated by means of 30-GHz-band Dual-electrode $LiNbO_3$ Mach-Zehnder Modulators with two different data. Each optical carrier was polarization-controlled to match the polarization axis of the MZM. The power of the RF signal applied to each arm of MZM was -3dBm. The 90^0 coupler used in the simulation generated a phase difference of 90^0 between two drive electrodes. Each MZM had a dc 2.5V on both electrodes, the $V\pi$ was 5V. In such a configuration, three groups of OTSSB signals, i.e. three channel signals were generated [see Figure 7.2 (a), (b) and (c)]. A 100m long DCF connected channel 2 and a 200m long DCF connected channel 3 before the WI-Mux were employed to decrease the correlation among the three channel signals. The three channel signals, centered at 1550nm, 1549.8nm and 1549.6nm respectively, were multiplexed by a WI-Mux, resulting in the optical wavelength-interleaved TSSB/SCM/DWDM RoF signals (see Figure 7.3). These multiplexed signals were amplified by an EDFA and then transmitted over a 50km-long SMF to remote BSs.

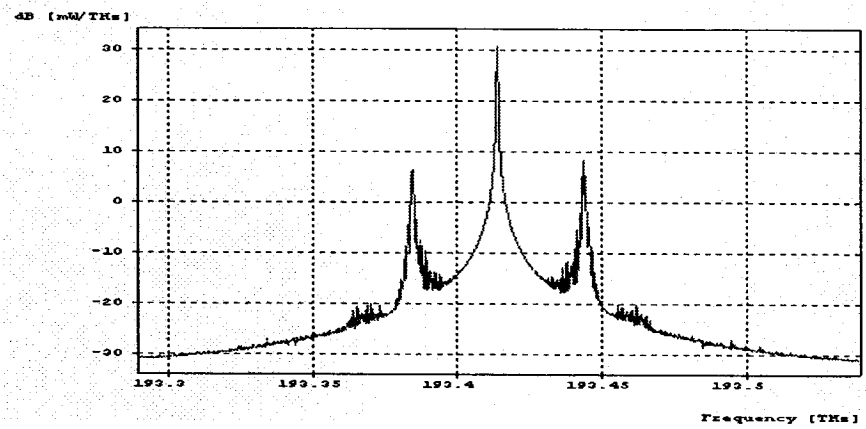

(a)

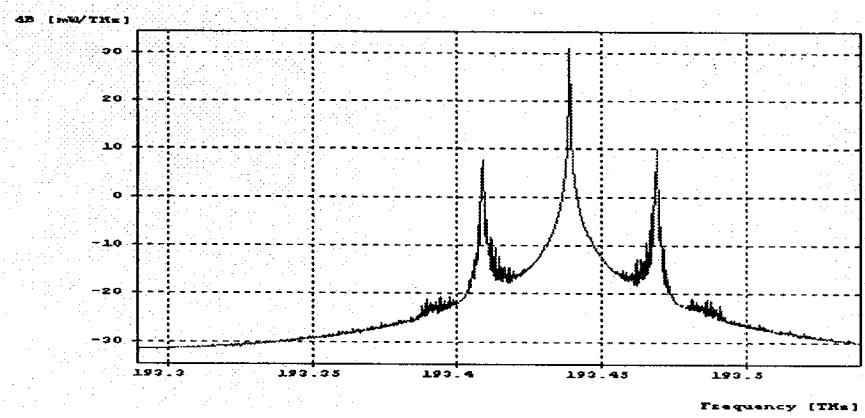

(b)

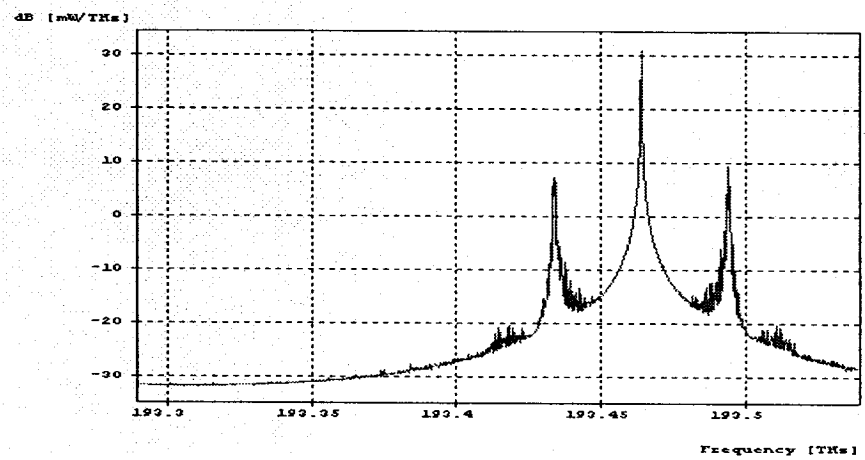

(c)

Figure 7.2 The simulated spectra of OTSSB signals, (a), (b) and (c) were measure at A, B, and C in Figure 7.1, respectively.

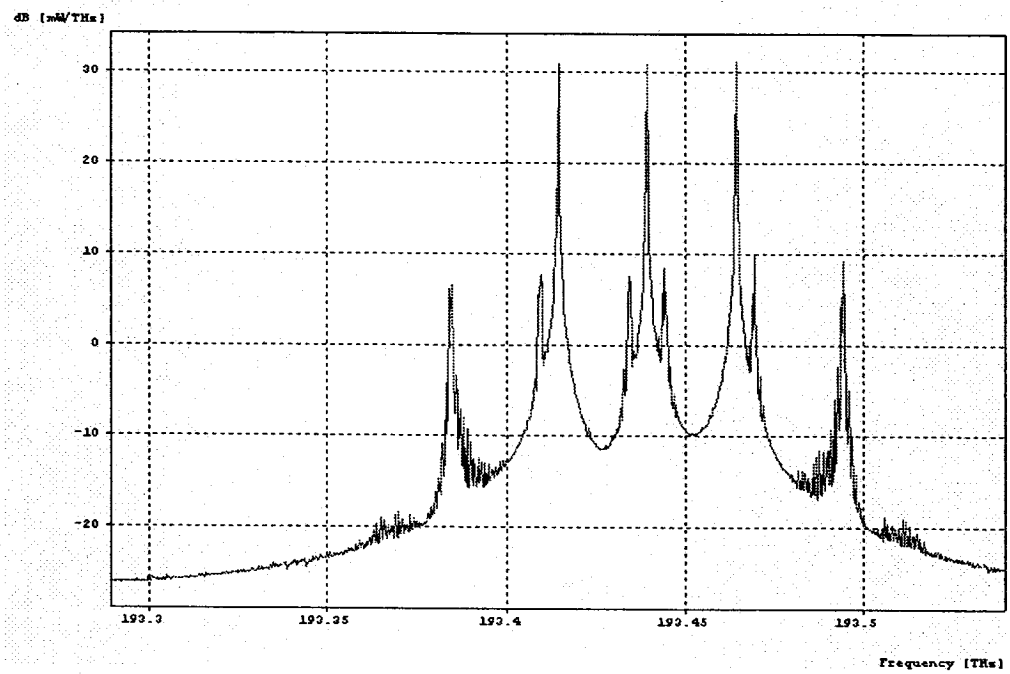

Figure 7.3 The simulated spectra of frequency- interleaved TSSB/SCM/DWDM RoF signal, measured at the D in Figure 7.1

7.2.1 Simulation Demonstration in the WI-OADM Branch

The interleaved optical signals were firstly passed through the WI-OADM. We designed that the optical carrier at λ_{c3} and its corresponding two sidebands were reflected from the WI-OADM and dropped at WI-OADM output port. The simulated optical spectrum at the drop port is shown in Fig. 7.4(a). A following coupler split the dropped signals into two parts. The BPF_5 filtered out the carrier and up-sideband signals. The simulated optical spectrum of the filtered out signals is shown in Figure7.4 (b). Then the carrier and up-sideband signals were photodetected to regenerate Data 5 at 30GHz by the high-speed PD_5 with responsivity of 0.875, quantum efficiency of 0.7 and dark current 1nA. Note that other PDs used in our simulations had the same characteristics as PD_5. The following Butterworth filter

with a 3-dB bandwidth of 310 MHz was used to eliminate the undesired components from other channels. The simulated electrical spectrum before and after the Butterworth filter is shown in Figure7.5 (a) and 7.5(b), respectively. Finally, the Data 5 was demodulated by a DPSK demodulator at 30GHz. The BER, Q and eye diagram were simulated by an error detector, a Q estimator and an electrical scope, respectively. Figure 7.6 (a) shows the simulated BER versus the received optical power before PD_5. Figure 7.6 (b) shows the simulated Q versus the received optical power before PD_5. Figure 7.6 (c) shows the eye diagram simulated at the back-to-back. In another branch after the optical coupler, following the same process above, the Data 6 in channel 3 was successfully extracted at 30GHz. Figure 7.6 (a) also shows the simulated BER versus the received optical power before PD_6. Figure 7.6 (b) shows the simulated Q versus the received optical power before PD_6.

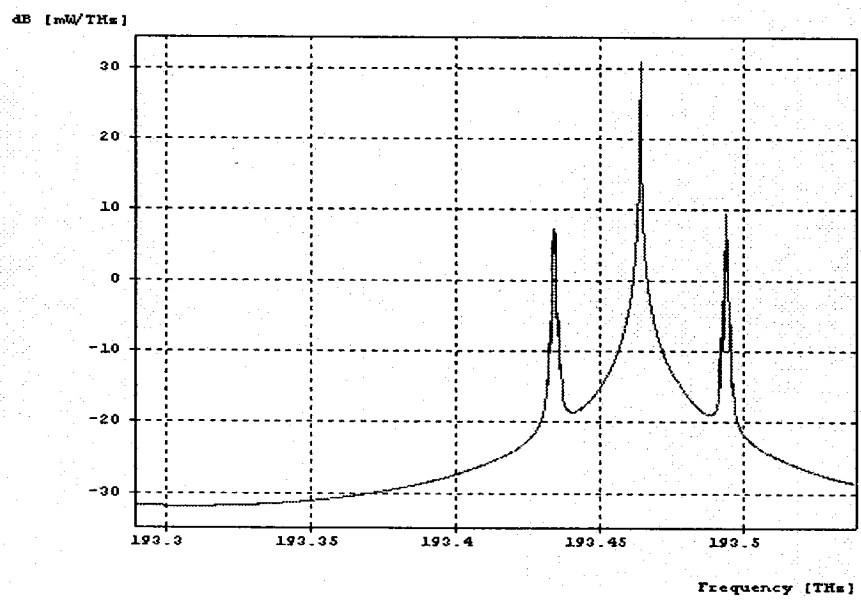

(a)

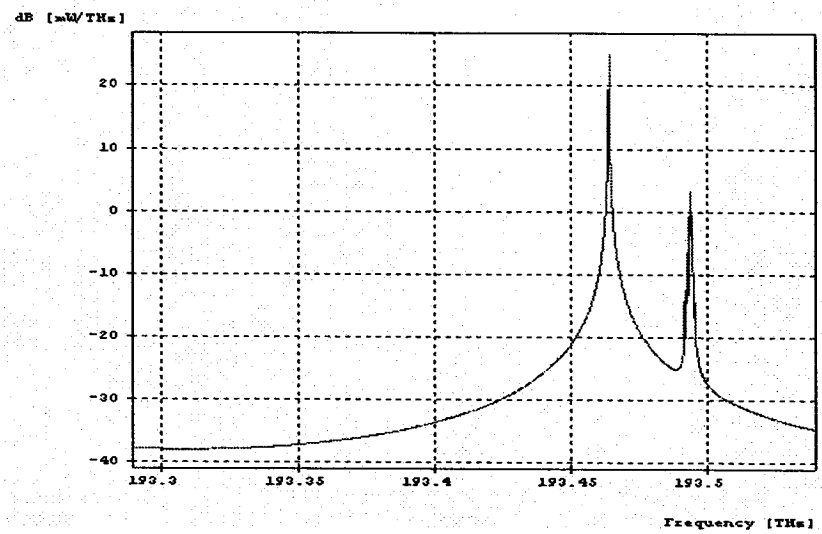

(b)

Figure 7.4 (a) The simulated optical spectrum of the dropped signals (channel 3);

(b) The simulated optical spectrum of the filtered out signals by BPF_5.

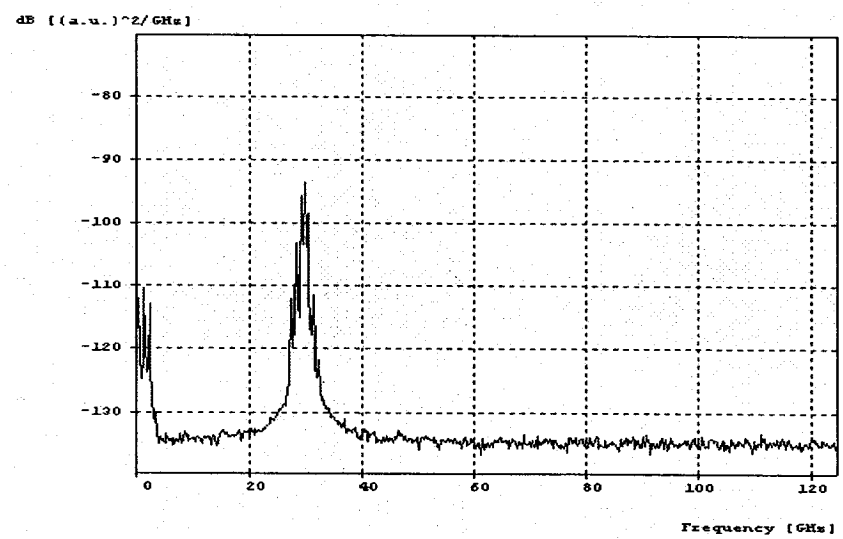

(a)

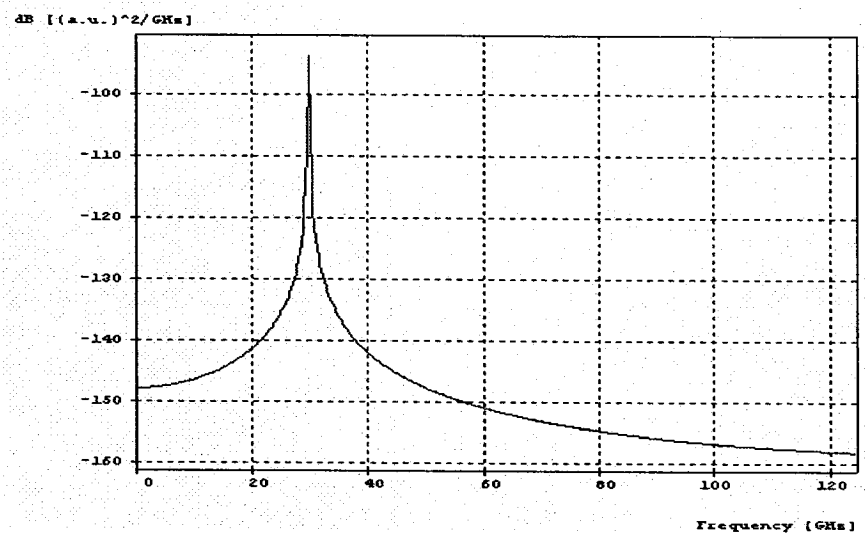

(b)

Figure 7.5 (a) The simulated electrical spectrum of the one of regenerated downlink signals at 30GHz. (b) The simulated electrical spectrum after the Butterworth filter.

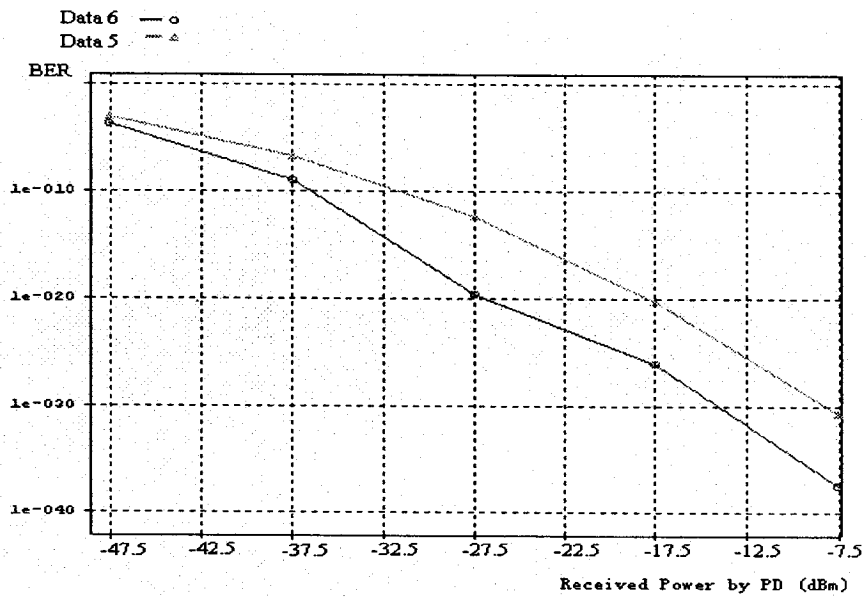

(a)

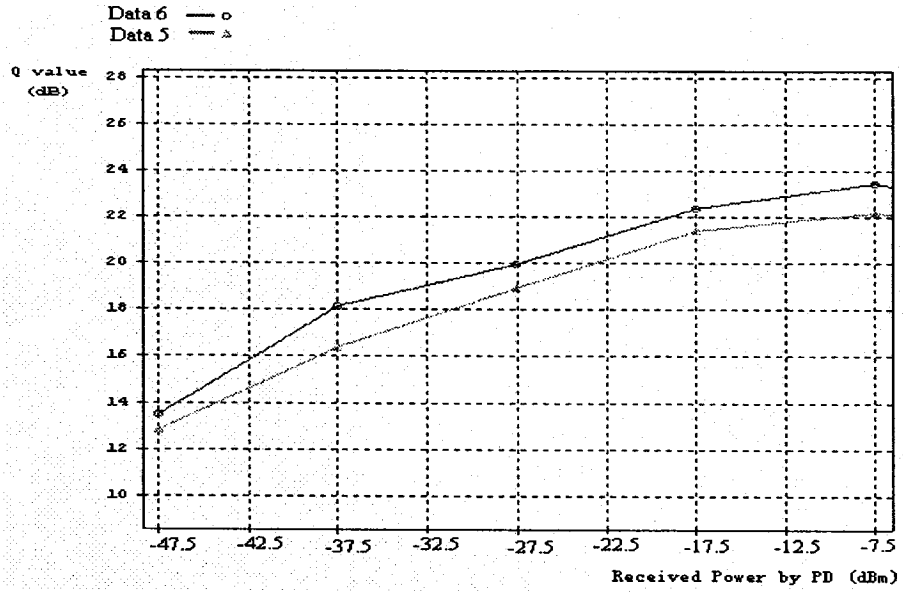

(b)

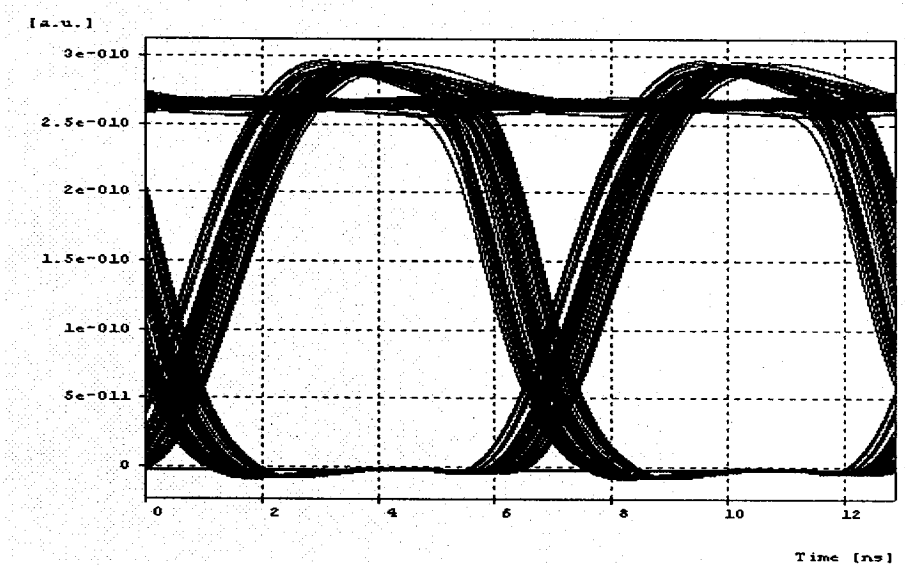

(c)

Figure 7.6 (a) BER versus received optical power by PD. (b) Q versus received optical power by PD. (c) Eye diagram of Data 5 in channel 3 simulated at the back-to-back.

7.2.2 Simulation Demonstration in the WI-DeMux Branch

As described in Section 7.2.1, λ_3 and its corresponding two sideband signals were reflected from the WI-OADM. The remainder of the input signals were then transmitted to the PDs for detection in BSs. They consisted of λ_1, λ_2 and their corresponding sideband signals (see Figure7.7). The following WI-DeMux demultiplexed the input signals into two channel signals. Here the signals in channel 1 were consisted of λ_1 and its corresponding two sideband signals; the signals in channel 2 were consisted of λ_2 and its corresponding two sideband signals. Then, the ORC in each channel split the channel signal power into two parts, one part for detection in BSs, and another part for providing optical carrier to the uplink. The spectra of recovered two channel signals are shown in Figure7.8. The following process of how to extract the data1 and data2 in channel 2 or extract the data3 and data4 in channel 2 at 30GHz is the same as the corresponding process described in Section 7.2.1. Their performances are shown in Figure7.9.

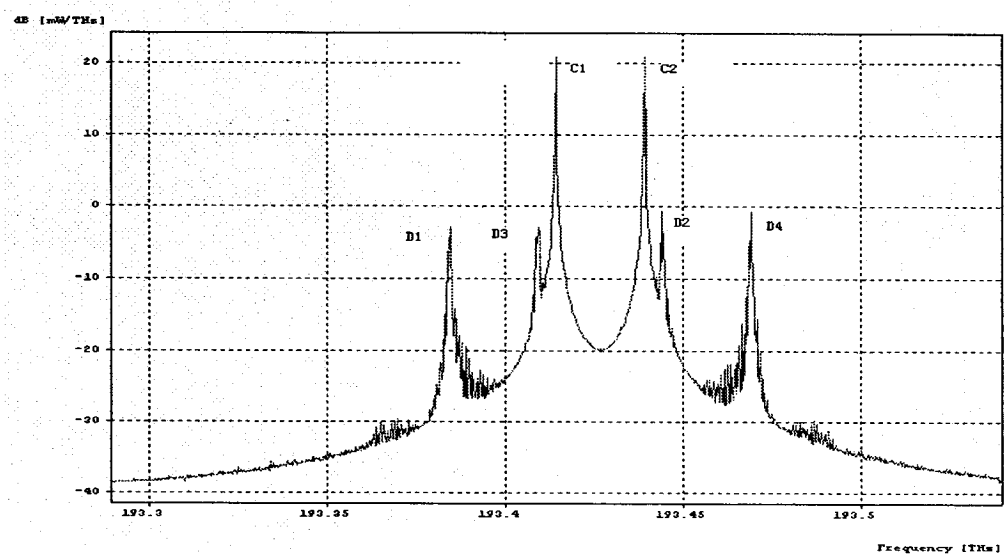

Figure 7.7 The simulated optical spectrum of the downlink signals after the WI-OADM.

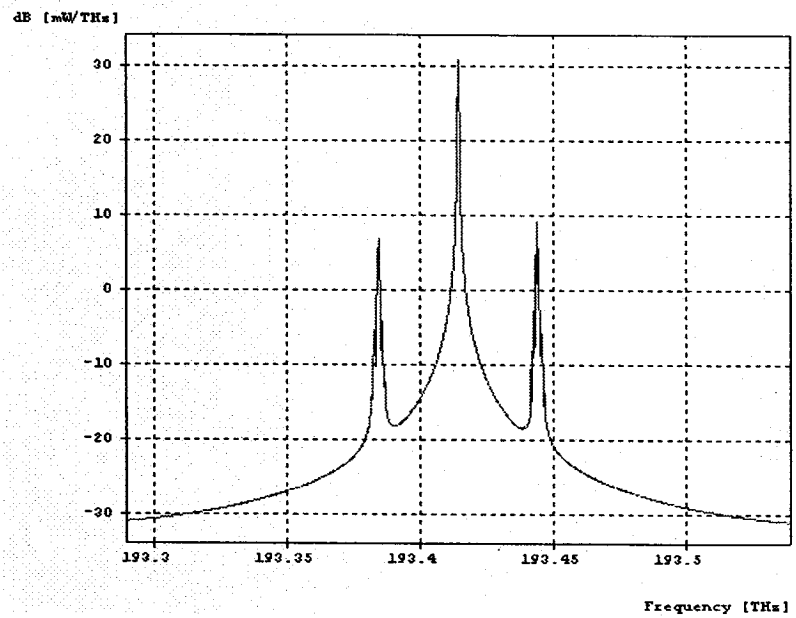

(a)

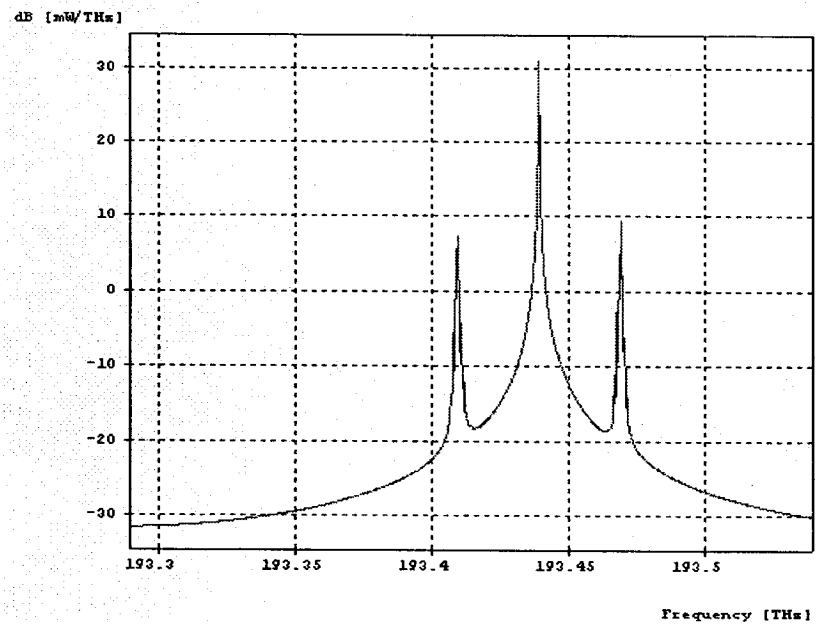

(b)

Figure 7.8 (a) The spectrum of recovered signals from channel 1.

(b) The spectrum of recovered signals from channel 2.

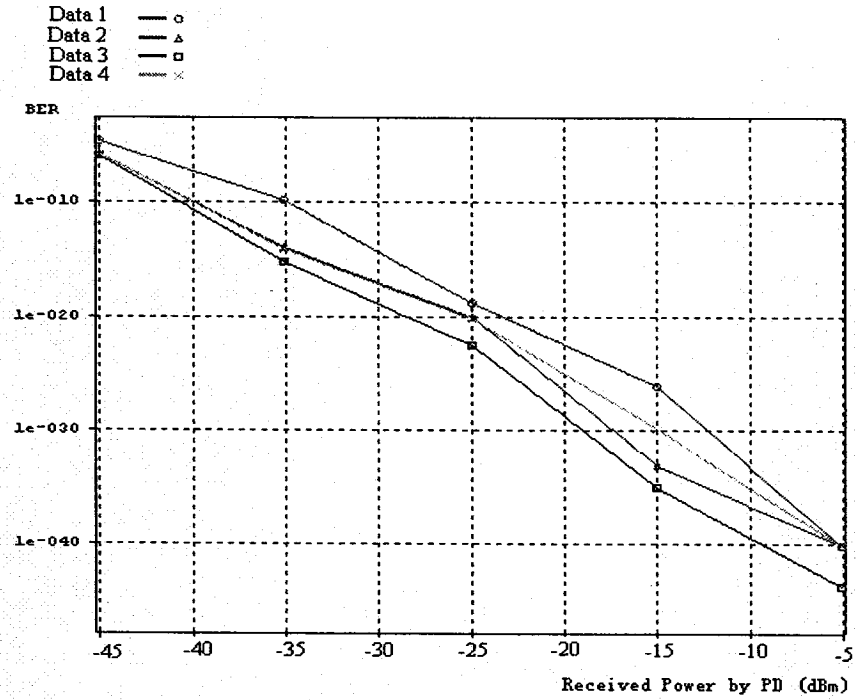
Data 1
Data 2
Data 3
Data 4
BER
1e-010
1e-020
1e-030
1e-040
-45
-40
-35
-30
-25
-20
-15
-10
-5
Received Power by PD (dBm)

(a)

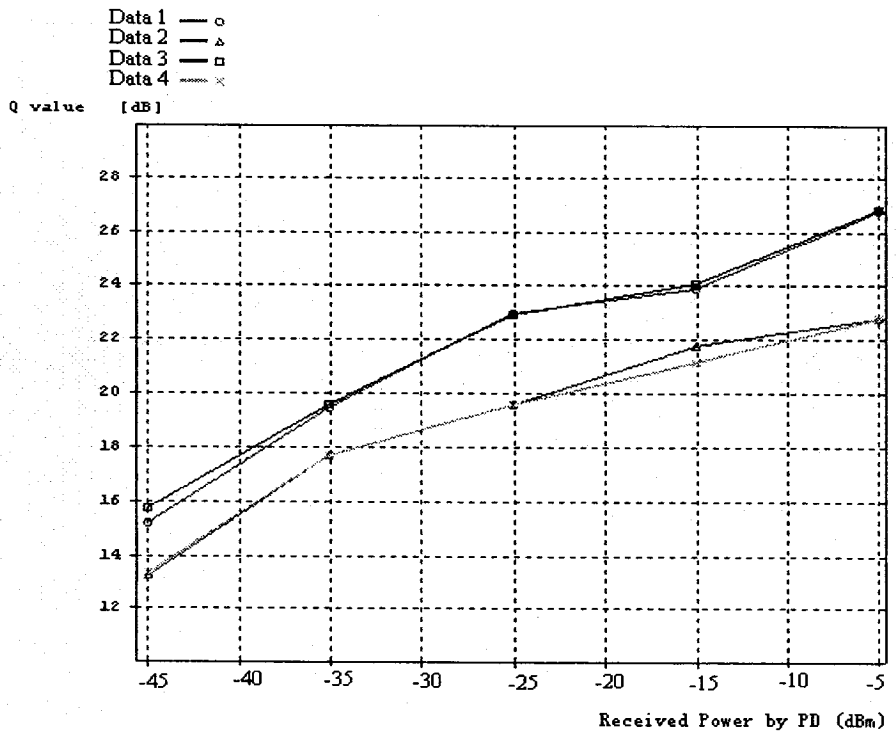
Data 1
Data 2
Data 3
Data 4
Q value [dB]
28
26
24
22
20
18
16
14
12
-45
-40
-35
-30
-25
-20
-15
-10
-5
Received Power by PD (dBm)

(b)

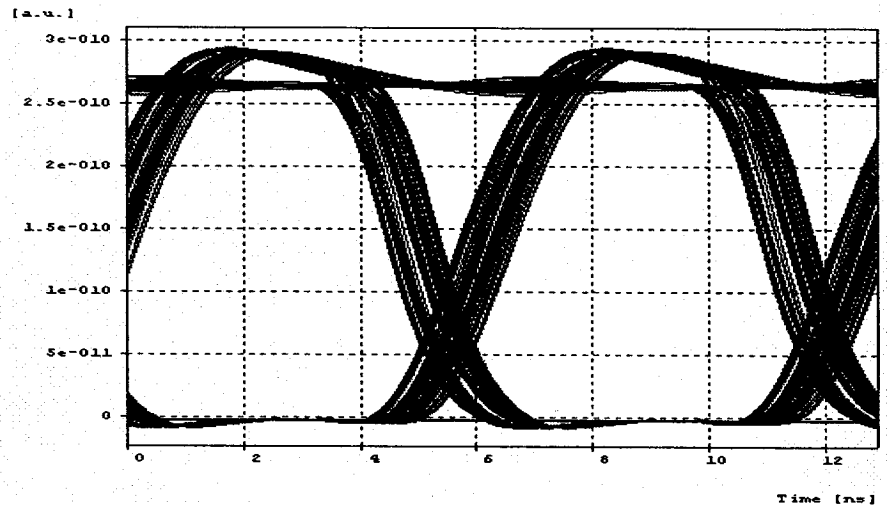

(c)

Figure 7.9 (a) BER versus received optical power by PD.

(b) Q versus received optical power by PD.

(c) Eye diagram of Data1 in channel 1 simulated at the back-to-back.

7.2.3 Result Discussion for the downlink

7.2.3.1 Fiber Chromatic Dispersion and ASE

In Figure 7.6 and Figure 7.9, they clearly indicate that the BER and Q of the decoded 155Mb/s data are simulated as a function of the received optical power, and no BER floor or Q roof were observed. Also no noticeable power penalty in the received data due to the chromatic dispersion of the transmission was observed. This is because only carrier and one of two sidebands are detected by a particular PD. The optical power of each LD in the simulation is -5dBm with the linewidth 10MHz. For a general case, an OBPF following an EDFA can be employed to reduce excess ASE noise. However, the satisfied performance achieved in the downlink had made it not necessary to be adopted in the downlink. Moreover, the EDFA could be removed if the received optical power was large enough to achieve a BER of 10^{-9}. If, for example,

the EDFA that was used for power compensation in the simulation can be removed, the SNR of the two sideband signals will be improved by 3 dB at least because an ideal noise figure of EDFA is 3 dB. As a result, the minimum RF power to be applied to the MZM for the downlink could be reduced.

7.2.3.2 Crosstalk

In order to estimate the influence of interchannel interference on the power penalty, we simulated the power penalty with respect to optical crosstalk in channel 3. Figure7.10 shows the setup. In the simulation, we inserted a variable optical attenuator (VOA) right after the MZM_1 and MZM_2 to reduce the optical powers of channel 1 and channel 2. Here, we neglect the optical crosstalk from channel 1, thus, optical crosstalk is defined as the optical power ratio of the channel 2 to the channel 3. The simulation was made without transmission over the 50-km SMF. For the upper-sideband signal, the power penalty of 0.1 dB can be achieved when the optical crosstalk is -10 dB. For the lower-sideband signal, the power penalty of 0.13 dB can be achieved when the optical crosstalk is -10 dB. It is clear that these power penalties were not so serious that they would degrade the system performance. Therefore, the proposed WI-OADM scheme is a practical candidate for the bus branch.

Using the same analyzing approach described above, the relationship of the power penalty with respect to optical crosstalk in channel 1 or channel 2 also indicates that the system has enough tolerant ability for interchannel interference.

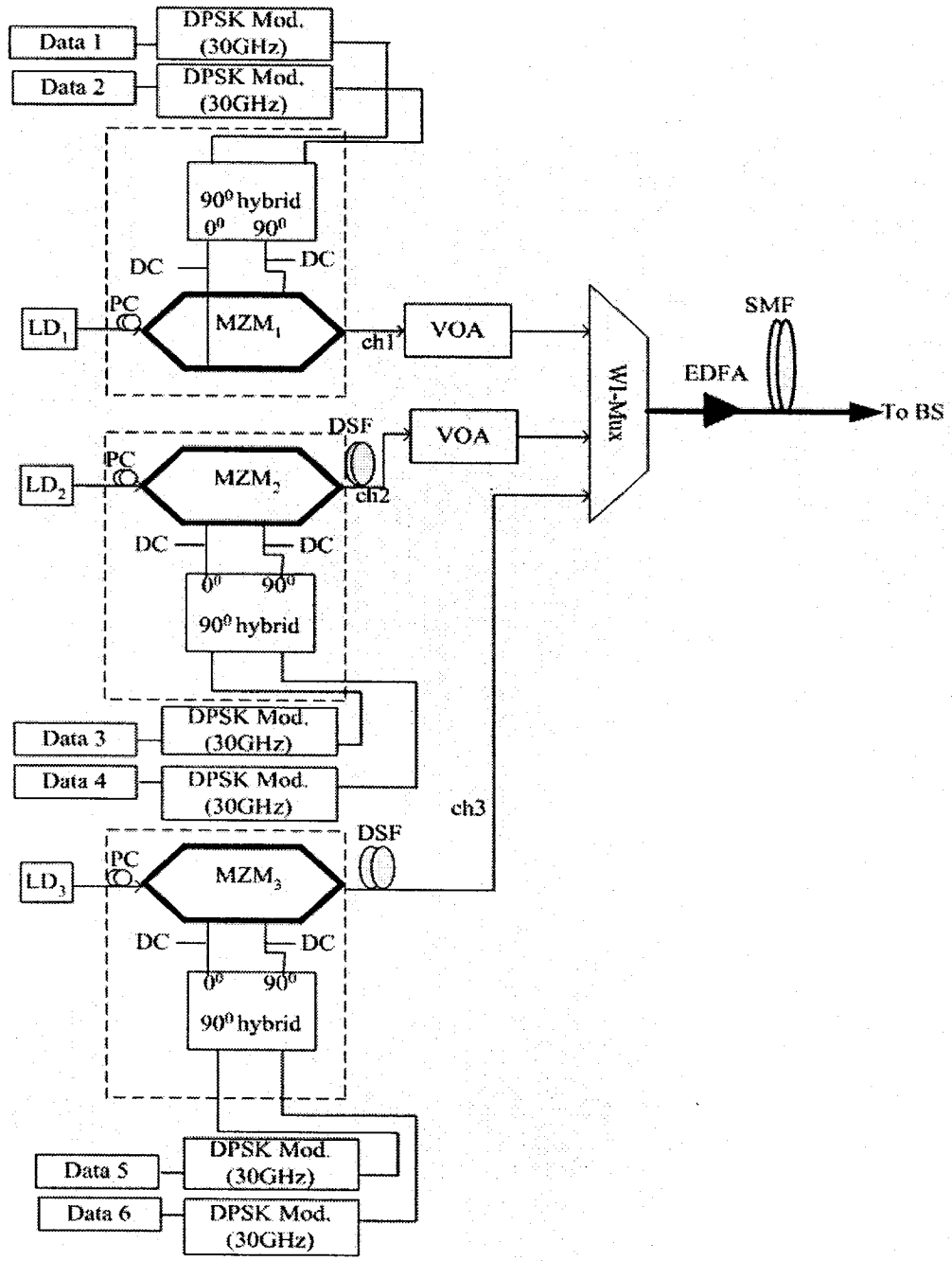

Figure 7.10 Setup for measuring power penalty versus optical crosstalk. The detection schemes, which are the same as the one in Figure7.1, are not shown.

7.2.3.3 IF over Fiber in Downlink

Finally, we would like to compare the "RF over fiber in downlink" with another approach for downlink transmission. This novel technique is to use IF subcarrier transmission over fiber in downlink as shown in Figure7.11 (a). Three 25GHz spaced DWDM optical carriers individually modulated by two 5GHz IF subcarriers with 155Mb/s DPSK data. A scenario inside this scheme is that a selected sideband signal should beat with a certain channel carrier to generate 30GHz RF at the receiver. For example, in order to extract D_2 at 30GHz, D_2 should beat with λ_1. In this scheme, D_2 and λ_1 were reflected from a customer designed WI-$OADM_1$ and dropped at WI-$OADM_1$ output port. Another scenario is that, for WI-$OADM_1$, the reflectivity at the wavelength of D_2 is set to 100%; while the reflectivity at the wavelength of λ_1 is set to 50%. The reason underlying this scenario depends on that each optical carrier has to beat with two different IF data, therefore, λ_1 should hold half power for another IF data to photodetect at another PD. In this simulation, the system parameters are the same as the one in Section 7.2.2 except for subcarrier frequency. An excellent eye diagram of extracted D_2 at 30GHz simulated at the back-to-back is shown in Figure 7.11(b). Other data can also be successfully extracted at RF without using the electrical frequency upconverter.

This novel technique can reduce expensive RF components in CO and all the optical components used in this scheme are commercial off-the-shelf. However, this technique is only suitable for the ring architecture.

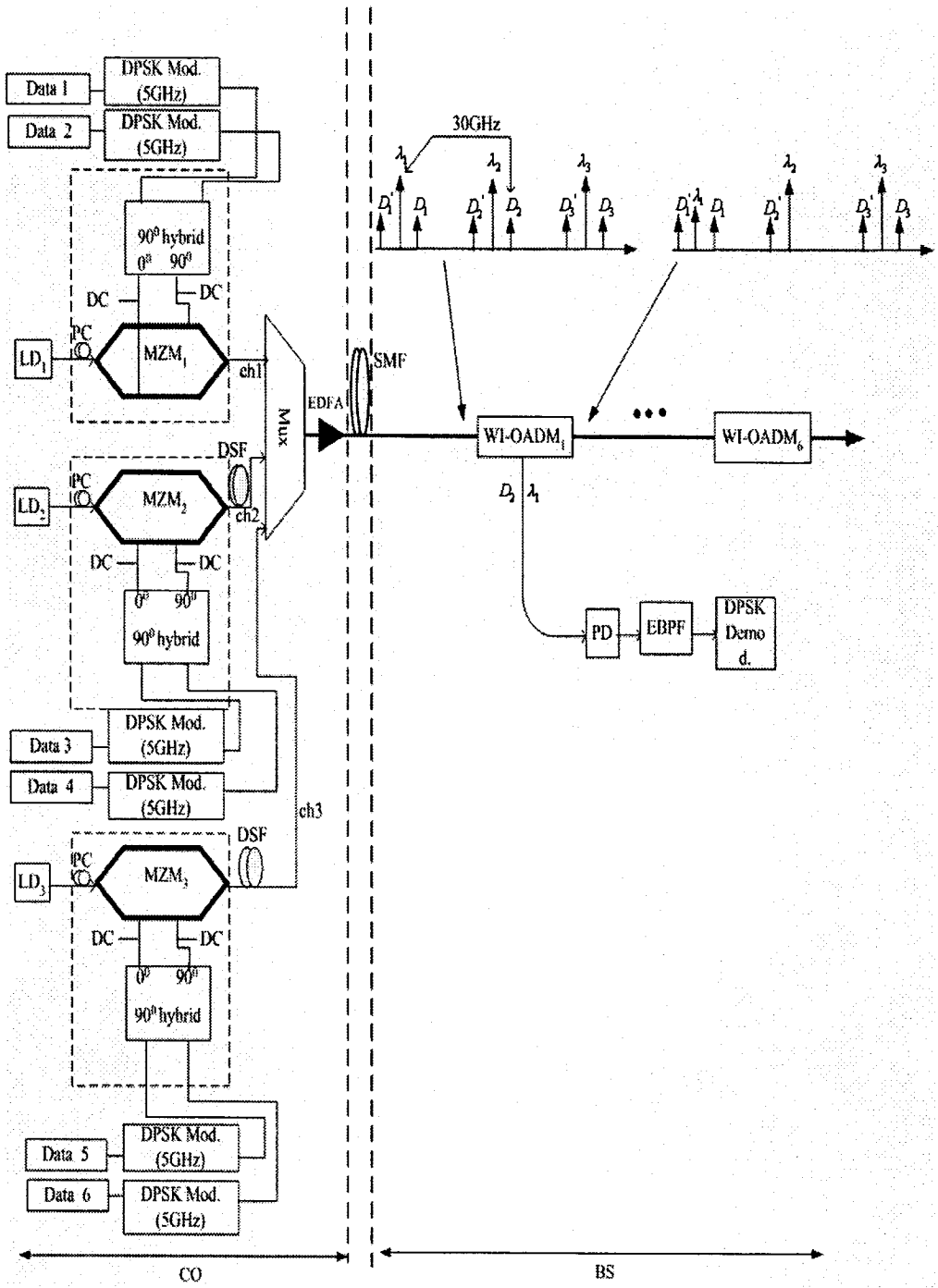
Data 1
DPSK Mod. (5GHz)
Data 2
DPSK Mod. (5GHz)
90⁰ hybrid
0⁰ 90⁰
DC
DC
PC
LD1
MZM1
ch1
Mux
EDFA
SMF
DSF
PC
LD2
MZM2
ch2
DC
DC
0⁰ 90⁰
90⁰ hybrid
Data 3
DPSK Mod. (5GHz)
Data 4
DPSK Mod. (5GHz)
ch3
DSF
PC
LD3
MZM3
DC
DC
0⁰ 90⁰
90⁰ hybrid
Data 5
DPSK Mod. (5GHz)
Data 6
DPSK Mod. (5GHz)
CO
30GHz
WI-OADM1
WI-OADM6
PD
EBPF
DPSK Demo d.
BS

(a)

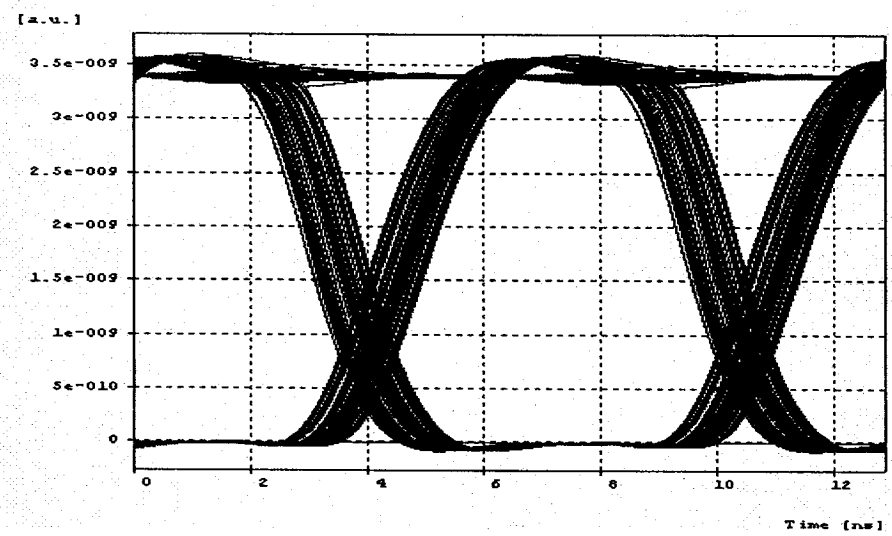

(b)

Figure 7.11 (a) Simulation setup for IF subcarrier transmission over fiber. (b) Eye diagram of the extracted D_2 simulated at the back-to-back., which was upconverted to 30GHz at the receiver without an electrical frequency upconverter.

7.3 RF over Fiber in uplink

As described in Section 7.2.1, λ_3 and its corresponding two sideband signals were dropped by the WI-OADM. However, another channel data, its carrier wavelength is λ_3 with corresponding two sidebands can also be added at the same WI-OADM to transmit through the fiber to BSs. Since there are no LDs in BSs in our system design, the optical powers for the uplink are provided by downlink signals. Therefore, three ORCs were used to provide optical powers for the uplink by using the technique in Section 4.2. The block diagram of the simulation setup is shown in Figure7.12.

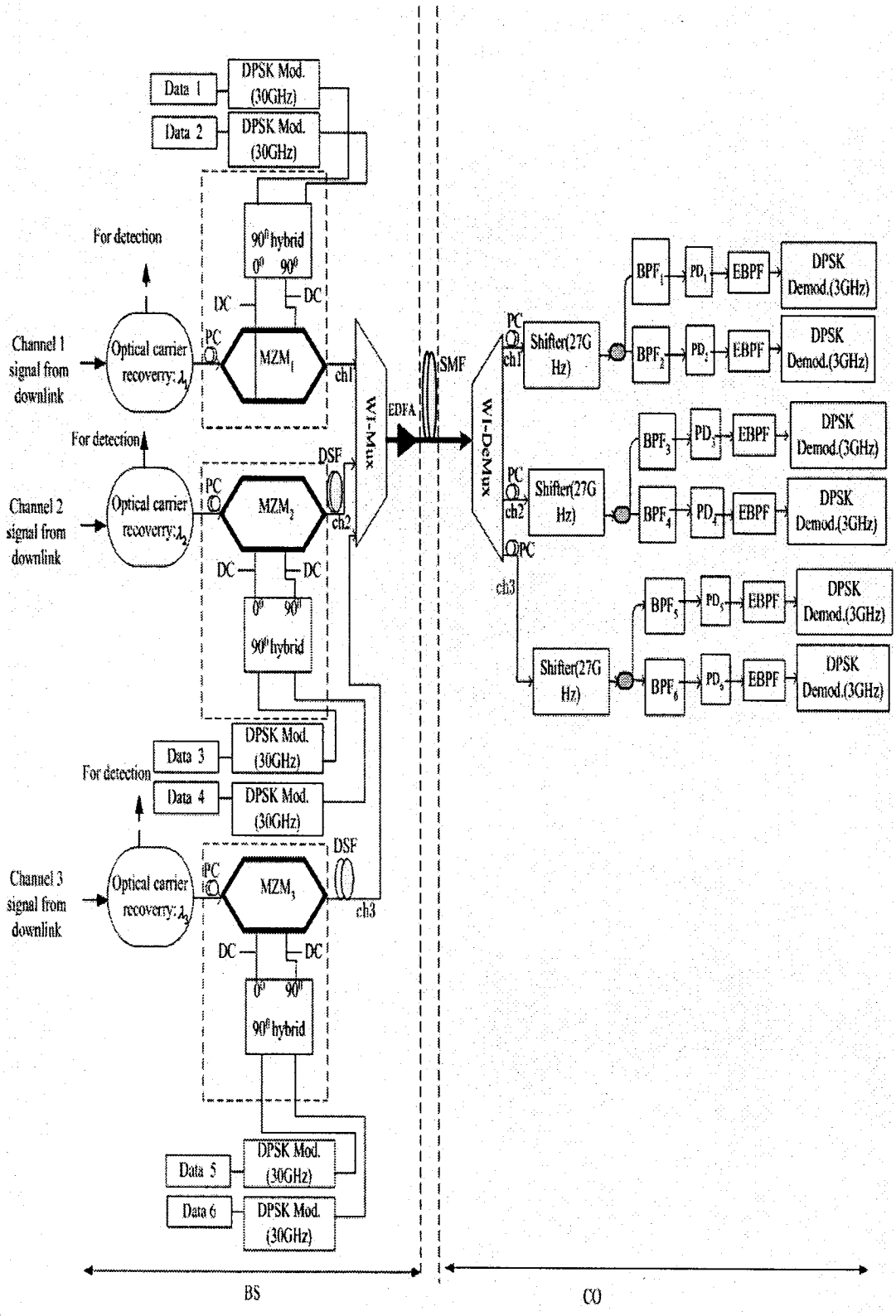

Figure 7.12 Simulation setup of millimeter-wave-band RF over fiber for the uplink.

7.3.1 Simulation Demonstration in the uplink

The recovered optical carriers were 1550nm, 1549.8nm and 1549.6nm from the channel 1, channel 2 and channel 3, respectively. Each recovered optical carrier was polarization-controlled to match the polarization axis of the MZM and again intensity modulated with two 30-GHz uplink RF data with rate of 155 Mb/s by MZM biased at quadrature. Thus, the output signal from a MZM was OTSSB signal again. The three channel OTSSB signals were interleaved and multiplexed by a WI-Mux. The formed OTSSB/SCM/DWDM signals were again amplified by another EDFA to compensate for the insertion losses of MZMs. Finally, these signals were transmitted over a 50-km-long SMF to the CO.

At the receiver, the uplink signal that was looped back to the CO was demultiplexed by WI-DeMux. Then, the demultiplexed channel signal was again polarization-controlled by a PC in each channel. Using the frequency-down-conversion technique described in Section 6.2, three recovered channel signals were frequency-down-shifted 27GHz by three shifters, respectively. Inside the shifter, $V\pi$ was 5V, the bias DC voltage was 2.5V on each MZM electrode. The spectrum after frequency-down-shifting is shown in Figure7.13. At Figure7.13, there are six frequency components on the spectrum of each channel. Among them, three frequency components are previous one, i.e. the carrier and its corresponding two sidebands; another three frequency components are the copies from the previous spectrum. These signal powers after frequency-down-shifting were split into two parts by a 3dB coupler, only interested signal pair with frequency interval of 3GHz was selected by a BPF in each branch.

Each interested signal pair was photodetected to regenerate a 3GHz uplink signal by a fast PD. The following Butterworth filter with a 3-dB bandwidth of 310 MHz

was used to eliminate the unwanted frequency components. The simulated electrical spectra after the Butterworth filters are shown in Figure7.14. Finally, each uplink data was demodulated by a DPSK demodulator at 3GHz. Figure 7.15 shows the simulated BER, Q versus the received optical power, and the back-to back eye diagram for the channel 1, channel 2, and channel 3.

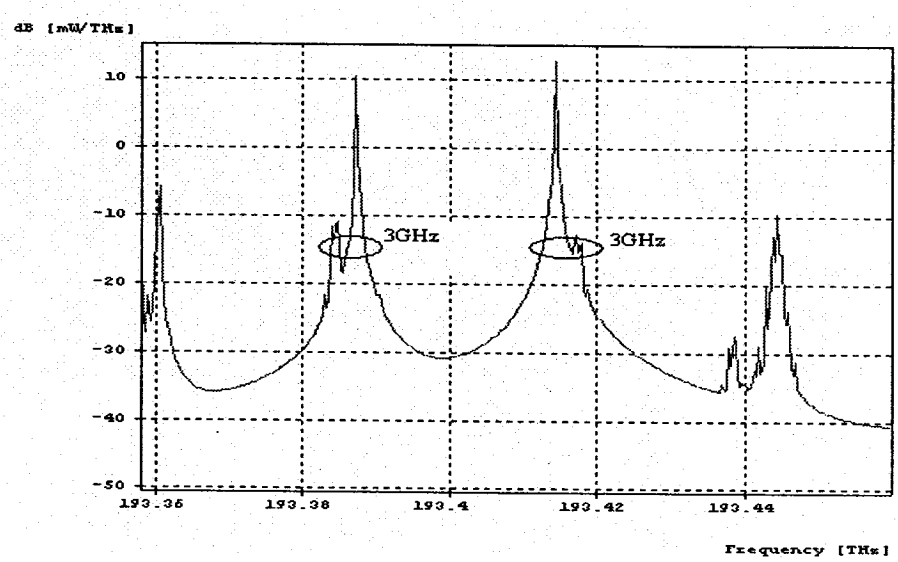

(a)

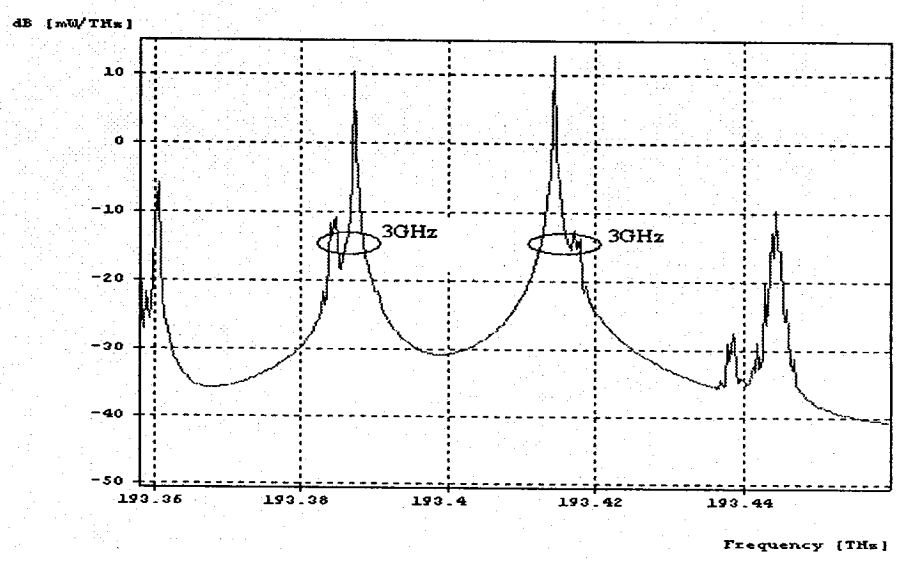

(b)

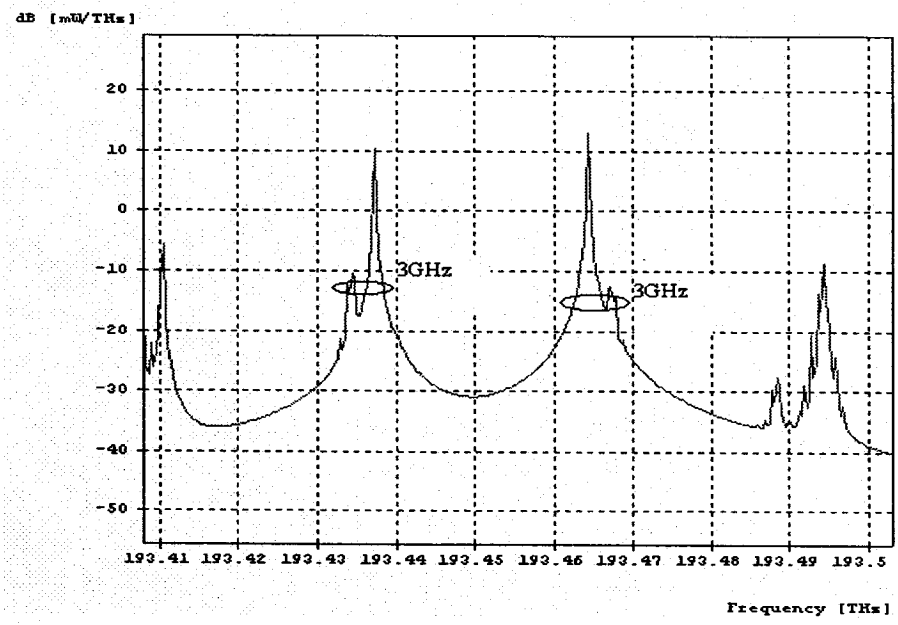

(c)

Figure 7.13 (a), (b) and (c) are the simulated optical spectra after frequency-down-shifting form the channel 1, channel 2 and channel 3, respectively.

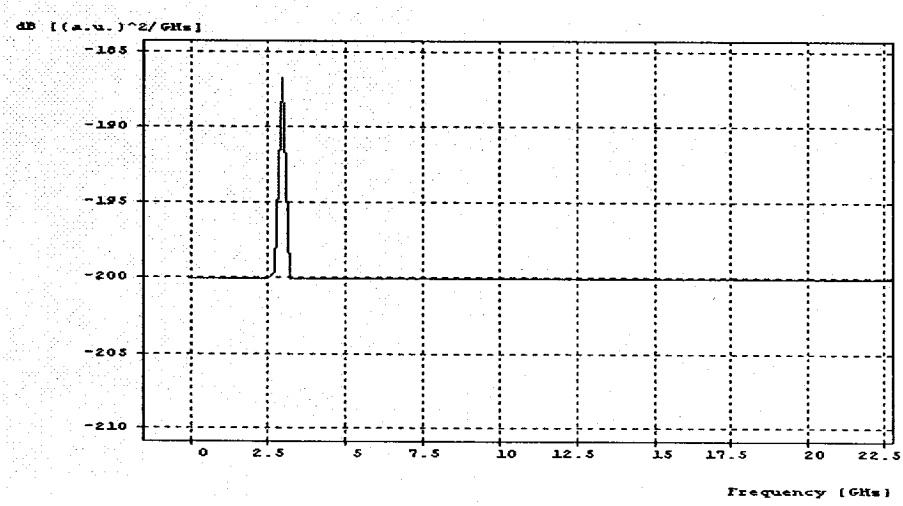

(a)

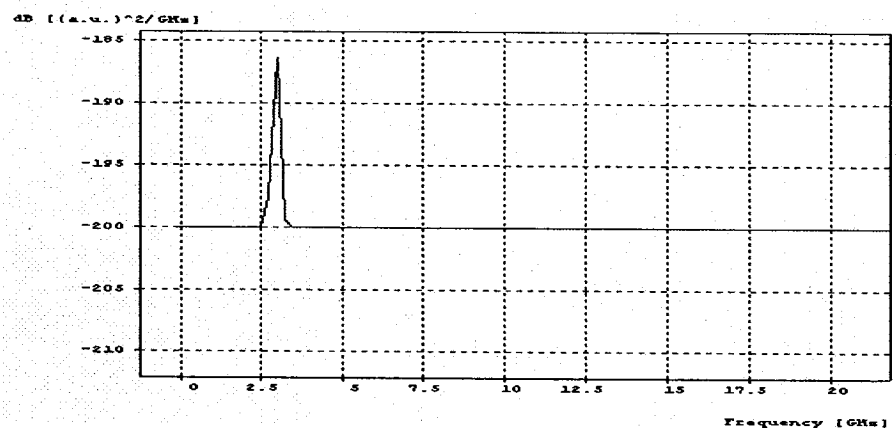
dB [(a.u.)^2/GHz]
-185
-190
-195
-200
-205
-210
0
2.5
5
7.5
10
12.5
15
17.5
20
Frequency [GHz]

(b)

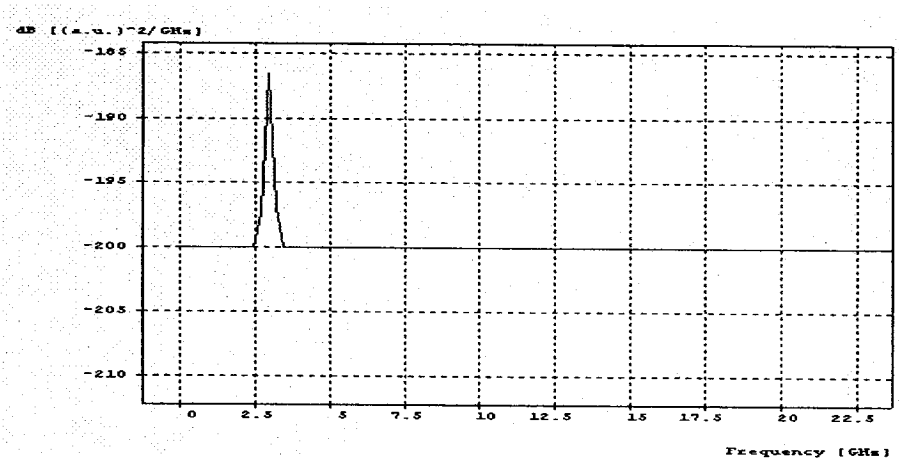
dB [(a.u.)^2/GHz]
-185
-190
-195
-200
-205
-210
0
2.5
5
7.5
10
12.5
15
17.5
20
22.5
Frequency [GHz]

(c)

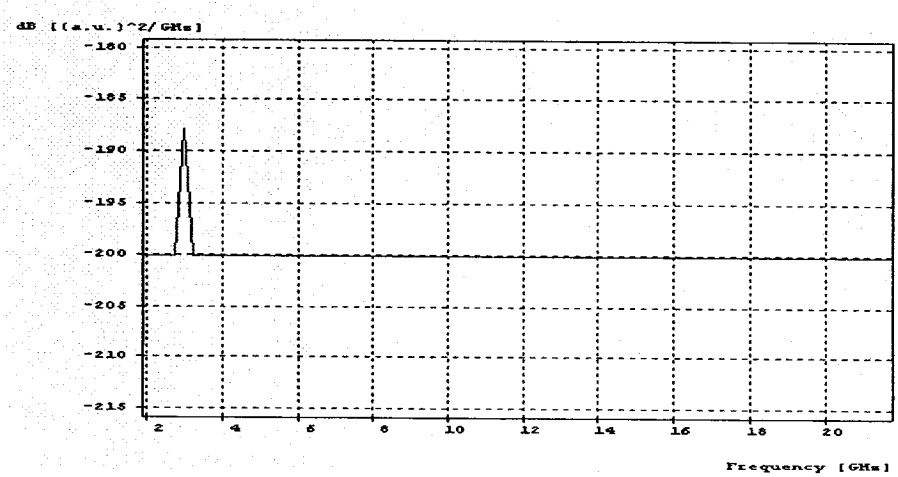
dB [(a.u.)^2/GHz]
-180
-185
-190
-195
-200
-205
-210
-215
2
4
6
8
10
12
14
16
18
20
Frequency [GHz]

(d)

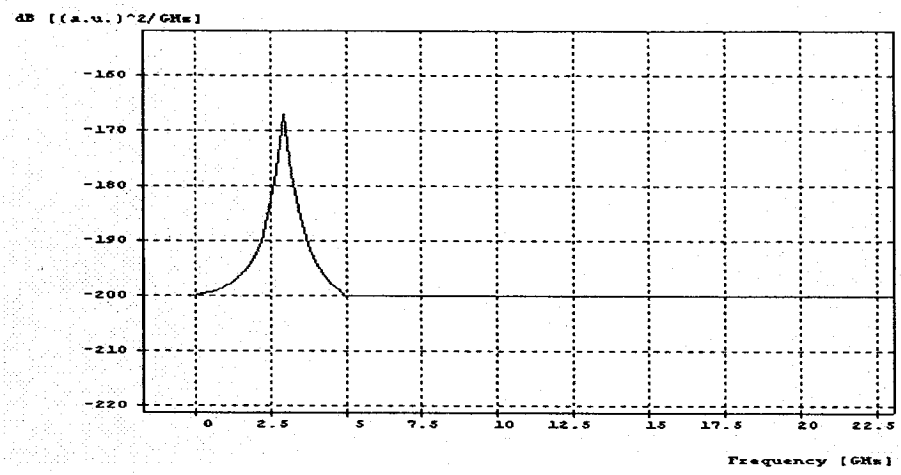

(e)

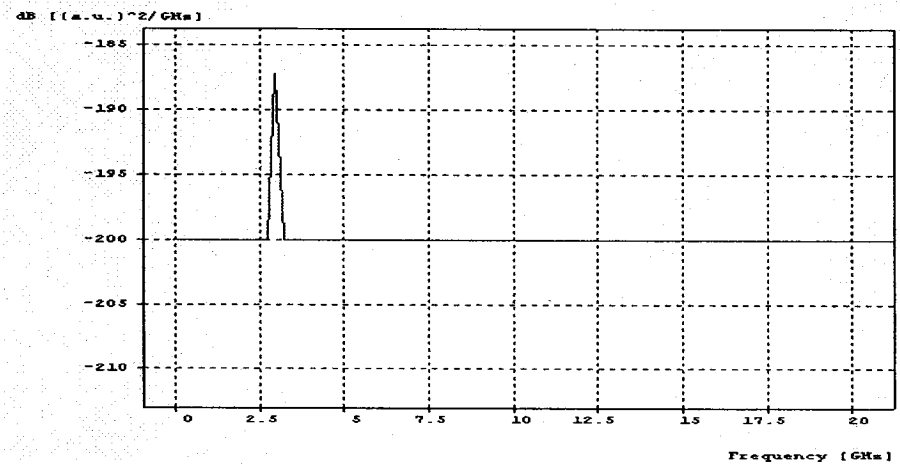

(f)

Figure 7.14 The simulated electrical spectra at the electrical BPFs. (a) Data1. (b) Data 2. (3) Data 3. (d) Data 4. (e) Data 5. (f) Data 6.

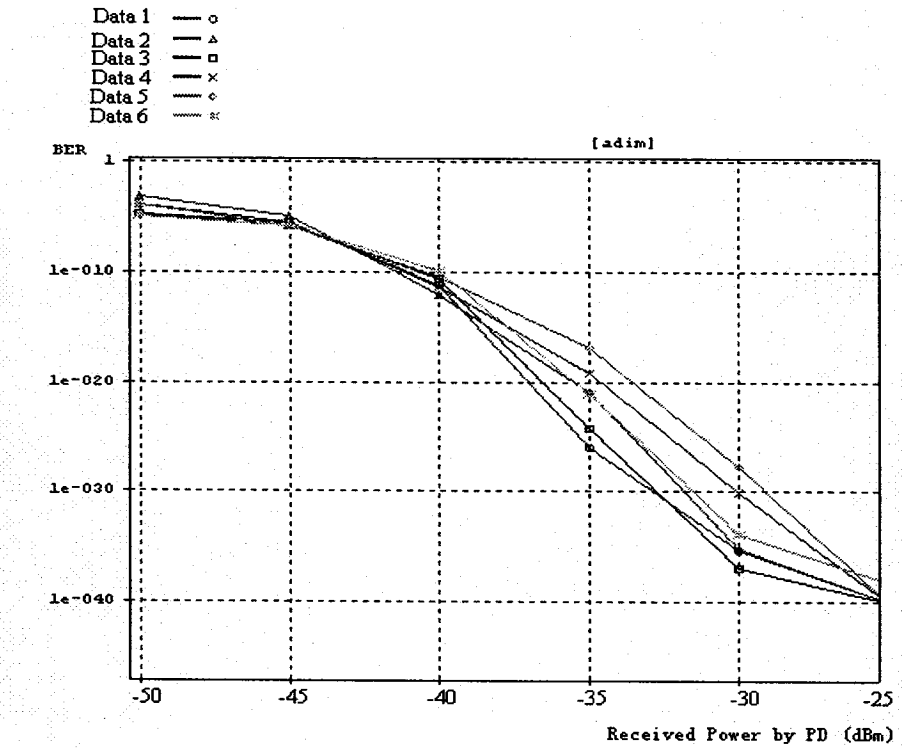
Data 1
Data 2
Data 3
Data 4
Data 5
Data 6
BER
[adim]
1
1e-010
1e-020
1e-030
1e-040
-50
-45
-40
-35
-30
-25
Received Power by PD (dBm)

(a)

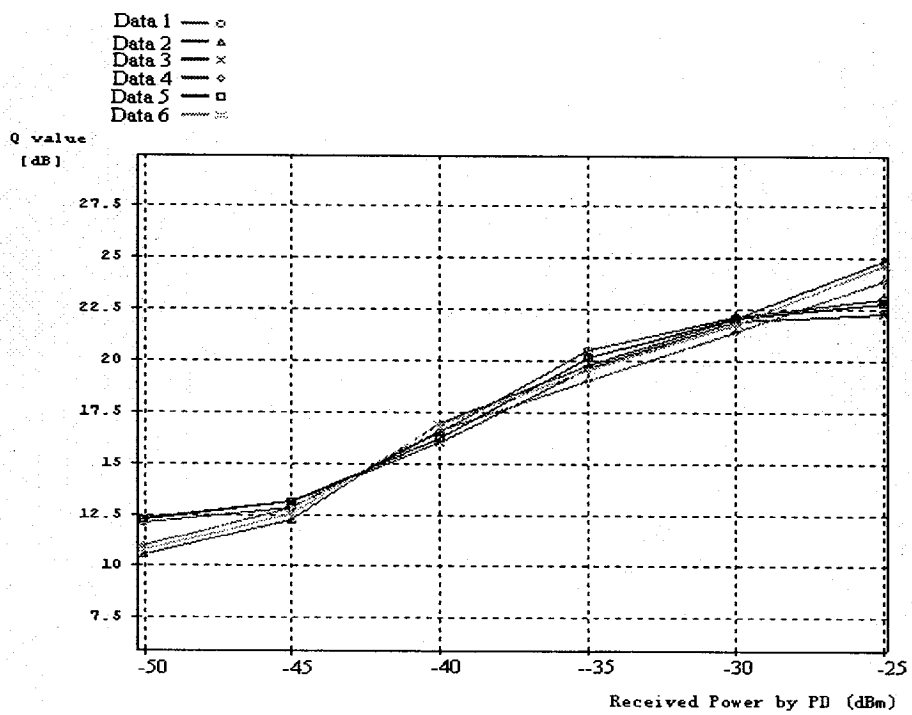
Data 1
Data 2
Data 3
Data 4
Data 5
Data 6
Q value
[dB]
27.5
25
22.5
20
17.5
15
12.5
10
7.5
-50
-45
-40
-35
-30
-25
Received Power by PD (dBm)

(b)

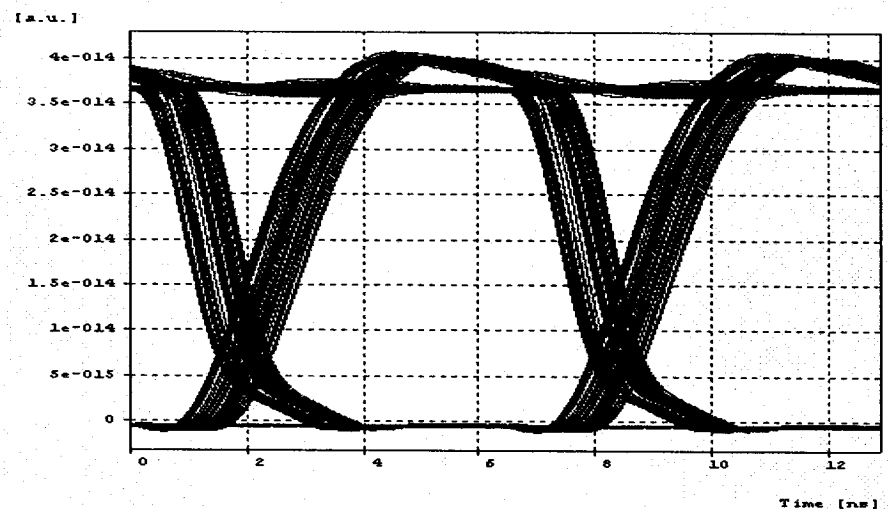

(c)

Figure 7.15 (a) BER versus received optical power by PD. (b) Q versus received optical power by PD. (c) Eye diagram of Data 1 simulated at the back-to-back.

7.3.2 Result Discussion for the uplink

In the uplink, undesired components generated by PD can be easily eliminated by EBPF. Figure14 shows the electrical spectra simulated at the output of EBPF. It can be seen that the desired data was successfully selected through the optical heterodyne detection by frequency-down-shifting without serious effects due to chromatic fiber dispersion. However, some level differences in the simulated IF signals were observed. Although it is difficult to identify the cause of these differences exactly, we think they were due to incomplete polarization matching and the different frequency densities in the spectrum.

Figure7.15 indicates that the BER and Q of the decoded 155Mb/s data are simulated again as a function of the received optical power; no BER floor, no Q roof and no noticeable power penalty due to fiber chromatic dispersion or laser phase noise were

observed. Moreover, the uplink system also has enough tolerant ability for inter-channel interference. Based on all of these satisfied results, they show the practicality of our frequency-down-shifting scheme for application to DWDM/SCM ROF uplink system.

Another approach for extracting the desired data at IF is to use only single frequency-down-shifter serving the all uplink receivers (see Figure 7.16). Here, for the sake of simplifying the analysis, we assume that there are only two interleaved optical channel signals are launched into a fiber, i.e. the carrier λ_1 with the corresponding upper-sideband signal D_1 and low-sideband $D_1^{'}$; the carrier λ_2 with the corresponding upper-sideband signal D_2 and low-sideband $D_2^{'}$. The channel spacing is 25GHz and RF is 30 GHz. The received wavelength-interleaved DWDM signals from BSs are directly put in a frequency-down-shifter. The signals from the shifter are consisted of the previous input signals and the corresponding copy signals. Then these signals are input into a demultiplexer to separate the four pairs of interested optical signals, which are related to generating the desired IF components. The frequency of the shifting is set to 33GHz instead of 27GHz to avoid a smaller spacing between two LOs. Finally, each of the selected four pairs of optical signals feeds to a PD to beat out the desired the IF signals.

The adjacent spacing for sidebands and carriers should be set wider enough to minimize crosstalk [52], [53]. However, in this approach, after frequency-down-shifting, the increased DWDM interleaving density would place tight restrictions on the rolloff and full-width at half-maximum (FWHM) of the filters in the demultiplexer. In Figure7.16 (c), the closest interval is only 2GHz, which is between $D_1^{'}$ and D_2, thereby making this approach very difficult to realize in practice. As a result, the frequency-

down-shifting technique described in Section 7.3.1 is clearly more practical option to extract data at IF in the uplink receiver.

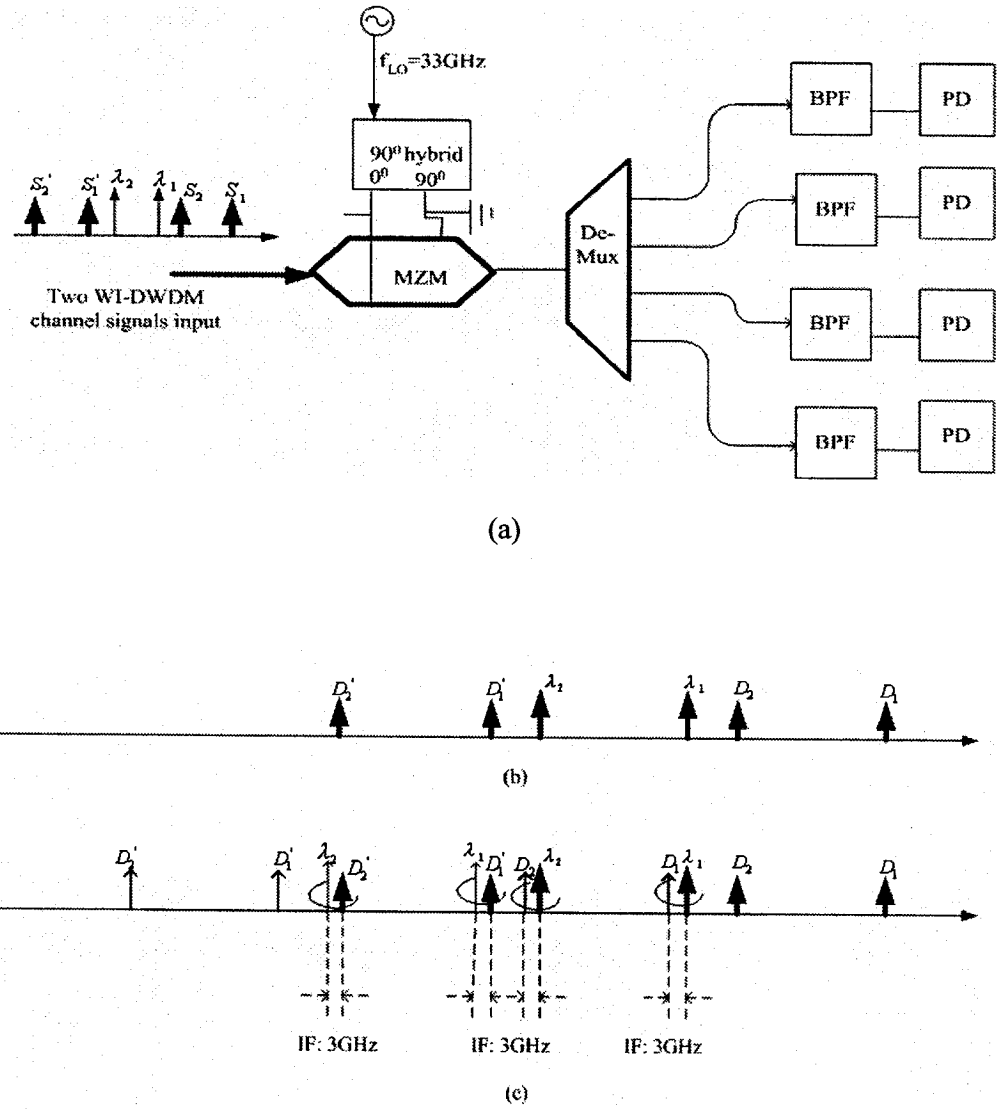

Figure 7.16 (a) Schematic diagram of the setup for using a single frequency- down-shifter to extract the desired data at IF. (b) The input spectrum before frequency-down-shifter. (c) The output spectrum after frequency-down-shifter. (The thick lines represent the original frequency components, the thin lines represent the shifted frequency components)

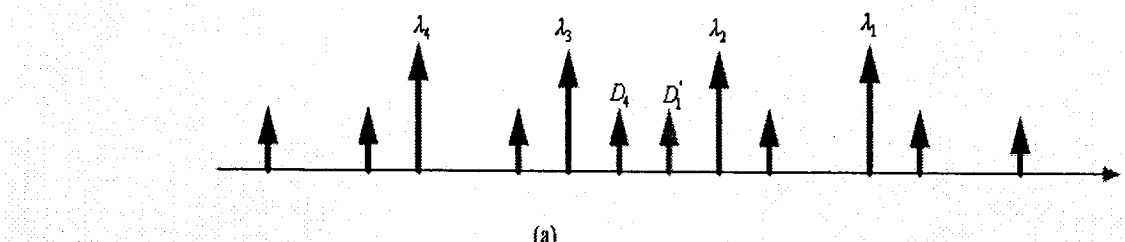
λ4
λ3
λ2
λ1
D4
D1'

(a)

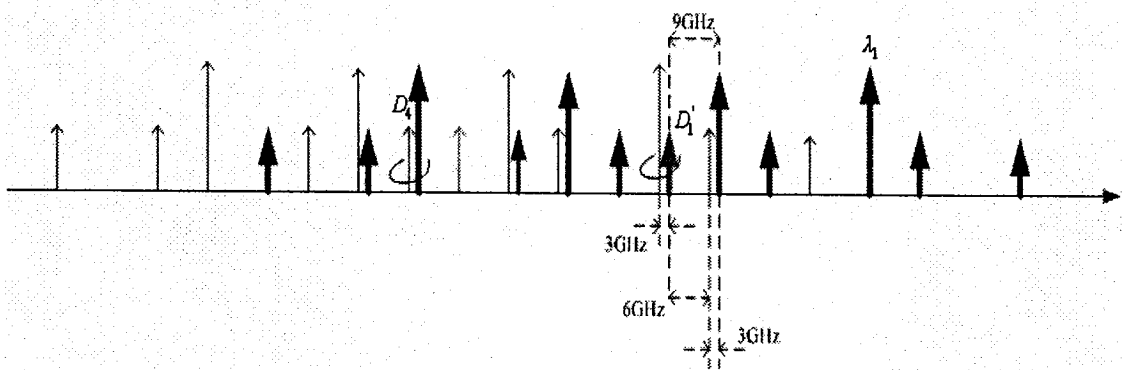
9GHz
λ1
D4
D1'
3GHz
6GHz
3GHz

(b)

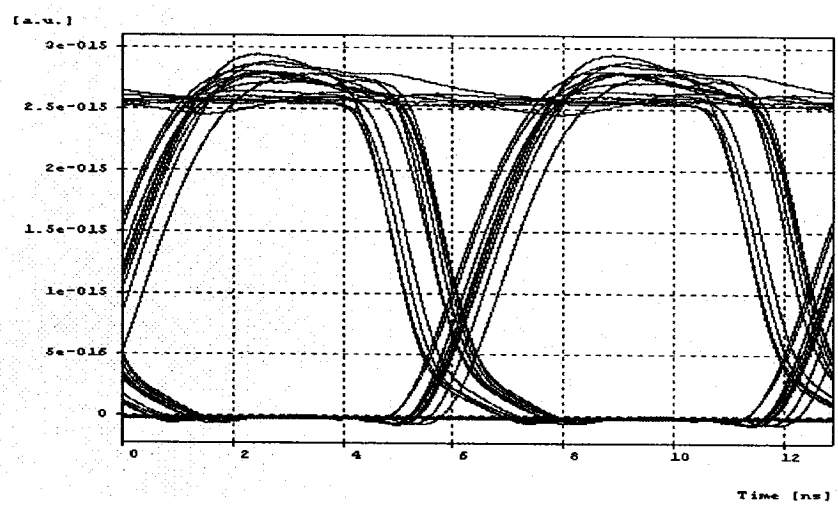
[a.u.]
3e-015
2.5e-015
2e-015
1.5e-015
1e-015
5e-016
0
0
2
4
6
8
10
12
Time [ns]

(c)

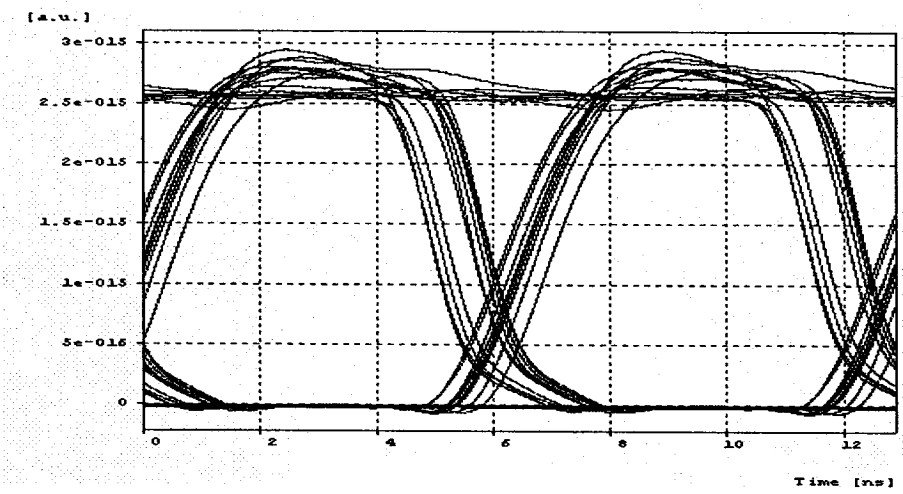

(d)

Figure 7.17 (a) The input spectrum before the frequency-down-shifter. (b) The output spectrum after the frequency-down-shifter. (c) The eye diagram of $D_1^{'}$ simulated at the back-to-back. (d) The eye diagram of D_4 simulated at the back-to-back.

However, if we consider changing the subcarrier frequency from 30GHz to 34GHz, the tight restrictions on the rolloff and full-width at half-maximum (FWHM) of the filters in the demultiplexer are disappeared. The reason is that the closest frequency interval is 6-GHz here, and nowadays the available smallest bandwidth of an optical filter is round 2.5-GHz. Therefore, we can use commercial off-the-shelf filters to separate the desired signals in practice. The schematic diagram of the simulation setup is similar as the Figure 7.16 (a). Here, we employ four channel input signals to verify using single frequency-down-shifter for the whole uplink receiver. The optical carrier is 1550nm, 1549.8nm, 1549.6nm and 1549.4 nm, respectively. The shifting frequency is set to 37GHz. The spectra and achieved eye diagrams are show in Figure 7.17. As

an example, we only show that the eye diagrams of D_1' and D_4 are successfully extracted at 3GHz.

7.4 Optical Power Budget and Capacity Analysis

Base on the architectures of both downlink and uplink in our simulation, an ideal link budget model of the network is devised. Figure7.18 shows the schematic of the link budget model. At the CO, three DWDM channel signals are multiplexed together using a WI-Mux, and the modulated optical signals are transported to the remote node (RN) via an optical fiber network. At the RN, the DWDM channels are demultiplexed using a WI-DeMux before being routed to the designated BS. In the uplink path, multiple DWDM channels are multiplexed at the RN via a WI-MUX and transported over the optical fiber network back to the CO.

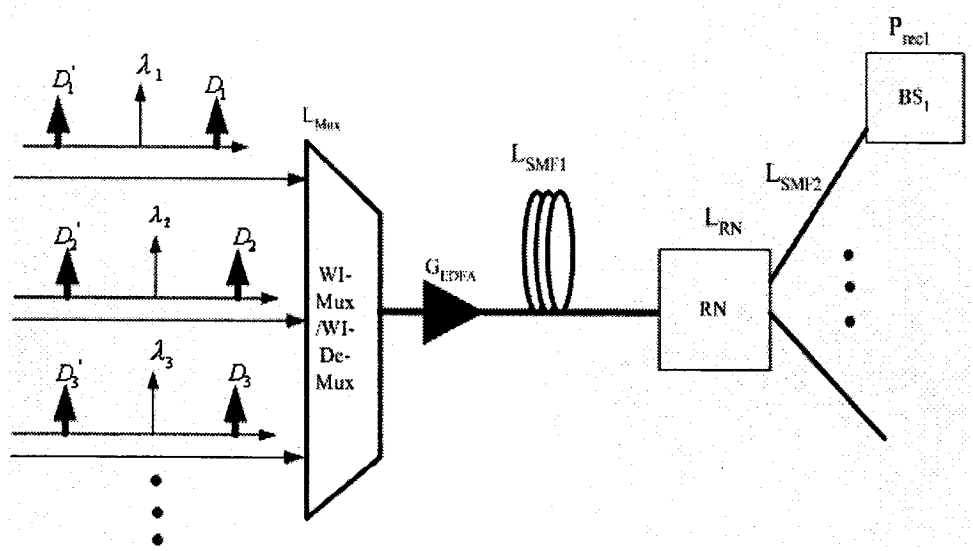

Figure 7.18 Schematic diagram of the RoF backbone network link budget model.

Here we neglect higher order sidebands, the total average optical power for a single DWDM channel can then be approximated using the optical carrier and the first-order sideband. These channels are multiplexed together at the CO and here optical

crosstalk effects due to a nonideal optical WI-MUX or WI-DeMUX and the effects of fiber dispersion are not taken into account for the sake of simplicity. A black-box erbium-doped fiber amplifier [54] was used in the model to provide the optical amplification in the optical link. Table7.2 shows the loss and gain values and also other parameters used in the model for the various components within the optical link, which are gotten from simulation parameters. Base on the link budget model and the simulation parameters, a power budget can be arranged. The EDFA used in our simulation has a small-signal gain of 40 dB and an output saturation power of 36 dBm, neglecting the requirement of system margin, the network reach is total 50km ($L_{SMF1}+L_{SMF2}$) . The half of total powers form the downlink will be provided for the uplink, the remainder of the power in each channel will again be shared by two BSs. Note that power gain and loss are additive, and thus the power budget reduces to straight-forward addition or subtraction. Then, the input optical power to the MZM per DWDM channel is set to -4dBm to achieve BER of 10^{-9} at the downlink receiver. In the uplink, when the gain from the preamplifier is set to 26 dB, then the received power before each PD in CO is -40dBm, BER of 10^{-9} is expected to achieve in the uplink receiver. Note that the BER is the function of the received power before PD described in Section 7.2.3 and 7.3.2.

In our simulation, the optical bandwidth of 30nm is available via the EDFA gain bandwidth, a total of 150 interleaved DWDM channel can be theoretically deployed if the network has sufficient link budget. However, Due to EDFA saturation effects and signal quality degradation, the maximum capacity of 150 channels will decrease. Incorporating an amplified RN architecture (postamplification) can significantly increase the overall capacity [55].However, such an amplification arrangement is

accompanied by an increased cost and network management complexity tradeoffs, which must also be taken into account.

Multiplexer loss (L_{Mux})	10dB
Small-signal EDFA gain (G_{EDFA})	40dB
EDFA maximum output power	36dBm
MZM insert loss	13dB
Fiber attenuation	0.2dB/km
Remote node loss (L_{RN})	13dB
Receiver sensitivity	-40dBm

Table 7.2 The table showing the loss/gain other parameters used in the analytical model for power budget.

Chapter 8

Conclusion and Future Work

8.1 Conclusion

A full-duplex 30-GHz millimeter-wave-band RoF system using frequency-interleaved OTSSB/SCM/DWDM scheme incorporating a single light source technique after transmitting over a 50-km-long SMF was successfully demonstrated. The applications of the novel WI-OADM, WI-Mux and WI-DeMux are indispensable to realize wavelength-interleaved DWDM millimeter-wave-band RoF networks. The satisfied results from our simulations demonstrate the effectiveness of the WI-OADM, WI-Mux and WI-DeMux in multiplexing and demultiplexing the carriers and their corresponding sidebands with potential for improved reduction in crosstalk.

Moreover, using a single light source configuration for full-duplex system leads to fewer optical components than conventional systems because its configuration is simpler due to the BS having no local light. The additional optical amplifiers, which compensate for the insertion losses, can be shared effectively with the DWDM systems. Since the optical downlink and uplink signals are in the OTSSB modulation format, there has been no serious dispersion problem. BERs of 10^{-9} have been simultaneously achieved for fiber-optic transmission of 30-GHz-band with data rate of 155Mb/s DPSK wireless signals in both the downlink and uplink.

In addition, a novel optical heterodyne detection using frequency-down-shifter for OTSSB/SCM/DWDM RoF system in the uplink has been demonstrated. In this scheme, the channel selection is carried out by frequency-down-shifting. This proposed scheme has a number of distinctive features:

1) Channel selection for multiplexed RoF signals;

2) No optical narrow BPF needed;

3) IF-band signal processing;

4) High receiver sensitivity;

5) Reduction of optical noise sources;

6) No OPLLs.

8.2 Future Work

Throughout our work, a 30GHz full duplex RoF system, which is considered as the best platform for next generation optically driven wireless networks, has been demonstrated.

Our techniques used in this 30GHz system can be easily applied to other 24-100 GHz millimeter-wave-band RoF systems. The next work in our research emphasis will particularly focus on:

1) Developing multi-gigabit/s wireless links based on millimeter-wave photonic techniques;

2) In our current system, MZM is used to double the spectral utilization comparing with using EAM. Unfortunately, MZM needs external voltages to bias it at BSs. A more realistic modulation technique should be devised to simultaneously achieve high spectral utilization and electrically maintenance-free at BSs;

3) Expanding the design of the optical wavelength-interleaved components in relation

to bandwidth limitation, noise problem, nonlinearity as well as inter-channel crosstalk; 4) Full-duplex millimeter-wave-band RoF system will theoretically and experiment ally be identified and studied with only one fiber transmission incorporating hybrid topologies suitable for DWDM application.

8.3 Summary of Contributions

Finally, we would like to mention the main contributions of this thesis that are listed below.

1) High Volume Transmission Capacity

Integrating optical wavelength-interleaving, optical tandem SSB format, subcarrier and DWDM technologies into one millmeter-wave-band RoF system, which has not existed in the current literature, can achieve the capability to deal with large amount of data.

2) Novel Optical Wavelength-interleaving Components

We have offered three proposals with practical approaches on designing novel WI-OADM, WI-Mux and DeMux components, which are indispensable to realize wavelength-interleaved DWDM transmission systems.

3) Novel Frequency-Down-Shifting Technique

This technique can successfully implement the channel selection and extract the desired data at IF for providing IF-band signal processing in CO. Many other advantages of this technique are described in Chapter 6 and Chapter 7.

4) IF Subcarrier Transmission over Fiber in Downlink

Here we introduced a new technique to realize IF subcarrier transmissions over fiber in the downlink while the subcarrier at RF can be achieved without electrical frequency-upconvertion in the BS. This technique can reduce expensive RF components in CO and have less fiber chromatic influence than RF subcarrier

transmission. All the optical components used in this scheme are commercial off-the-shelf.

5) Effective Architecture of Millimeter-Wave-Band RoF Network

We have designed an effective architecture of the millimeter-wave-band RoF network with the optimal solutions to the two critical challenges, i.e. maximizing spectral utilization and low-cost BS configuration. This work would be helpful for researchers to make system design and analysis of future broad-band wireless access.

References

[1] U. Gliese, "Multi-functional fiber-optic microwave links," *Opt. & Quantum Electron.*, vol. 30, pp. 1005–1019, 1998.

[2] H. Ogawa, D. Polifko, and S. Banba, "Millimeter-wave fiber optics systems for personal radio communications," *IEEE Trans. Microwave Theory Tech.*, vol. 40, pp. 2285–2292, 1992.

[3] J. J. O'Reilly and P. M. Lane, "Remote delivery of video services using mm waves and optics," *J. Lightwave Technol.*, vol. 12, pp. 369–375, Feb. 1994.

[4] G. H. Smith, D. Novak, and C. Lim, "A millimeter-wave full-duplex fiber-radio star-tree architecture incorporating WDM and SCM," *IEEE Photon. Technol. Lett.*, vol. 10, pp. 1650–1652, 1998.

[5] L. Noel, D. Wake, D. G. Moodie, D. D. Marcenac, L. D. Westbrook, and D. Nesset, "Novel techniques for high-capacity 60 GHz fiber-radio transmission systems," *IEEE Trans. Microwave Theory Tech.*, vol. 45, pp. 1416–1423, 1997.

[6] K. Kitayama, "Architectural considerations of fiber-radio millimeter-wave wireless access systems," *Fiber Integr. Opt.*, vol. 19, pp.167–186, 2000.

[7] T. Kuri, K. Kitayama, and Y. Takahashi, "Simplified BS without light source and RF local oscillator in full-duplex millimeter-wave radio-on-fiber system based upon external modulation technique," in *IEEE Int. Microwave Photonics Topical Meeting Technical Dig.*, Paper T-7.3, pp. 123–126, 1999.

[8] K. Kitayama, T. Kuri, A. St¨ohr, and Y. Ogawa, "Fiber-optic millimeter-wave downlink system using 60-GHz-band external modulation," *J.Lightwave Technol.*, vol. 17, May 1999.

[9] S.V. Kartalopoulos, "DWDM Networks, Devices, and Technology," *IEEE Press*, Secs.3, New York, 2003.

[10] Hiroyuki Toda, Tsukasa Yamashita, Toshiaki Kuri, and Ken-ichi Kitayama, "Demultiplexing Using an Arrayed-Waveguide Grating for Frequency-Interleaved DWDM Millimeter-Wave Radio-on-Fiber Systems," *IEEE .J. Lightwave technol.,* vol. 21, pp, 1735-1740, Aug 2003

[11] Meslener, G.J. "Chromatic dispersion induced distortion of modulated monochromatic light employing direct detection" *IEEE J. Qantum., 1984, 20, pp.1208-1216*

[12] D. Novak, Z. Ahmed, G. H. Smith, and H. F. Liu, "Techniques for millimeter-wave optical fiber transmission systems (invited)," in *Microwave Photon. Topical Meeting Tech. Dig.*, Duisbrug, Germany, Sept. 1997, TH1-3, pp. 39–42.

[13] T. Kuri and K. Kitayama, "Laser phase noise free optical heterodyne detection technique for 60GHz –band radio-on-fiber systems ," in *2000 Int.Topical meeting Microwave Photonics(MWP2000) Tech.Dig.*, vol. WE1.5, Oxford, K, ,pp.141-144, Sep.2000

[14] http://www.ictc.com.cn/2000/paper/34.pdf, "Mm-wave Radio over fiber system."

[15] G.P.Agrarwal, "Fiber optical Communication System," Sec.2, New York, Wiley, 2002.

[16] K. Yonenaga and N. Takachio, "A fiber chromatic dispersion compensation technique with an optical SSB transmission in optical homodyne detection systems," *IEEE Photon. Technol. Lett.*, vol. 5, pp. 949–951, Aug. 1993.

[17] P.-Y. Pi-Yang Chiang and W. I.Winston I. Way, "Ultimate capacity of a laser diode in transporting multichannel M-QAM signals," *J. Lightwave Technol.*, vol. 15, pp. 1914–1924, Oct. 1997.

[18] C. F. Lam, "A simplified model for estimating the capacity limit of an optical

link in transporting multichannel M-QAM signals," *IEEE Photon. Technol. Lett.*, vol. 12, pp. 1579, Nov. 2000.

[19] S. L. Zhang, P. M. Lane, and J. J. O'Reilly, "Assessment of the nonlinearity tolerance of different modulation schemes for millimeter-wave fiber-radio systems using MZ modulators," *IEEE Trans. Microwave Theory Tech.*, vol. 45, pp. 1403–1409, Aug. 1997.

[20] G. H. Smith, D. Novak, and Z. Ahmed, "Technique for Optical SSB Generation to Overcome Dispersion Penalties in the fibre-radio systems," *Electron. Lett.*, vol. 33, pp. 74-75,1997.

[21] A. Djupsjobacka, "Residual chirp in integrated-optic modulators," *IEEE Photon. Technol. Lett.*, vol. 4, pp. 41–43, Jan. 1992.

[22] F. Devaux, Y. Sorel, and J. F. Kerdiles, "Simple measurement of fiber dispersion and of chirp parameter of intensity modulated light emitter,"*J. Lightwave Technol.*, vol. 11, pp. 1937–1940, Dec. 1993.

[23] R. A. Griffin, H. M. Salgado, P. M. Lane, and J. J. O'Reilly, "System capacity for millimeter-wave radio-over-fiber distribution employing an optically supported PLL," *J. Lightwave Technol.*, vol. 17, pp. 2480–2487, Dec. 1999. pp. 167–186, 2000.

[24] M.Y. Frankel and R. D. Esman, "Optical single sideband suppressed carrier modulator for wide-band signal processing," *J. Lightwave Technol.*, vol. 16, pp. 859, May 1998.

[25] K. Kitayama, "Highly spectrum efficient OFDM/PDM wireless networks by using optical SSB modulation," *J. Lightwave Technol.*, vol. 16, pp. 969–976, June 1998.

[26] S. Ohmori, "Toward future wireless multimedia communication systems using mm-waves," in *IEEE Int. Microwave Photonics Topical MeetingTechnical*

Dig., Melbourne, Australia, Nov. 1999, Paper W-1.1, pp. 3.

[27] I. Seto, H. Shoki, and S. Ohshima, "Optical subcarrier multiplexing transmission for base station with adaptive array antenna," *IEEE Trans. Microwave Theory Tech.*, vol. 49, pp. 2036–2041, Oct. 2001.

[28] D. Wake, C. R. Lima, and P. A. Davies, "Optical generation of millimeter-wave signals for fiber-radio systems using a dual-mode DFB semiconductor laser," *IEEE Trans. Microwave Theory Tech.*, vol. 43, pp. 2270–2276, Sept. 1995.

[29] T. Kuri, K. Kitayama, and Y. Ogawa, "Fiber-optic millimeter-wave uplink system incorporating remotely fed 60-GHz-band optical pilot tone," *IEEE Trans. Microwave Theory Tech.*, vol. 47, pp. 1332–1337, July 1999.

[30] A. Nirmalathas, C. Lim, D. Novak, and R. Waterhouse, "Optical interface without light sources for base-station designs in fiber-wireless systems incorporating WDM," in *IEEE Int. Microwave Photonics Topical Meeting Technical Dig.*, Melbourne, Australia, Paper T-7.2, pp. 119–122, Nov. 1999.

[31] T. Kuri, K. Kitayama, and K. Murashima, "Error-free DWDM transmission of 60-GHz-band fiber-radio signals with square-like response fiber Bragg gratings," in *IEEE Int. Microwave Photonics Topical Meeting Technical Dig.*, Paper Tu.2-6, pp. 69–72, Jan. 2001.

[32] D. Castleford, A. Nirmalathas, D. Novak, and R. S. Tucker, "Optical crosstalk in fiber-radio WDM networks," *IEEE Trans. Microwave Theory Tech.*, vol. 49, pp. 2030–2035, Oct. 2001.

[33] Jean-Pierre Laude. "DWDM fundamentals, components, and application," Boston, Artech House, pp.27-51, 2002.

[34] N.Gote, H.Venghaus, 'Fiber Optical Communication Devices', Sec.3-4, Berlin, Springer, 2001.

[35] H. Toda, T. Yamashita, K. Kitayama, and T. Kuri, "A DWDM mm-wave fiber-radio system by optical frequency interleaving for high spectral efficiency," in *Proc. MWP*, Long Beach, CA, pp. 85–88, 2001.

[36] C. Lim, A. Nirmalathas, D. Novak, R. Tucker, and R. Waterhouse, "Novel technique for increasing spectral efficiency in millimeter-wave fiber-radio systems," *Electron. Lett.*, vol. 37, pp. 1043–1045, 2001.

[37] R. Zengerle and O. Leminger, "Phase-shifted Bragg-grating filters with improved transmission characteristics," *J. Lightwave Technol.*, vol. 13, pp. 2354–2358, 1995.

[38] L. Wei and J. Lit, "Phase-shifted Bragg grating filters with symmetrical structures," *J. Lightwave Technol.*, vol. 15, pp. 1405–1409, 1997.

[39] F. Bakhti and P. Sansonetti, "Design and realization of multiple quarter-wave phase-shifts UV-written bandpass filters in optical fibers," *J. Lightwave Technol.*, vol. 15, pp. 1433–1437, 1997.

[40] T. Erdogan, "Fiber grating spectra," *J. Lightwave Technol.*, vol. 15, pp.1277 1294, 1997.

[41] G. P. Agarwal, "Fiber Optic Communication Systems," Sec.10, New York, Wiley, 2002.

[42] S. Betti, G. de Marchis, and E. Iannone, "Coherent Optical Communication System ," Sec.7,Willey, New York, 1995.

[43] A. Narasimha, X. J. Meng, M. C. Wu, and E. Yablonovitch, "Tandem single sideband modulation scheme to double the spectral efficiency of analog fiber links," *Electron. Lett.*, vol. 36, no. 13, pp. 1135, June 2000.

[44] T. Kuri and K. Kitayama, "Optical heterodyne detection of millimeter-wave band radio-on-fiber signals with a remote dual-mode local light source," *IEEE Trans. Microwave Theory Technol.*, vol. 49, pp. 2025–2029, Oct. 2001.

[45] H. Sotobayashi and K. Kitayama, "Cancellation of the signal fading for 60 GHz subcarrier multiplexed optical DSB signal transmission in nondispersion shifted fiber using midway optical phase conjugation," *J. Lightwave Technol.*, vol. 17, pp. 2488–2497, Dec. 1999.

[46] E. Suematsu and N. Imai, "A fiber optic/millimeter-wave radio transmission link using HBT as direct photodetector and an optoelectronic upconverter," *IEEE Trans. Microwave Theory Tech.*, vol. 44, pp. 133–143, Jan. 1996.

[47] H. M. Salgado and J. J. O'Reilly, "Accurate performance modeling of subcarrier multiplexed fiber/radio systems: Implications of laser nonlinear distortion and wide dynamic range," *IEEE Trans. Commun.*, vol. 44, pp. 988–996, Aug. 1996.

[48] Y. Ozeki, K. Higuma, S. Oikawa, M. Kishi, and M. Tsuchiya, "A 60-GHz optoelectronic mixing scheme of high image and carrier rejection ratios with an integrated optical single-sideband modulator employed," *IEEE Microwave Theory Tech.*, vol. 49, pp. 1986–1991, Oct. 2001.

[49] A. Loayssa, C. Lim, A. Nirmalathas, and D. Benito, "Optical single sideband modulator for broad-band subcarrier multiplexing systems," *IEEE Photon. Technol. Lett.*, vol. 15, pp. 311–313, Feb. 2003.

[50] S. Betti, G. D. Marchis, and E. Iannone, "Coherent Optical Communications Systems," Sec. 9. New York: Wiley, 1995,

[51] C. G. Schäffer, M. Sauer, K. Kojucharow, and H. Kaluzni, "Increasing the channel number in WDM mm-wave systems by spectral overlap," in *2000 Int. Topical Meeting Microwave Photonics (MWP2002) Tech. Dig.*, vol. WE2.4, Oxford, U.K., Sept. 2000, pp. 164–167, pp. 85–88, Jan. 2002.

[52] K. Kikuchi and K. Katoh, "Optical heterodyne receiver for selecting densely frequency division multiplexed signals," *Electron. Lett.*, vol. 38, no. 6, pp.

283–285, Mar. 2002.

[53] B. J. Dixon, R. D. Pollard, and S. Iezekiel, "Orthogonal frequency-division multiplexing in wireless communication systems with multimode fiber feeds," *IEEE Trans. Microwave Theory Tech.*, vol. 49, pp.1404–1409, Aug. 2001.

[54] X. Zhang and A. Mitchell, "A simple black box model for erbium-doped fiber amplifiers," *IEEE Photon. Technol. Lett.*, vol. 12, pp. 28–30, 2000.

[55] C. Lim, A. Nirmalathas, D. Novak, and R. B. Waterhouse, "Capacity analysis for a WDM fiber-radio backbone incorporating wavelength-interleaving," in *Proc. OFC*, Anaheim, CA, pp. 355–357, 2002.